



Remediation of an Arsenic-Contaminated Anoxic Aquifer in Hjärtevad with Zerovalent Iron

– Assessment and Modelling of Sorption Strength
and Solubility of Arsenic

Kathrin Leicht

Master Thesis in Environmental Science • 30 ECTS
Swedish University of Agricultural Sciences, SLU
Department of Soil and Environment
EnvEuro – European Master in Environmental Science
Examensarbeten, Institutionen för mark och miljö
Uppsala 2021



Remediation of an Arsenic-Contaminated Anoxic Aquifer in Hjärtevad with Zerovalent Iron – Assessment and Modelling of Sorption Strength and Solubility of Arsenic

Kathrin Leicht

Supervisor: Thiago Formentini, SLU, Department of Soil and Environment
Assistant supervisor: Geert Cornelis, SLU, Department of Soil and Environment
Assistant supervisor: Markus Puschenreiter, University of Natural Resources and Life Sciences, Institute of Soil Research
Examiner: Jon Petter Gustafsson, SLU, Department of Soil and Environment

Credits: 30 ECTS
Level: Second cycle, A2E
Course title: Independent Project in Environmental Science – Master thesis
Course code: EX0897
Programme/education: EnvEuro – European Master Environmental Science
Course coordinating dept: Soil and Environment

Place of publication: Uppsala
Year of publication: 2021

Keywords: Arsenic Remediation, Zerovalent Iron, Anoxic Aquifer

Swedish University of Agricultural Sciences
Faculty of Natural Resources and Agricultural Sciences
Department of Soil and Environment

Publishing and archiving

Approved students' theses at SLU are published electronically. As a student, you have the copyright to your own work and need to approve the electronic publishing. If you check the box for **YES**, the full text (pdf file) and metadata will be visible and searchable online. If you check the box for **NO**, only the metadata and the abstract will be visible and searchable online. Nevertheless, when the document is uploaded it will still be archived as a digital file.

If you are more than one author you all need to agree on a decision. Read about SLU's publishing agreement here: <https://www.slu.se/en/subweb/library/publish-and-analyse/register-and-publish/agreement-for-publishing/>.

YES, I/we hereby give permission to publish the present thesis in accordance with the SLU agreement regarding the transfer of the right to publish a work.

NO, I/we do not give permission to publish the present work. The work will still be archived and its metadata and abstract will be visible and searchable.

Abstract

In-situ injection of zerovalent Iron (ZVI) particles to remediate contaminated groundwater is a widely applied approach. However, studies assessing the remediation and immobilisation mechanisms of Arsenic (As) under anoxic field conditions with zerovalent iron particles are lacking, especially for nanosized sulphidated ZVI (S-nZVI) and oxidic shell free ZVI (OSF-nZVI). This study aimed to assess the suitability of nanosized S-nZVI and OSF-nZVI sorbents for the remediation of an anoxic aquifer contaminated with As from chromated copper arsenate (CCA) wood preservative solution and compare them with micro-sized S-mZVI and mZVI sorbents. Batch experiments were conducted under anoxic conditions by mixing sorbents with contaminated sediment and artificial groundwater, mimicking the conditions in the natural aquifer. Sorbent performance was assessed at uncontrolled pH and at pH acidified to field pH. Fractionation of As in the solid phase was assessed by extraction with phosphate and oxalate and by microwave-assisted aqua regia digestion of the samples. Based on this, three fractions were defined, namely specifically sorbed As, As associated with amorphous Fe-(hydr)oxides and residual As. Results showed As removal efficiencies of all four ZVI sorbents of at least 85 % at uncontrolled and acidified pH. All four ZVI sorbents showed resistance towards As release at acidification despite increased Fe dissolution. Fractionation results at uncontrolled pH showed a dominating As immobilisation mechanism for ZVI sorbents by formation of amorphous Fe-As-coprecipitates. In the S-mZVI treatment, formation of additional As-S compounds was indicated at uncontrolled pH. Acidification did not affect As immobilisation in the nanosorbent treatments. In the micro-sorbent treatment, As immobilisation changed upon acidification from coprecipitation towards specifically sorbed As and formation of recalcitrant As-Fe (mZVI) or As-S compounds (S-mZVI). All four tested ZVI sorbents were potentially suitable for the remediation of the contaminated anoxic aquifer. S-mZVI was assessed as the most suitable of the four ZVI sorbent due to the highest As removal efficiency and the highest As immobilisation strength.

Keywords: Arsenic Remediation, Zerovalent Iron, Anoxic Aquifer

Popular science summary

Arsenic (As) is an environmental contaminant of major worldwide concern due to its widespread occurrence and high toxicity. The predominant risk to humans from As arises via contaminated drinking water. Since groundwater is an important source of drinking water, elevated As concentrations in the groundwater have been shown to cause severe health problems. Consequently, developing strategies to tackle elevated As concentrations in the groundwater is important. Such a strategy is the application of iron-based sorbents, so-called zerovalent iron (ZVI). Regular ZVIs were already successfully applied for the remediation of As contaminated groundwater. In recent years, new modifications of ZVI showed increasing remediation efficiencies. In this study, the As remediation efficiency of four different ZVI sorbents was tested, namely, uncoated and sulphidated nanosized, and microsized sorbents, respectively. Batch experiments mimicked the natural conditions of an As contaminated site in Sweden (Hjältevad). The site was contaminated with As by application of an As-containing wood preservative and showed steadily increasing dissolved As concentrations in the groundwater. In all experiments, natural As contaminated sediment was mixed with artificial groundwater reflecting the composition at the site. In order to simulate field conditions, all experiments were conducted at an O₂-lacking, so-called anoxic atmosphere. The experiments showed that all four ZVI sorbents sufficiently reduce dissolved As concentrations. This indicates that all four ZVI sorbents are suitable for the remediation of As under anoxic conditions. For the specific site, microsized uncoated ZVI was assessed as the best suitable sorbent due to the highest As remediation efficiency, strongest As immobilisation and lowest change in natural conditions. However, for a more exhaustive evaluation of the suitability of the four ZVI sorbents for the specific site, further experiments that address, amongst others, the mobility of the sorbents are required.

Table of contents

List of tables	I
List of figures.....	II
List of formulas	V
List of Abbreviations.....	VI
1. Introduction.....	1
2. Theoretical Background	3
2.1. Chemistry of Arsenic	3
2.2. Interaction of Arsenic with Zerovalent Iron	5
2.2.1. Corrosion of the Fe(0) core.....	5
2.2.2. Arsenic Immobilisation Mechanisms.....	6
2.2.3. Influencing Factors of Arsenic Remediation Efficiency.....	7
2.2.4. Zerovalent Iron Characteristics.....	8
3. Description of the Study Site (Hjältevad).....	11
3.1. Overview.....	11
3.2. Hydrogeological Conditions.....	12
3.3. Contamination History	12
3.4. Previous Decontamination Actions.....	12
3.5. Current Pollution Situation.....	13
4. Materials and Methods.....	15
4.1. Sediment.....	15
4.2. Batch Experiments	16
4.2.1. Zerovalent Iron Sorbents	16
4.2.2. Artificial Groundwater	17
4.2.3. Phosphate and Oxalate Extraction of Solid Samples	21
4.2.4. Digestion of Solid Samples.....	23
4.3. pH-dependent Arsenic Solubility under Oxidic Conditions.....	25
4.4. Data Processing	26
4.4.1. Classification of Fractions.....	26
4.4.2. Statistical Analysis	28

4.4.3.	Differences of Arsenic Fractionation (F1-F4).....	28
4.5.	Simulations with Visual MINTEQ.....	29
5.	Results.....	32
5.1.	Iron in the Solid Phase (Fe_{F3} , Fe_{F4}).....	32
5.2.	Solution Chemistry	33
5.2.1.	pH	33
5.2.2.	Oxidation Reduction Potential	34
5.2.3.	Dissolved Arsenic (F1).....	35
5.2.4.	Arsenic Speciation	36
5.2.5.	Dissolved Iron (Fe_{F1}).....	38
5.3.	Fractionation of Arsenic in the solid phase (F2-F4)	39
5.3.1.	Sorbent Performance at Uncontrolled pH (T1) vs. Untreated Sediment (T0)	40
5.3.2.	Sorbent Performance at pH Adjusted to Field pH (T2) vs. Untreated Sediment (T0).....	41
5.3.3.	Sorbent Performance at pH Adjusted to Field pH (T2) vs. Uncontrolled pH (T0)	42
5.4.	Modelled pH-dependent Dissolved Arsenic Concentrations at Changing Redox Conditions.....	43
6.	Discussion.....	45
6.1.	Field Conditions.....	45
6.2.	Changing Conditions Induced by Sorbents	46
6.3.	Arsenic Removal Efficiency	47
6.4.	Arsenic Immobilisation Mechanisms	50
6.4.1.	Uncontrolled pH (T1)	50
6.4.2.	pH Adjusted to Field pH (T2)	51
6.5.	Assessment of the Overall Sorbent Performance	53
7.	Conclusions	55
	References	VI
	Acknowledgements.....	XIV
	Appendix	XV

List of tables

Table 1: Composition of artificial groundwater used in batch experiments.....	17
Table 2: Characteristics of added ZVI sorbents. SSA: Specific Surface Area. N/S: not specified.....	18
Table 3: Amounts of ZVI sorbents [ml/mg] added and the resulting normalised Fe dose [g/L].....	20
Table 4: Sampling Timepoints and number of samples per treatment at T0 and T1.	20
Table 5: HCl addition to each treatment.....	21
Table 6: Sample List for extractions. All extractions were run in duplicates.....	22
Table 7: Model Input Parameters.....	31
Table 8: Iron concentration in the solid phase (Fe_{F3} , Fe_{F4} , Fe_{tot}) [mg/kg]. T0: untreated sediment. T1: uncontrolled pH. T2: pH adjusted to field pH. Fe_{F3} : amorphous Iron. Fe_{F4} : crystalline Iron. Fe_{tot} : total Iron.....	33
Table 9: As fractionation (F1-F4) [mg/kg]. T0: Untreated sediment. T1: uncontrolled pH. T2: pH adjusted to field pH.....	40
Table 10: Assessment of the overall sorbent performance of all four ZVI sorbents in relation to each other based on selected factors. T1: uncontrolled pH. T2: pH adjusted to field pH. Red: lowest performance; Yellow: moderate performance; Green: highest performance.	54
Table 11: Groundwater composition in 2017 at groundwater sampling points (1708 and 1709) closest to sediment sampling point 1904 (16-17 m distance) and median values of 34 sampling points throughout the whole area (2016-2018) including the classification of the median values according to SGU's classification (1: very low – 5: too high). ¹ : SGU (2013).....	XV
Table 12: pH in extracts after phosphate extractions.....	XVII
Table 13: Input data for Visual Minteq.	VI
Table 14: Total Concentrations [mg/kg] of metals in the sediment of sampling point 1904 analysed by hot-plate digestion (SE-SOP-0021).1: Chrome VI (predominant in groundwater).....	VI
Table 15: Dissolved Sulphide [$\mu\text{g/L}$] in the untreated sediment (T0), in ZVI treatments at uncontrolled pH (T1), and pH adjusted to field pH (T2)...	VI

List of figures

- Figure 1: A: Eh-pH diagram of aqueous arsenic species at equilibrium in the system As-O₂-H₂O at 25°C and 1 bar (adapted from Smedley and Kinniburgh, 2002, p. 521). B: Bidentate, binuclear complex of As(V) on a Fe-oxide surface (Loeppert et al., 2003, p. 44).....4
- Figure 2: Possible follow-up reactions of dissolved Fe²⁺ (adapted from Shi et al., 2015, p. 19).....5
- Figure 3: Possible immobilisation mechanisms of As(III) and As(V) with nZVI and S-nZVI particles (adapted from Singh et al. (2021), p. 10).....10
- Figure 4: A: Location of the former wood impregnation site in Hältevad. (OpenStreetMap). B: Close-Up aerial view of the area (Google Earth). ..11
- Figure 5: Calculated distribution of As concentrations from results of dynamic groundwater sampling in 34 points (2016-2018) (SWECO, 2019). A: Interpolation of maximum measured concentrations (adapted according to Figure 54, p. 107). B: Weighted averages over the depth of the aquifer (adapted according to Figure 60, p. 117).....14
- Figure 6: Experimental Workflow. Red: anoxic conditions; blue: oxic conditions. T0: before treatment; T1: uncontrolled pH. T2: pH adjusted to field pH. AGW: Artificial Groundwater; ORP: Oxidation Reduction Potential.24
- Figure 7: pH in AGW. T0: untreated Sediment. T1: uncontrolled pH. T2: pH adjusted to field pH. Values show means ($n \geq 2$). Error bars express standard deviation ($n > 2$). For S-mZVI, error bars express absolute deviation (T1, $n = 2$) and only one value is shown for T2. Statistically significant differences ($p < 0.05$) are shown for Kruskal-Wallis with post-hoc Bonferroni, and (1) one-way ANOVA with post-hoc Tukey HSD. Non-Italic letters refer to statistical differences within treatments at T1 and between T0 and T1. Italic letters refer to statistical differences within treatments at T2 and between T0 and T2. Square brackets with asterisks indicate differences between T1 and T2 proven with Kruskal-Wallis with post-hoc Bonferroni.....34
- Figure 8: ORP [mV] in AGW. T0: untreated sediment. T1: uncontrolled pH. T2: pH adjusted to field pH. Values show means ($n \geq 2$). Error bars express standard deviation ($n > 2$). For S-mZVI, error bars express absolute deviation (T1, $n = 2$) and only one value is shown for T2. Significant differences ($p < 0.05$) are shown for Kruskal-Wallis with post-hoc Bonferroni, and (1) one-way ANOVA with post-hoc Tukey HSD. Non-Italic letters refer to

	differences within treatments at T1 and between T0 and T1. Italic letters refer to differences within treatments at T2 and between T0 and T2.....	35
Figure 9:	Dissolved As [$\mu\text{g/L}$] in AGW (F1). T0: untreated sediment. T1: uncontrolled pH. T2: pH adjusted to field pH. Values show means ($n \geq 2$). Error bars express standard deviation ($n > 2$). For S-mZVI, error bars express absolute deviation (T1, $n=2$) and only one value is shown for T2. Significant differences ($p < 0.05$) are shown for Kruskal-Wallis with post-hoc Bonferroni, and (1) one-way ANOVA with post-hoc Tukey HSD. Non-Italic letters refer to differences within treatments at T1 and between T0 and T1. Italic letters refer to differences within treatments at T2 and between T0 and T2.....	36
Figure 10:	Measured Eh-pH data points plotted in the Eh-pH diagram for the aqueous arsenic species in the system As-O ₂ -H ₂ O at 25°C and 1 bar total pressure (adapted from Smedley and Kinniburgh (2002), p. 521)..	37
Figure 11:	A: Dissolved As(III) [% total dissolved As]. B: Dissolved As(III) and As(V) [$\mu\text{g/L}$]. T0: untreated sediment. T1: uncontrolled pH. T2: pH adjusted to field pH. Values are means ($n \geq 2$). Error bars express standard deviation ($n > 2$). For S mZVI, error bars express absolute deviation (T1, $n=2$) and only one value is available for T2.	38
Figure 12:	Dissolved Fe [mg/L] (Fe_{F1}). T0: untreated sediment. T1: uncontrolled pH. T2: pH adjusted to field pH. Values are means ($n \geq 2$). Error bars express standard deviation ($n > 2$). For S-mZVI, error bars express absolute deviation (T1, $n=2$) and only one value is shown for T2. Significant differences ($p < 0.05$) are shown for Kruskal-Wallis with post-hoc Bonferroni, and (1) one-way ANOVA with post-hoc Tukey HSD. Non-italic letters refer to differences within treatments at T1 and between T0 and T1. Italic letters refer to differences within treatments at T2 and between T0 and T2. Square brackets with asterisks indicate differences between T1 and T2 proven with Kruskal-Wallis with post-hoc Bonferroni.	39
Figure 13:	As fractionation change in ZVI treatments at uncontrolled pH (T1) compared to the untreated sediment (T0) illustrated as absolute difference [mg/kg] of means at T1 and T0 of each fraction. Symbols show significant differences ($p < 0.05$) of absolute values between T0 and T1 in each fraction (#: one-way ANOVA with post-hoc Tukey HSD; *: Kruskal-Wallis with post-hoc Bonferroni).	41
Figure 14:	As fractionation change in ZVI treatments at pH adjusted to field pH (T2) compared to the untreated sediment (T0) illustrated as absolute difference [mg/kg] of means at T2 and T0 of each fraction. Asterisks show significant differences ($p < 0.05$) of absolute values between T0 and T2 in each fraction assessed with Kruskal-Wallis with post-hoc Bonferroni.....	42

Figure 15: As fractionation change in ZVI treatments at pH adjusted to field pH (T2) compared to uncontrolled pH (T1) illustrated as absolute difference [mg/kg] of means at T2 and T1 of each fraction. Asterisks show significant differences ($p < 0.05$) of absolute values between T1 and T2 in each fraction assessed with Kruskal-Wallis with post-hoc Bonferroni.....	43
Figure 16: Simulated pH-dependent dissolved As concentrations of the untreated sediment at -5, -120, and -275 mV. Simulations were conducted with Visual Minteq ver. 3.1. Simulated dissolved As(V) and dissolved total As (As_{tot}) concentrations at T0, T1, and T2 are displayed as a reference.....	44
Figure 17: Effect of different phosphate concentrations on As sorption onto ferrihydrite. Modelling was conducted with Visual Minteq ver. 3.1. ...	XVI
Figure 18: Phosphate extractable Fe [mg/L] (F2). T0: Untreated Sediment. T1: Uncontrolled pH. T2: pH adjusted to field pH. Values show means ($n \geq 2$). Error bars express standard deviation ($n > 2$) or absolute deviation ($n = 2$). Significant differences ($p < 0.05$) are shown for Kruskal-Wallis with post-hoc Bonferroni, and (1) one-way ANOVA with post-hoc Tukey HSD. Non-italic letters refer to differences within treatments at T1 and between T0 and T1. Italic letters refer to differences within treatments at T2 and between T0 and T2.	XVII
Figure 19: Added NaOH/HNO ₃ concentrations [mM] and resulting pH of pre-tests of the unfiltered supernatant after 5 days shaking.....	XVIII
Figure 20: Added NaOH/HNO ₃ concentrations [mM] and resulting average pH of the unfiltered supernatant after 5 ½ days shaking.	XVIII
Figure 21: Simulation of As solubility with changing Ferrihydrite concentrations. 100 % represent 0.18 g/L ferrihydrite. Measured means measured As concentrations in the supernatant of experiments in section 4.3.	VII

List of formulas

(1) Corrosion reaction of the Fe(0) core in water under oxic conditions (Ponder et al., 2000).....	5
(2) Corrosion reaction of the Fe(0) core in water under anoxic conditions (Ponder et al., 2000).....	5
(3) Dissolved Iron (Fe_{F1}).....	26
(4) Phosphate extractable Iron (Fe_{F2}).....	26
(5) Amorphous Iron (Fe_{F3}).....	26
(6) Crystalline Iron (Fe_{F4}).....	26
(7) Total Iron (Fe_{tot}) of the ZVI treatments.....	27
(8) Dissolved Arsenic (F1)	27
(9) Specifically sorbed As (F2).....	27
(10) Strongly bound Arsenic to amorphous Iron (F3)	27
(11) Residual Arsenic (F4)	28
(12) Total Arsenic (Tot).....	28
(13) Differences of Arsenic Fractionation (F1-F4).....	28

List of Abbreviations

AD	Absolute Deviation	HNO ₃	Nitric Acid
Al	Aluminium	K	Potassium
ARD	Aqua Regia Digestion	L/S	Liquid to Solid Ratio
As	Arsenic	mZVI	Micro Zerovalent Iron
As(III)	Arsenite	MAMSL	Meter Above Mean Sea Level
As(V)	Arsenate	Mg	Magnesium
AGW	Artificial Groundwater	Mn	Manganese
Ba	Barium	N ₂	Nitrogen
Ca	Calcium	Na	Sodium
CCA	Chromated Copper Arsenate	Ni	Nickel
Cd	Cadmium	NH ₄	Ammonium
Cl ⁻	Chloride	NO ₃ ⁻	Nitrate
Co	Cobalt	NOM	Natural Organic Matter
Cr	Chromium	OE	Oxalate Extraction
Cu	Copper	ORP	Oxidation Reduction Potential
DM	Dry Matter	OSF-nZVI	Oxidic Shell Free Nano Zerovalent Iron
DOC	Dissolved Organic Carbon	O ₂	Oxygen
EC	European Commission	P	Phosphorous
Eh	Redox Potential	Pb	Lead
EU	European Union	PE	Phosphate Extraction
E ⁰	Standard Redox Potential	pH _{PZC}	Point of zero charge
FA	Fulvic Acid	PO ₄	Phosphate
Fe	Iron	SD	Standard Deviation
Fe _{F1}	Dissolved Iron	SEPA	Swedish Environmental Protection Agency
Fe _{F2}	Iron Extracted by Phosphate	S	Sulphur
Fe _{F3}	Amorphous Iron	S-nZVI	Sulphidated Nano Zerovalent Iron
Fe _{F4}	Crystalline Iron	SOM	Soil Organic Matter
Fe _{tot}	Total Iron	SO ₄ ²⁻	Sulphate
F1	Dissolved Arsenic	TCE	Trichlorethylene
F2	Specifically Sorbed Arsenic	TOC	Total Organic Carbon

F3	Arsenic Strongly Bound to Amorphous Iron	T0	Conditions Before Treatment
F4	Residual Arsenic	T1	Sorbent Performance at Uncontrolled pH
HA	Humic Acid	T2	Sorbent Performance at pH Adjusted to Field pH
HCl	Hydrochloric Acid	V	Vanadium
HCO ₃	Hydrogen Carbonate	WHO	World Health Organisation
Hg	Mercury	Zn	Zink

1. Introduction

Arsenic (As) is the 20th most abundant element in the earth's crust and a widespread environmental contaminant of major concern due to its high toxicity (Kanel *et al.*, 2005; Wenzel, 2013; Wu *et al.*, 2018). Elevated As concentrations can be caused by geogenic background concentrations or anthropogenic activities.

Geogenic As is predominantly present in sulphide minerals such as pyrite (FeS₂), with concentrations up to 7.7 wt% (Smedley and Kinniburgh, 2002). Weathering of rocks containing As or deposition of atmospheric As lead to accumulation of the element in soils (Matschullat, 2000). Soils are known to serve as an As sink due to the limited mobility of As (approximate retention time 1,000-3,000 a) (Wenzel, 2013). The average background concentration of As in soils worldwide is estimated between 5 and 10 mg/kg (Smedley and Kinniburgh, 2002). In groundwater, As accumulates due to rock and soil weathering (Matschullat, 2000). Uncontaminated groundwater concentrations are usually below 1 µg/L As (Matschullat, 2000). Naturally elevated As groundwater concentrations predominantly occur in arid or semi-arid areas in aquifers with high pH, and very little water flow, or in aquifers with reducing conditions (e.g. alluvium) (Smedley and Kinniburgh, 2002). In As-enriched groundwater and soils, As can be taken up by plants and may accumulate along the food chain (Wenzel, 2013).

Anthropogenically, environmental pollution of As originates primarily from mining, fossil fuel combustion, and use of As in industrial products, e.g. as a decolouring agent for glass production or as an antibacterial in wood preservatives such as chromated copper arsenate (CCA) (Matschullat, 2000). The mobilisation of As from the earth's crust caused by mining is in the same magnitude as the natural mobilisation induced by weathering and volcanic activity (Wenzel, 2013). Once mobilised by one of these processes, As is released to the atmosphere, deposited in surface waters or accumulates in soils, sediments and groundwater (Matschullat, 2000).

The predominant risk to humans from As is via contaminated drinking water (Tuček *et al.*, 2017). Thus, naturally-occurring and anthropogenically-driven elevated As concentrations in groundwater are a major concern (Tuček *et al.*, 2017). Worldwide, over 100 million people are potentially exposed to As-polluted aquifers (Polya *et al.*, 2019). The most infamous cases are Bangladesh and West Bengal in India, where consumption of As-enriched groundwater alongside As accumulation

in crops such as rice have led to deaths and long-term adverse health effects such as cancer or coronal heart disease (Matschullat, 2000; Kanel *et al.*, 2005; Wenzel, 2013). Indeed, groundwater and surface water concentrations in South Asia are the highest worldwide and vary between ca. 50 to >3,000 µg/L As (Tuček *et al.*, 2017). These values exceed the set threshold As concentration of 10 µg/L for drinking water by more than 300 times (WHO, 2017). This threshold value was set in 1993, in compliance with former treatment and measurement feasibility. Currently, there is some debate as to whether the current threshold value is sufficient to prevent adverse health effects (WHO, 2004, 2017, Ahmad and Bhattacharya, 2019).

In order to mitigate As contamination in soils and groundwater, several different approaches have been used such as adsorption, flocculation/filtration, ion exchange, photooxidation, reverse osmosis, microbial transformation, lime softening, electro-dialysis, and usage of iron (Fe) and manganese (Mn) minerals (Tuček *et al.*, 2017; Hao *et al.*, 2018). Treatment of As-contaminated sites by adsorption is considered to be the most cost-efficient method (Mohan and Pittman, 2007). Due to their availability, environmental friendliness, and cost-efficiency, the majority of sorbents are iron-based materials such as zerovalent iron (ZVI) (Tuček *et al.*, 2017).

Several size and surface modifications of these sorbents have been tested in the last decade (Cundy, Hopkinson and Whitby, 2008; Yan *et al.*, 2013; Sun *et al.*, 2016; Fan *et al.*, 2017; Hao *et al.*, 2018; Wang *et al.*, 2021). Promising modifications for As remediation depict nanosized zerovalent iron (nZVI), oxidic shell free ZVI (OSF-ZVI), as well as sulphidated ZVI (S-ZVI).

The As removal efficiency of micro and nano ZVI has already been tested in several studies from lab- to field-scale with removal efficiencies of up to 38 mg As/g nZVI (Yuan and Lien, 2006; Li *et al.*, 2014; Gil-Díaz *et al.*, 2016; Tiberg *et al.*, 2016; Zou *et al.*, 2016; Kumpiene *et al.*, 2021; Wang *et al.*, 2021). In lab-scale experiments, OSF-ZVI and S-nZVI have indicated a very high potential for the removal of As(III) under anoxic conditions (Tuček *et al.*, 2017; Wu *et al.*, 2018). However, their efficiency, and immobilisation mechanisms for remediation of As at field conditions have not yet been assessed.

In this study, four different ZVI sorbents (S-nZVI, OSF-nZVI, S-mZVI, and mZVI) were applied to an anoxic sediment/groundwater system contaminated by CCA at uncontrolled pH and at field pH in order to:

1. Quantify and compare the As removal efficiency according to particle size (micro vs. nano) and coating (uncoated vs. sulphidated)
2. Identify possible As immobilisation mechanisms
3. Compare sorbent performance at uncontrolled pH and field pH
4. Propose the most suitable ZVI sorbent for the remediation of the CCA contaminated site

2. Theoretical Background

2.1. Chemistry of Arsenic

Arsenic (As) occurs in the environment predominantly in four different redox states: -3, 0, +3, +5 (Flora, 2015). The prevailing redox states in sediments and groundwater are the trivalent arsenite (As(III)), and the pentavalent arsenate (As(V)) (Bowell *et al.*, 2014). Figure 1A shows an Eh-pH equilibrium diagram of aqueous As species, where Eh represents the redox potential based on the potential of the standard hydrogen electrode, the lines indicate the equilibrium of the respective As redox pairs (Smedley and Kinniburgh, 2002; Huang, 2016). It shows that oxyanions of As(V) are favoured at high redox potentials (> 200 mV) and/or high pH (> 9) whereas oxyanions of As(III) prevail at low redox potentials (< -200 mV) and/or low pH (< 6). Redox-driven speciation of As is mainly impacted by oxygen (O_2) concentration, microbial activity, and by the presence of other redox-active substances (Sasaki *et al.*, 2009). Most redox transformations may have kinetic constraints so that As(III) and As(V) can coexist in the environment, leading to the presence of As(III) at oxidising and As(V) at reducing conditions to some extent (Loeppert *et al.*, 2002).

Organic As species such as monomethylarsonic acid (MMA) and dimethylarsinic acid (DMA) may be formed by microbial transformations (Wang and Mulligan, 2006). In sulphidic environments, thioarsenic species can occur either as mono-, di-, tri-, thioarsenate or thioarsenite (Herath *et al.*, 2018). In these cases, sulphur (S) replaces O_2 forming As-SH or As=S species (Herath *et al.*, 2018).

In most pH ranges of soils (3-9) at oxidising conditions, one or two times negatively charged hydrolysis species of As(V) ($H_2AsO_4^-$; $HAsO_4^{2-}$) predominate and show strong association with Fe-(hydr)oxides (Kanel *et al.*, 2005, Wenzel, 2018). Thus, As(V) is usually rather immobile in soils, with a sorption maximum at pH 3 to 5 (Wang and Mulligan, 2006). With increasing pH, electrostatic repulsion caused by increasing negative charges at Fe-(hydr)oxides enhances desorption of As(V) (Wang and Mulligan, 2006).

Below pH 9.2 at reducing conditions, the neutral As(III) hydrolysis species $H_3AsO_3^0$ dominates (Kanel *et al.*, 2005). As(III) shows an increased toxicity and

mobility compared to As(V) due to the low sorption affinity of the neutral hydrolysis species with sorption maxima between pH 7 and pH 9 (Goh and Lim, 2005; Kanel *et al.*, 2005). In reducing, sulphur containing environments, As(III) can be immobilised by sorption onto metal sulphides or formation of As-sulphides (Loeppert, *et al.*, 2003).

Overall, mobility and toxicity of As(III) and As(V) in the environment is predominantly governed by sorption. It is known that As(III) and As(V) form inner-sphere bidentate, binuclear complexes with the OH-groups on the surface of Fe-(hydr)oxides (Figure 1B) (Loeppert *et al.*, 2002). As(V) and As(III) are also known to sorb on the surface of aluminium (Al)- and Mn-oxides, but with overall lower binding strengths and affinities compared to Fe-(hydr)oxides (Loeppert *et al.*, 2002; Martin *et al.*, 2014). Arsenic shows low affinity towards calcium and carbonate minerals as well as natural organic matter (NOM). Therefore, dissolved As concentrations may be increased in organic soils (Wenzel, 2013).

Dissolved As concentrations are relatively low in most soils and sediments. However, when the number of sorption sites is limited or the concentration of As is high, elevated dissolved As concentrations may be found (Loeppert *et al.*, 2002). These conditions can be caused in particular by low redox potentials that enhance the dissolution of Fe-(hydr)oxides and increase the presence of As(III) or by As inputs due to anthropogenic pollution (Loeppert *et al.*, 2002). Furthermore, the presence of competing anions can reduce adsorption of As in soils. Due to the chemical similarity of PO_4^{3-} and As oxyanions, PO_4^{3-} was observed to be the strongest competitor for As(III) as well as for As(V) (Hongshao and Stanforth, 2001; Caporale *et al.*, 2013; Gao *et al.*, 2013). Other dissolved inorganic anions, e.g. sulphate (SO_4^{2-}), chloride (Cl^-), nitrate (NO_3^-) show significantly lower competition with As (Wenzel, 2013). Furthermore, NOM is known to increase dissolved As concentration by surface competition or formation of aqueous complexes (Wang and Mulligan, 2006).

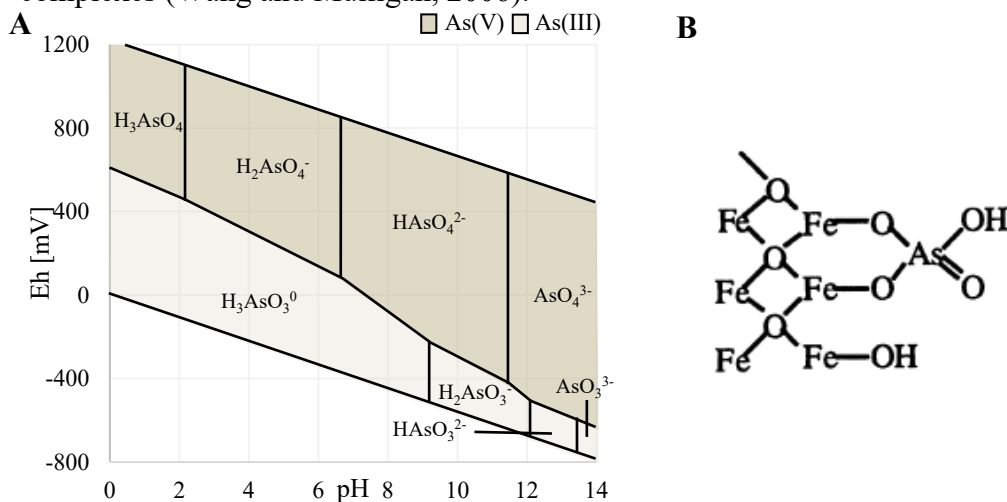


Figure 1: A: Eh-pH diagram of aqueous arsenic species at equilibrium in the system As-O₂-H₂O at 25°C and 1 bar (adapted from Smedley and Kinniburgh, 2002, p. 521). B: Bidentate, binuclear complex of As(V) on a Fe-oxide surface (Loeppert *et al.*, 2003, p. 44).

2.2. Interaction of Arsenic with Zerovalent Iron

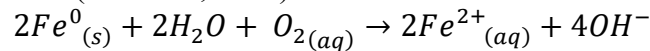
The use of ZVI for the removal of metals and metalloids from environmental media has been widely applied within the past two decades. ZVI is known to be cost-efficient, environment friendly, and easy to implement (Bae and Hanna, 2015; Zou *et al.*, 2016; Tuček *et al.*, 2017). Sections 2.2.1-2.2.4 give an overview of ZVI characteristics, immobilisation mechanisms towards As, factors influencing the remediation efficiency, and surface modifications.

2.2.1. Corrosion of the Fe(0) core

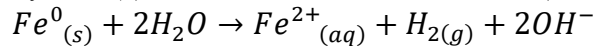
On the surface of regular nanosized ZVI (nZVI), a several nanometres-thick layer of Fe-(hydr)oxide surrounds the Fe(0) core in aqueous solutions (Bae and Hanna, 2015).

Under oxic conditions, this is caused by oxidation of the Fe(0) core by dissolved oxygen according to equation (1) (Ponder *et al.*, 2000).

Under anoxic conditions, corrosion of the Fe(0) core takes place by reduction of H₂O to H₂ according to equation (2) (Ponder *et al.*, 2000). Overall, corrosion of nZVI is enhanced compared to microsized ZVI (mZVI) due to the higher reactive surface area of nZVI (Shi *et al.*, 2015).



(1) Corrosion reaction of the Fe(0) core in water under oxic conditions (Ponder *et al.*, 2000).



(2) Corrosion reaction of the Fe(0) core in water under anoxic conditions (Ponder *et al.*, 2000).

Reactions (1) and (2) lead to increasing pH in unbuffered systems, with a more pronounced impact under oxic conditions, which favours the formation of Fe(III)-precipitates such as Fe(OH)₃ (Figure 2; (1), (2)) (Schmid *et al.*, 2015; Shi *et al.*, 2015). Under anoxic conditions, Fe(II)-oxides such as Fe(OH)₂ or mixed-valent Fe-oxides (Fe(II,III)) such as magnetite (Fe₃O₄) are formed (Figure 2; (3)) (Filip *et al.*, 2014; Shi *et al.*, 2015). Further, corrosion of the Fe(0) core causes a shift towards reducing conditions, in particular under anoxic conditions due to the formation of H₂ (Schmid *et al.*, 2015).

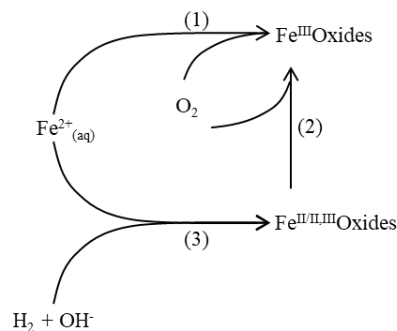


Figure 2: Possible follow-up reactions of dissolved Fe^{2+} (adapted from Shi *et al.*, 2015, p. 19).

The formation of an oxidic shell and H₂ passivate the surface of the ZVI particles and formation of Fe-(hydr)oxide precipitates depletes the Fe(0) core which may decrease contaminant removal (Kanel *et al.*, 2005). On the other hand, Fe-(hydr)oxide precipitates can serve as additional sorbent surfaces which can promote contaminant removal (see section 2.2.2) (Wang *et al.*, 2021). Reaction (2) is substantially less rapid compared to reaction (1), thus the reactivity efficiency of ZVI towards contaminant immobilisation under anoxic conditions is higher (Liu and Lowry, 2006; Schmid *et al.*, 2015).

2.2.2. Arsenic Immobilisation Mechanisms

Immobilisation of As by ZVI predominantly takes place by reduction, oxidation, sorption, and coprecipitation (Yan, Ramos, *et al.*, 2012; Filip *et al.*, 2014; Wang *et al.*, 2021) The processes may occur simultaneously or sequentially, and the extent and efficiency of the individual processes depends on the site-specific conditions and sorbent specifications (see sections 2.2.3, 2.2.4) (Wang *et al.*, 2021). Figure 3 gives an overview of possible immobilisation mechanisms of As(III) and As(V) with nZVI and sulphidated nZVI (S-nZVI).

Sorption of As(III) and As(V) mainly takes place by the formation of inner-sphere complexes on the surface of the oxidic shell of the Fe(0) core or Fe-precipitates formed during corrosion of the Fe(0) core (see section 2.2.1) (Wu *et al.*, 2018; Wang *et al.*, 2021) (Figure 3, (1)-(4)). Overall, As can form monodentate or bidentate complexes, with the latter being more stable (Fendorf *et al.*, 1997; Wang *et al.*, 2010; Dong *et al.*, 2012). Sorption of As(V) to Fe-(hydr)oxides is generally higher compared to As(III) and decreases with increasing pH (see section 2.1). The stability of As(V)- and As(III)-nZVI complexes towards phosphate extraction significantly increases with ageing time up to 60 days, indicating irreversible sorption or further transformation processes (Su and Puls, 2001b; Dong *et al.*, 2012).

Fe(0) is a strong reductant ($\text{Fe}^{2+}/\text{Fe}(0)$: $E^0 = -0.45 \text{ V}$) which thermodynamically enables reduction of As(V) to As(III) and As(V) to As(0) ($\text{As(V)}/\text{As(III)}$: $E^0 = 0.58 \text{ V}$; $\text{As(V)}/\text{As(0)}$: $E^0 = 0.499 \text{ V}$) (Sasaki *et al.*, 2009). Bang *et al.* (2005) showed that reduction of As(III) to As(0) becomes thermodynamically possible under anoxic conditions. Overall, two different hypotheses for the reduction of As(III) by nZVI under anoxic conditions are proposed. Yan, *et al.* (2012) suggested that As(III) is reduced on the surface of the oxidic shell of nZVI and diffuses into the interface between the oxidic shell and Fe(0) core where it forms a heterogeneous Fe-As intermetallic phase. Tuček *et al.* (2017) proposed As(III) reduction by the Fe(0) core and immobilisation of As(0) between the freshly formed oxidic shell of initially oxidic-shell-free nZVI (OSF-nZVI) and the Fe(0) core without the formation of an intermetallic phase. Figure 3 (5) provides a simplified illustration of the processes proposed by Yan, *et al.* (2012) and Tuček *et al.* (2017). Singh *et*

al. (2021) and Tuček *et al.* (2017) showed step-wise reduction of As(V) to As(III) and As(0) upon reaction with nZVI under anoxic conditions with decreased removal efficiencies compared to As(III). Singh *et al.* (2021) assumed reduction of sorbed As(V) on the Fe-oxide surface followed by reduction to As(III) and diffusion and subsequent reduction to As(0) on the interface between the Fe(0) core and oxidic shell (Figure 3, (6, 7)). Tuček *et al.* (2017) showed that formation of As(0) only takes place under anoxic conditions. According to Yan *et al.* (2012), reduction of As(III) only takes place during treatment with nanosized ZVI but not microsized ZVI.

Yan *et al.* (2012) showed that oxidation of As(III) to As(V) is a relatively fast process occurring on the surface of the oxidic shell of ZVI (Figure 3 (8)). Under anoxic conditions, oxidation of As(III) was explained by adsorbed Fe^{2+} on the oxidic shell (Manning *et al.*, 2002; Ramos *et al.*, 2009; Amstaetter *et al.*, 2010; Yan *et al.*, 2010; Yan, Ramos, *et al.*, 2012; Singh *et al.*, 2021). Amstaetter *et al.* (2010) proposed that, in a first step, an inner-sphere Fe-oxide-Fe(II)-As(III)-complex forms which is subsequently oxidised to an intermediate Fe-oxide-Fe(III)-As(III) complex. In a second step, complexed As(III) ions are oxidised by the intermediate Fe(III) phase and a Fe-oxide-Fe(II)-As(V) complex is finally formed. This localised oxidation may lead to adsorption of As(III) at the oxidic shell despite electrostatic repulsion at alkaline pH (Ramos *et al.*, 2009). Consequently, oxidised As(V) is mainly located on the surface of ZVI particles (Yan, Ramos, *et al.*, 2012). Overall oxidation of As(III) to As(V) is promoted under oxic conditions due to presence of dissolved O_2 as a strong oxidant (Tuček *et al.*, 2017).

Coprecipitation takes place between As and products of the corrosion of the Fe(0) core (Singh *et al.*, 2021) Figure 3 (9-11). As may either coprecipitate after adsorption on corrosion products or directly with released Fe^{2+} ions (Yan, Ramos, *et al.*, 2012; Wang *et al.*, 2021). Coprecipitation of As with nZVI corrosion products in the form of $Fe_3(AsO_4)_2 \cdot 8H_2O$ at alkaline pH and anoxic conditions was observed at high As concentrations (500 mg/L; 2-10 g/L nZVI) (Li *et al.*, 2014). Overall, coprecipitation strongly depends on the redox conditions, pH value and initial As concentrations (Singh *et al.*, 2021).

2.2.3. Influencing Factors of Arsenic Remediation Efficiency

The most important influencing factors of As remediation are dissolved O_2 , pH, and co-existing anions.

Different immobilisation mechanisms of As by ZVI dominate depending on the prevailing redox conditions. Under oxic conditions, i.e. when the concentration of dissolved O_2 is elevated, oxidation, sorption and coprecipitation dominate whereas under anoxic conditions, i.e. when no dissolved O_2 is present, sorption followed by reduction is more prevalent (Tuček *et al.*, 2017). Overall, it was observed that As removal by ZVI is more efficient under oxic conditions compared to anoxic

conditions, in particular for As(V) (Lackovic *et al.*, 2000; Bang *et al.*, 2005; Bang *et al.*, 2005). This is because under anoxic conditions, less sorption sites caused by the formation of Fe precipitates by Fe(0) corrosion are formed (Peng *et al.*, 2017). However, recently, immobilisation of As(III) by oxidic shell free ZVI has been observed to be more efficient under anoxic compared to oxic conditions due to the strongly reducing Fe(0) core (Tuček *et al.*, 2017).

As mentioned in section 2.2.2, sorption plays an important role in immobilisation of As with ZVI. Arsenic sorption depends strongly on pH, with sorption maximum at pH 3-5 for As(V) and 7-9 for As(III) (section 2.1). Further, the electrical charge of ZVI particles and thus the point of zero charge (pH_{PZC}) changes with pH with a common pH_{PZC} of ZVI at neutral pH, meaning that ZVI are predominantly positively charged at pH<7 and negatively charged at pH>7 (Kanel *et al.*, 2005). Therefore, As(V) removal was observed to be enhanced at initial acidic pH and decreased with rising pH due to increasing electrostatic repulsion of negatively charged aqueous As(V) species and negatively charged ZVI (Tanboonchuy *et al.*, 2011). As(III) removal showed slightly lower removal efficiencies at high pH compared to As(V) under oxic conditions (Tuček *et al.*, 2017). According to Zou *et al.* (2016), the best contaminant removal efficiency of most nZVI materials is achieved at pH 4-7 and 100 % sorption of As(III) onto synthesised nZVI was observed at pH 4.5-8 under anoxic conditions (Kanel *et al.*, 2005). Apart from sorption, reduction of As during nZVI treatment was also observed to increase at lower pH (Bang *et al.*, 2005; Tuček *et al.*, 2017).

In general, the presence of anions requires higher ZVI dosage to obtain the same As removal efficiency compared to pure water since anions compete for sorption sites with As (Wang *et al.*, 2021). High mass ratios, i.e. between 50 to 2000 (nZVI/As) need to be applied in order to obtain sufficient removal capacities (Bae and Hanna, 2015; Wu *et al.*, 2018). Different anions impact the As removal to different extents. HCO₃⁻, CO₃²⁻, and SO₄²⁻ showed no or small effects and H₂PO₄⁻ as well as SiO₃²⁻ and PO₄³⁻ showed inhibitory effects on the immobilisation of As by ZVI with the latter being the most significant (Su and Puls, 2001a; Tanboonchuy *et al.*, 2012; Wang *et al.*, 2021). Zhu *et al.* (2009) have shown that, at high pH, PO₄³⁻ has a lower adverse effect on the As(III) removal compared to As(V). Furthermore, humic acid (HA) was observed to occupy adsorption sites on the oxidic shell of ZVI by formation of Fe-HA complexes (Wang *et al.*, 2021). Additionally, HA was also shown to lower the amount of sorption sites by suppressing Fe(0) corrosion (Wang *et al.*, 2021).

2.2.4. Zerovalent Iron Characteristics

As already indicated above, ZVI characteristics significantly influence As removal efficiencies. The most important characteristics are (Sun *et al.*, 2016; Tuček *et al.*, 2017; Wang *et al.*, 2021):

- Adsorption capacity (availability of active sites)
- Point of zero charge
- Extent of surface corrosion
- Particle size
- Surface structure
- Mobility

Aggregation of uncoated nZVI particles reduces their reactivity and increases their size leading to reduced mobility (Schmid *et al.*, 2015). By coating nZVI particles with polyelectrolytes, surfactants or sulphides, aggregation can be reduced and the stability as well as the reactivity and mobility of the particles can be increased (Schmid *et al.*, 2015). Since removal processes predominantly occur on the surface of the sorbents, surface alteration has a great potential to increase efficiencies (Wu *et al.*, 2018). However, reactivity may also be decreased by coating due to blocking of reactive surface sites (Phenrat *et al.*, 2009). Out of the numerous surface modification methods of ZVI particles, sulphidation offers a relatively new and promising approach for As removal.

2.2.4.1. Sulphidated Zerovalent Iron

Sulphidated ZVI (S-ZVI) particles are prepared by the addition of an sulphur (S) compound (e.g. Na₂S or FeS) during or after ZVI synthesis (Kim *et al.*, 2011; Han and Yan, 2016; Gu *et al.*, 2017). S-ZVI are commonly flake-like nanoparticles with an Fe-oxide and Fe-sulphide shell (FeS) (Wu *et al.*, 2018) (Figure 3, right).

The major benefit of S-ZVI compared to bare ZVI is their increased kinetics of As removal and reactivity lifespan (up to 10 years) (Fan *et al.*, 2017). The S coating reduces corrosion of the Fe(0) core and thus increases longevity of particles (Singh *et al.*, 2021). S-mZVI showed an increased electron sufficiency of up to 99 % meaning that only about 1 % of electrons are lost to the hydrolysis of water (Han and Yan, 2016; Gu *et al.*, 2017). Additionally, with increasing sulphidation (increasing S/Fe ratio) increasing surface roughness and shell thickness create more binding sites for As (Wu *et al.*, 2018). Wu *et al.* (2018) showed increasing As removal efficiencies up to a S/Fe ratio of 0.28. Furthermore, S-ZVI showed an increased mobility due to a lower pH_{PZC} compared to ZVI. The pH_{PZC} of nZVI and S-ZVI particles prepared by Wu *et al.* (2018) had pH_{PZC} of 7.5 and 5.5, respectively. Thus, S-ZVI are negatively charged and have a decreased tendency to form homoaggregates at natural pH of most aquifers (Wu *et al.*, 2018).

Arsenic immobilisation by S-ZVI particles was stated to be more complex than ZVI due to the dual character of the Fe-oxide/FeS shell (Wu *et al.*, 2018). It is widely known that Fe-S minerals, e.g., pyrite or mackinawite can bind As (Farquhar *et al.*, 2002). Wolthers *et al.* (2005) and Farquhar *et al.* (2002) have observed that under anoxic conditions, As(III) and As(V) form outer-sphere complexes at low As concentrations and coprecipitates at higher concentrations on the surface of

mackinawite with higher sorption of As(V) compared to As(III). Wu *et al.* (2018) showed that the predominant immobilisation pathways of As(III) by S-nZVI are the formation of inner-sphere complexes on the surface of the FeS/Fe-oxide shell, and coprecipitation as Fe/As/S-hydroxides (Wu *et al.*, 2018) (Figure 3, (12)-(15)). An optimum immobilisation pH was observed between 5 and 8 with a maximum As removal capacity of 240 mg/g (Wu *et al.*, 2018). Throughout the whole tested pH range, S-nZVI showed higher As removal efficiency compared to nZVI, likely caused by the lower dissolution of S-nZVI compared to nZVI (Wu *et al.*, 2018). On the contrary, Singh *et al.* (2021) suggest formation of outer-sphere surface complexes of As(III) and As(V) and coprecipitation of mainly As(III) as As_2S_3 and low amounts of As(V) with released S^{2-} ions (Figure 3, (16)-(19)). Coprecipitation in the form of Fe-As-hydroxides (similar during reactions with nZVI particles, see section 2.2.2) may occur due to the dual character of the Fe-oxide/FeS shell (Figure 3, (15), (20)) (Singh *et al.*, 2021). Reduction of As(III) or As(V) was not observed after reaction with S-nZVI for 24 h (Singh *et al.*, 2021). Overall, As removal was higher under oxic conditions as compared to anoxic conditions due to the formation of Fe-S-H groups induced by dissolved O_2 and oxidation of As(III) by FeS and Fe-oxide (Wu *et al.*, 2018). It was also observed that, under oxic conditions, S-nZVI particles formed flake-like deposits whereas the core-shell structure was maintained under anoxic conditions (Wu *et al.*, 2018).

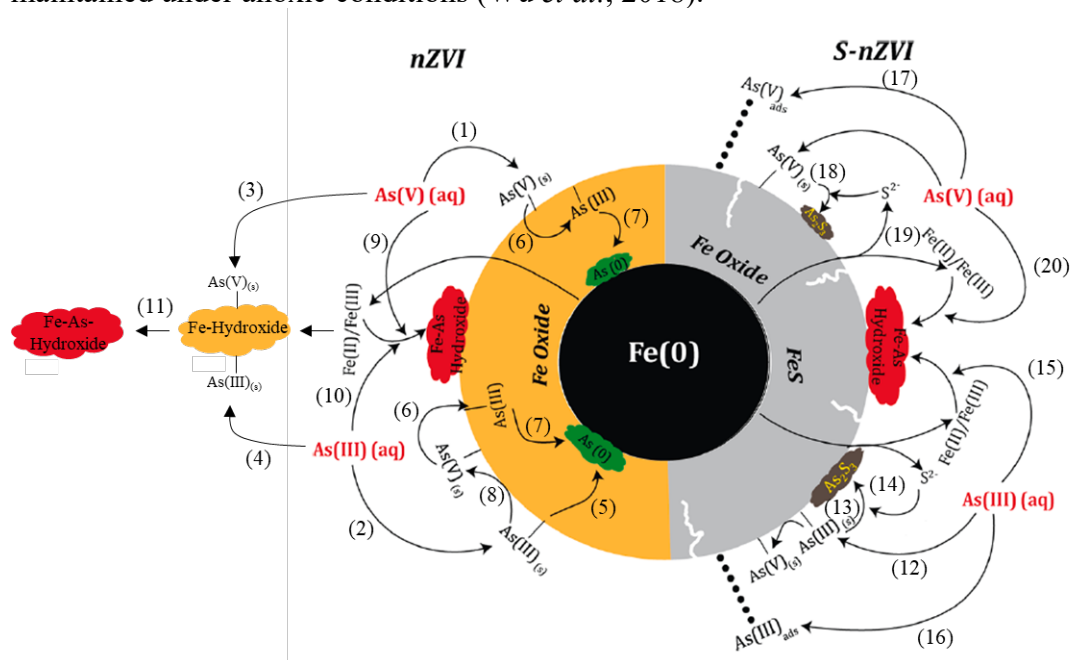


Figure 3: Possible immobilisation mechanisms of As(III) and As(V) with nZVI and S-nZVI particles (adapted from Singh *et al.* (2021), p. 10).

3. Description of the Study Site (Hjältevad)

The As contaminated site where the sediment, that was used for all laboratory experiments, was sampled, is described in the present section. All the information, if not stated otherwise, was taken from SWECO (2019).

3.1. Overview

The contaminated site has an area of ca. 5.3 ha and is located 168 meters above mean sea level (MAMSL) in the locality of Hjältevad, which is part of the municipality Eksjö, Jönköping County, Southern Sweden (Figure 4A). From 1949-1985, a wood impregnation plant involving the storage and application of water-based wood preservatives, in particular chromated copper arsenate (CCA), was located on the site. Currently, a forest is located on the north-western part of the area and a soccer field was established in the south-eastern part of the area (Figure 4B).

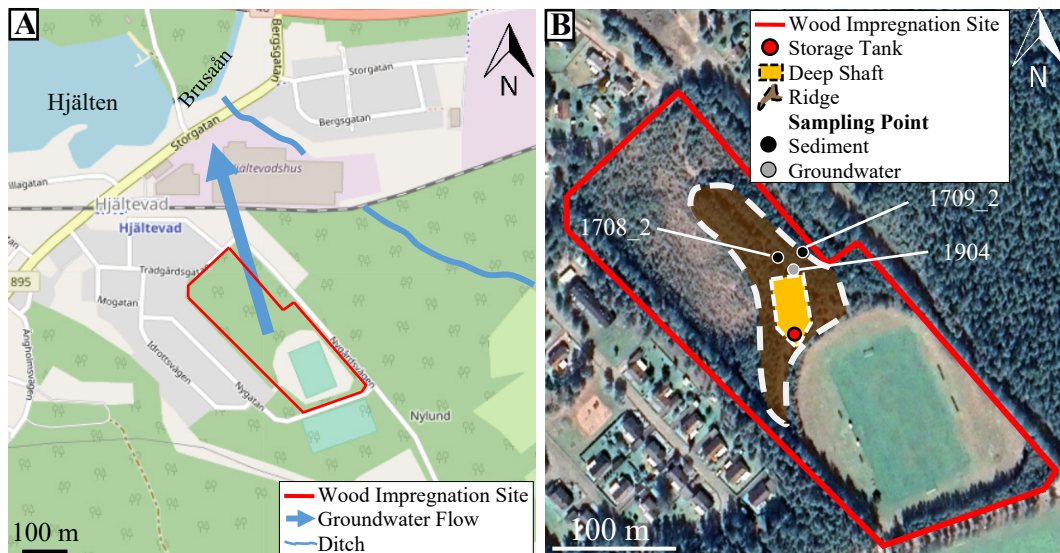


Figure 4: A: Location of the former wood impregnation site in Hjältevad. (OpenStreetMap). B: Close-Up aerial view of the area (Google Earth).

3.2. Hydrogeological Conditions

The underlying bedrock of the area is granite, located at a depth of ca. 40 m below the soil surface. It is mainly overlain by glacial sediments originating from a ground moraine with increasing particle size towards the surface from silt, sand to gravel. Groundwater flows northwest (343.0 ° clockwise from the north) with an average hydraulic gradient of 0.16 %, discharging directly or indirectly in the river Brusaån via a ditch located east of the area (Figure 4A). The overall hydraulic conductivity reaches rather high values (10^{-5} to 10^{-3} m/s) with decreasing amounts at increasing depth. No groundwater is currently used for drinking water and only superficial groundwater unaffected by the As plume is used for irrigation. An overview of the groundwater composition is given in Table 11 in the Appendix.

3.3. Contamination History

The composition of the wood preservative solution stored on the site and used for the impregnation of telephone poles varied at the beginning of the plant operation, but As in the form of Diarsenic Pentoxide (As_2O_5) was the most applied throughout. From 1952, the preservative CCA solution K33 containing ca. 34 % As_2O_5 was used. A 2 wt% solution was used, resulting in 4.4 g/L As. It is estimated that ca. 500 t of As was processed throughout the 36 years of plant operation. K33 also contained 26.6 % Chromium Trioxide (CrO_3), 14.8 % Copper Oxide (CuO), and 24.6 % water. In 1968, the leaking of a steel tank containing 50 m³ of CCA located 0.5 m below the groundwater surface (164 m MAMSL) was detected (Figure 4B). It was estimated that roughly 65-80 kg of As has leaked. Continuous overfilling of the storage tank alongside unprotected impregnation and drying of telephone poles in the northern part of the area are assumed to have significantly contributed to enhanced As pollution.

3.4. Previous Decontamination Actions

Shortly after the leaking was detected in 1968, ca. 1,000 m³ of groundwater near the storage tank was treated by As immobilisation via pump and treat followed by ex-situ disposal of treated water. This approach caused the As levels near the storage tank to decrease by a factor of 1,000; from 2.5 g/L to 2.6 mg/L. Between 1984 and 1995, additional in-situ groundwater remediation by aeration and re-infiltration was implemented. In total, six wells spread on the area northwest of the storage tank with depths between 4 and 10 m below ground (158 -164 MAMSL) were used. This enabled the treatment of ca. 296,000 m³ water and the removal of about 200 kg As.

Between 1988 and 1997, the buildings of the former impregnation plant were demolished. In 1997, As was removed from superficial soil layers by excavation and on-site soil washing. Soil with As \geq 15 mg/kg up to 1 m below the ground surface and As \geq 40 mg/kg underneath was excavated. The latter was treated in an on-site soil washing plant. In the former storage area of impregnated telephone poles, soil up to 5 m below the surface was excavated. Within direct proximity to the former storage tank, an area of 800 m² and 10 m depth (7 m below the groundwater surface) was excavated (Figure 4B; deep shaft). Uncontaminated soil was backfilled up to the groundwater surface. Washed and unwashed soil with As \leq 40 mg/kg was put on top of that and on parts of the adjacent area creating a ridge (Figure 4B; ridge). This was finally covered with 1 m thick soil with As concentrations \leq 15 mg/kg. With this measure, ca. 4,600 kg As corresponding to 2/3 of the total amount of As present in 1997, was removed. Remaining pollution was estimated to amount to ca. 1.4 t As in the ridge area.

3.5. Current Pollution Situation

In 1997, leaching tests using eight soil samples from the backfilled soil area showed a slow spread of the pollution plume (K_d : 1,000 L/kg). In the groundwater, K_d was 50 L/kg and As concentrations were $<$ 50 μ g/L.

From 1997 to 2018, monitoring of pollutant concentrations in four different wells located downstream of the former storage tank showed a continuous increase in As concentrations, from ca. 40 μ g/L up to ca. 500 μ g/L in the sampling point located closest to the former storage tank. 30 % of the 185 dynamic groundwater samples performed in 34 sampling points (2016-2018) showed As concentrations above the drinking water threshold value of 10 μ g/L. In sampling points 1708_2 and 1709_2 located 16-17 m from the sediment sampling point 1904, the As concentration was between 300 and 1500 μ g/L, with As(III) shares of 80-90 % (Appendix Table 11).

Figure 5 shows the modelled distribution of As in the groundwater of the contaminated area. In Figure 5A, the highest detected As concentration in each of the 34 sampling points was used for interpolation and in Figure 5B, the average detected As concentrations over the depth of each sampling point was used for interpolation.

Figure 5A shows high As concentrations of 1,000-3,000 μ g/L in the groundwater, at 20 to 50 m distance from the former storage tank, and an expanding As plume with concentrations up to 100 μ g/L 200 m downstream, already outside the area of the former impregnation plant. Figure 5B shows As concentrations of 300 μ g/L in the groundwater at 20 to 100 m distance from the former storage tank and 10-30 μ g/L at 200 m distance.

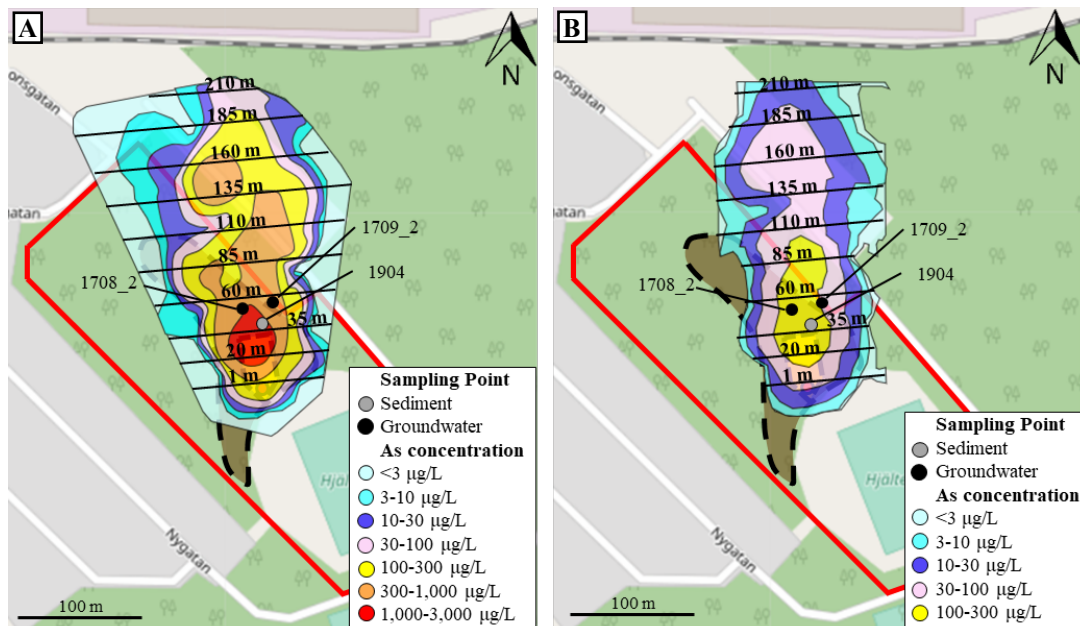


Figure 5: Calculated distribution of As concentrations from results of dynamic groundwater sampling in 34 points (2016-2018) (SWECO, 2019). A: Interpolation of maximum measured concentrations (adapted according to Figure 54, p. 107). B: Weighted averages over the depth of the aquifer (adapted according to Figure 60, p. 117).

For comparison, in 2017, 36 out of 74 soil and sediment samples of the area showed As contents above the national 90th percentile for Swedish sediment soils (7.4 mg/kg). Sampling points adjacent to the area do not show high levels of As in the soil. Highest As concentrations occur 20 m downstream of the former shaft with 238 mg/kg (169 MAMSL). Significantly increased As concentrations were found in the area of the former deep shaft below the former shaft bottom (168 MAMSL).

In 2017, As concentrations in the ditch located northeast of the area were <2 µg/L and below background concentrations (<0.4 µg/L) for the river Brusaån. Thus, an immediate impact of the As plume on the surface water can be excluded. Nevertheless, a further expanding pollutant plume may pose a risk on water extraction in the surrounding area.

4. Materials and Methods

All element analyses, if not stated otherwise, were performed by ALS Scandinavia AB with an ICP-MS. The lab is accredited by the Swedish national accreditation body (SWEDAC, reg. nr. 2030) and complies with the requirements of ISO 9001:200.

4.1. Sediment

The sediment that was used for all laboratory experiments was collected in 2019 in sampling point 1904, 16 – 18 m below the soil surface (Figure 4B). The sample was taken as a core using a Sonic Geo Drill. During the sampling it was ensured that as little O₂ as possible entered the sampling system. A rubber gasket that separates the core from the piston and a so-called “aqualock” that prevents penetration of O₂ during sample transfer by pressurised water were used. During the transfer of the cores from the drill tubes to the hard plastic tubes for storage, nitrogen (N₂) was applied on the bottom of the plastic tube. In the plastic tube, the 2 m sediment core was compressed to 1 m solid sample and the nitrogen hoses were quickly removed before the tube was sealed with a rubber stopper, tape, and an air-tight plastic bag. Within a few hours after sampling, the core was frozen and stored at -20 °C until further use.

The frozen sediment core was transferred into a glovebox (Labconco[®], Protector[®] Controlled Atmosphere Glove Box, atmosphere leak specification according to ISO 10648-2 Class 1 with Auto Pressure Control) with controlled anoxic atmosphere (purified N₂ (AtmosPure[®] Re-Gen Gas Purifier)) and catalytic O₂ removal. Throughout the experiments, the O₂ level was monitored continuously (Alpha Omega Series 3000 Trace Oxygen Analyser) and kept below 20 ppm during daily operations and below 5 ppm overnight. In the glovebox, the sediment core was thawed, homogenized, split into subsamples in sealed aluminum foil bags (Mylar[®]), and stored at -20°C until further use.

Total concentration of major elements in the sediment sample (barium (Ba), cadmium (Cd), cobalt (Co), chromium (Cr), copper (Cu), manganese (Mn), mercury (Hg), nickel (Ni), lead (Pb), vanadium (V), and zink (Zn)) were determined by ALS Scandinavia AB after hot-plate digestion of air-dried sediment using 7 M

HNO₃ according to SE-SOP-0021. Total concentrations of As and Fe in the sediment were obtained after aqua regia microwave digestion according to ISO 11466:1995 (Milestone Ethos[®] Easy Advanced Microwave Digestion System, MAXI-44 rotor, 80 mL PTFE vessels) of 0.5 g oven-dried and sieved samples (see section 4.3), in triplicates.

4.2. Batch Experiments

4.2.1. Zerovalent Iron Sorbents

Four different zerovalent iron (ZVI) sorbents were used in this experiment. Two unsulphidated sorbents, i.e., nanosized, oxidic shell free ZVI (OSF-nZVI) and microsized ZVI (mZVI); and two sulphidated sorbents, i.e., nanosized sulphidated ZVI (S-nZVI) and microsized sulphidated ZVI (S-mZVI). The nZVI and S-nZVI suspensions were used within a week and the S-mZVI slurry was used within two months after delivery. All mixtures were stored in the dark at 4°C until usage. mZVI powder was stored in a plastic container at room temperature. Prior to usage, all four ZVI sorbents were transferred into the glovebox and opened at controlled anoxic atmosphere. An overview of the specifications of each ZVI sorbent is given in Table 2.

S-nZVI (NANOFEAR 25DS) was provided by Nano Iron as a slurry, suspended 1:5 (w/w) in water. Particles were prepared by treating nZVI particles in aqueous solutions of sodium sulphide (Na₂S) under anoxic conditions (Brumovský *et al.*, 2020, 2021). According to the manufacturer, the mixture contains 14-18 wt% Fe(0), 2-6 wt% Fe(II)-oxide, 0-1 wt% Fe(II)-sulphide, and 0-1 wt% carbon, leading to an approximate S/Fe ratio of 0.01. Brumovský *et al.* (2020) measured a S/Fe mass-ratio of 0.007 in dried NANOFEAR 25DS particles. Sulphur was mainly allocated on the particle shell as sulphide (S²⁻), suggesting a Fe(0)-FeS core-shell structure with a ca. 6 nm thick shell surrounding a ca. 50-100 nm core (Brumovský *et al.*, 2020, 2021). Formation of ca. 1 µm aggregates after groundwater injection was observed and a zeta potentials of -19 mV in 100 mM NaHCO₃ was measured (Brumovský *et al.*, 2020, 2021).

OSF-nZVI (NANOFEAR 25) was provided by Nano Iron as a slurry, suspended 1:5 (w/w) in water. As stated by the manufacturer, preparation of particles took place under anoxic atmosphere, followed by suspension in water. The mixture consisted of the same amounts of Fe(0), Fe(II)oxide, and carbon than S-nZVI. According to the manufacturer, the average single particle size is 50 nm. However, Schmid *et al.* (2015) observed an average size of 4.4±3.9 µm and a zeta potential of -10 mV using laser obscuration time method in a 100 times diluted slurry, indicating the formation of aggregates. Kašlík *et al.* (2018) confirmed the absence

of an oxidic-shell on the surface of fresh NANOFER 25 particles using X-ray diffraction.

S-mZVI; (S-MicroZVITM) was provided by Regenesis as a slurry, suspended ca. 1:2.5 (w/w) in Glycerine solution (ASTM[®] D6584). The mixture contains ca. 40 wt% Fe(0), and 1-2 wt% Fe(II)-sulphide (Regenesis, no date). According to the manufacturer, the particles are spherical-shaped with a particle diameter of ca. 2-3 μm (Regenesis, no date). Similarly to S-nZVI, the sorbent S-mZVI consist of a Fe(0) core with a Fe(II)-sulphide shell (Regenesis, no date).

mZVI (Ferox Target) was provided by Hepure as a powder. According to the manufacturer, the powder consists of 95 % pure zerovalent iron with minor impurities of sulphur, silicon, and phosphate, and a particle size of 44 μm (Hepure, 2016).

4.2.2. Artificial Groundwater

The experiments within this chapter were conducted in a glovebox (specifications see section 4.1) at a controlled anoxic atmosphere.

Artificial groundwater (AGW) was used to reproduce the ionic composition of the groundwater in the field (Appendix Table 11). The concentration of major ions in the field was estimated based on the average concentrations of sampling points 1708_2 and 1709_2 located 16 and 17 m downstream, respectively, from the sediment sampling point 1904 (Figure 4B). AGW was prepared in the glovebox by adding the components as salts to ultrapure water (Type I, ELGA PURELAB[®] ultra) (Table 1). Before usage, the ultrapure water was degassed with pure N₂ for an hour and immediately transferred into the glovebox. The pH of the final solution was adjusted to pH 6.0 by addition of 0.72 mM HCl.

Table 1: Composition of artificial groundwater used in batch experiments.

Element	Unit	Added Concentration
NH ₄ ⁺	mg/L	0.27
Ca ²⁺	mg/L	18.04
Mg ²⁺	mg/L	2.43
Mn ²⁺	mg/L	0.55
Na ⁺	mg/L	17.2
K ⁺	mg/L	2.0
Cl ⁻	mg/L	41.0
SO ₄ ²⁻	mg/L	19.2
PO ₄ ³⁻	mg/L	0.10
HCO ₃ ⁻	mg/L	48.8
Ionic Strength	mEq	2.34

Table 2: Characteristics of added ZVI sorbents. SSA: Specific Surface Area. N/S: not specified.

Sorbent	Commercial Name	Supplier	State	Dilution Factor (Medium)	Fe(0) [wt%]	Fe(II)O [wt%]	Fe(II)S [wt%]	Carbon [wt%]	Impurities [wt%]	Zeta Potential [mV]	Diameter	SSA [m ² /g]
S-nZVI	NANO FER 25DS	NANO IRON	Suspension	0.2 (Water)	14-18 ¹	2-6 ¹	0-1 ¹	0-1 ¹		-19 ²	50 nm ¹	> 25 ¹
OSF-nZVI	NANO FER 25	NANO IRON	Suspension	0.2 (Water)	14-18 ³	2-6 ³	-	0-1 ³		-10 ⁴	50 nm ³	> 25 ³
S-mZVI	S-MicroZVI™	REGENESIS	Slurry	0.4 (Glycerine (ASTM® D6584))	40 ⁵	-	1-2 ⁵	-		N/S	2-3 μm ⁶	N/S
mZVI	Ferox Target	Hepure	Powder	-	96.3-97.3 ⁷		-	1.5-2 ⁷	S: 0.1 ⁷ Si: 1-1.5 ⁷ PO ₄ ³⁻ : 0.1 ⁷	N/S	44 μm ⁷	5.15 ⁷

¹: Nanofer 25DS Safety Data Sheet; ²: S:Fe ratio 0.007, particle concentration: 242 mg/L in 100 mM NaHCO₃ (Brumovský et al., 2020); ³: Nanofer 25 Safety Data Sheet; ⁴: Measured 100 times diluted in water (Schmid et al., 2015); ⁵: S-MicroZVI Safety Data Sheet; ⁶: Regenesis (no date); ⁷: Hepure (2016).

4.2.2.1. Conditions Before Treatment (T0)

18 g of As-contaminated sediment (moisture content of 13 %) were mixed with 90 mL of AGW (initially free of As) in 100 mL centrifuge tubes (Brand[®], polypropylene) (Figure 6T0). This yielded to a liquid to solid (L/S) ratio of 5.9 considering the moisture content of the sediment. The tubes were sealed with parafilm and shaken using an end-over-end shaker. After 30, 33, 34, 40, 41, and 47 days of shaking time (Table 4), individual tubes were removed from the shaker and opened for further processing.

For the analysis of each batch, the workflow scheme shown in Figure 6T0, was followed. The sealed tubes were transferred out of the glovebox and centrifuged for 15 min at 2,500 rpm (Allegra X15R Beckman Coulter Centrifuge, rotor length: 207.8 mm). After centrifugation, the tubes were immediately transferred back into the glovebox. In a next step, 22 mL of the supernatant was withdrawn for pH measurement (Thermo Scientific[®] Orion[®] ROSS Ultra[®] pH Electrode) and oxidation reduction potential (ORP) measurement (Thermo Scientific[®] Orion[®] Metallic Combination Electrode; with Orion[®] Automatic Stirrer). The remaining supernatant was filtered through a 0.45 µm-syringe filter (Pall[®] Acrodisc[®], Supor[®] Membrane (polyethersulphone), 32 mm, acrylic housing, non-sterile). 15 mL of the filtered supernatant was passed through an As speciation cartridge (MetalSoft Center), acidified to 1 % HNO₃ and stored in 15 mL storage tubes for As(III) measurement. Another 15 mL aliquot of the filtered supernatant was directly transferred into a 15 mL storage tube and acidified to 1 % HNO₃ for measurement of total As (A_{Stot}) and Fe. All samples were stored at 4 °C until analysis. The remaining solid samples were flash frozen at liquid nitrogen at -47 °C (Mechatech Systems, Lyodry Compact) and stored at -18 °C until further use.

4.2.2.2. Zerovalent Iron Sorbent Performance at Uncontrolled pH (T1)

The four ZVI sorbents were added to the mixture of sediment and groundwater according to Table 3 (described in 4.2.2.1). The added concentration of mZVI was 5 times higher than S-mZVI, S-nZVI and OSF-nZVI, in order to account for the differences in application technique and specific surface area. mZVI has a significantly greater particle size than the other three ZVI sorbents, and injection of the particles as a slurry by direct push technology results in a higher dilution in the groundwater after soil passage (Geosyntec, 2020). On the contrary, S-nZVI, OSF-nZVI and S-mZVI have a similar size range and specific surface area (data for S-mZVI is not available, but is assumed) which enables injection of a water-like slurry based on natural permeation (Geosyntec, 2020).

The tubes containing sediments, AGW, and ZVI sorbents were sealed with parafilm and shaken with an end-over-end-shake for at least 23 days. Equilibrium conditions were assumed after ca. 23 days.

Table 3: Amounts of ZVI sorbents [ml/mg] added and the resulting normalised Fe dose [g/L].

Sorbent	Amount	Dilution	Fe [g/L]
S-nZVI	0.15 mL	0.2	0.4
OSF-nZVI	0.15 mL	0.2	0.4
S-mZVI	0.09 g	0.4	0.4
mZVI	0.18 g	-	1.9

At given times (Table 4), individual tubes were removed from the shaker and opened for further processing. For sampling and analysis of each treatment, the workflow scheme described in 4.2.2.1 and shown in Figure 6T1, was followed. There was one difference, which is that the supernatant of the nZVI and S-nZVI treatments was filtered through a 0.1 μm syringe filter (Pall[®] Acrodisc[®], Supor[®] Membrane (polyethersulphone), 32 mm, acrylic housing, non-sterile) rather than 0.45 μm , in order to account for the smaller particle sizes of these sorbents.

Table 4: Sampling Timepoints and number of samples per treatment at T0 and T1.

Treatments	Sampling Timepoints [d]	Total Number of Samples
Untreated	30, 33, 34, 40, 41	5
S-nZVI	23, 33 ¹ , 56	4
OSF-nZVI	23, 33 ¹ , 56	4
S-mZVI	30, 31, 33 ¹	4
mZVI	30, 33 ¹ , 62	4

¹: Samples taken in duplicates.

4.2.2.3. Zerovalent Iron Sorbent Performance at pH Adjusted to Field pH (T2)

Complementarily to the experiments at uncontrolled pH (see section 4.2.2.2), similar experiments were conducted but with the pH of each treatment being adjusted to 7 (Figure 6T2). In a first trial, one sample of each treatment that has been previously equilibrated at uncontrolled pH for at least 30 days was acidified using HCl and then shaken for an additional period (Table 5). In a second trial, the shaking time before acidification was standardised to 33 days for all treatments. After 33 days, samples of each treatment were acidified in duplicates to pH 7.0 and shaken for additional 3 days before sampling (Table 5). For sampling and analysis of each batch, the workflow scheme described in section 4.2.2.1, 4.2.2.2, and shown in Figure 6T2, was followed.

Table 5: HCl addition to each treatment.

Treatment	HCl Addition [M]	Shaking time before acidification [d]	Shaking time after acidification [d]
S-nZVI	0.01/0.01	56 ¹ /33 ²	4 ¹ /3 ²
OSF-nZVI	0.01/0.01	56 ¹ /33 ²	4 ¹ /3 ²
S-mZVI	0.01/0.005	31 ¹ /33 ²	3 ¹ /3 ²
mZVI	0.03/0.03	62 ¹ /33 ²	4 ¹ /3 ²

¹: First run of acidification. ²: Second run of acidification; samples taken in duplicates.

4.2.3. Phosphate and Oxalate Extraction of Solid Samples

The following analyses were conducted under oxic conditions, i.e. outside the glovebox at atmospheric air conditions. Atmospheric air conditions were chosen in order to avoid Fe dissolution induced by decreasing pH (pH 8 for phosphate and pH 3 for oxalate extraction) under anoxic conditions in the glovebox. It is expected that the crystallinity of Fe compounds does not change with changing atmospheric conditions and that changing speciation of As does not significantly affect the amount of extractable As. Thus, even though changing As speciation is known to affect As sorption (e.g. Dixit and Hering, 2003), the total amount of As extractable by phosphate should not change. This can be explained by the fact that both As(III) and As(V) are bound to the same surfaces, i.e. desorption of both species will be captured in the total extractable As.

Prior to the extraction experiments, all glassware was soaked in 1 % HNO₃ for 48 h and rinsed three times with deionised water and once with ultrapure water.

0.50 g ± 5 % of the dried solid phase that remained after centrifuging and filtering the mixtures described in section 4.2.2 was weighed in duplicates into 50 mL centrifugal tubes (Sarstedt polypropylene, sterile) (Figure 6). The samples used for extractions are listed in Table 6. Additionally, 0.50 g ± 5 % of dried and sieved sediment that has not been in contact with AGW or sorbents (see section 4.3) was used. The weighed samples were then subject to extraction according to the procedures described in section 4.2.3.1 and 4.2.3.2. Extracts were stored at +4 °C in the dark until analysis of As and Fe concentrations.

Table 6: Sample List for extractions. All extractions were run in duplicates.

Treatment	Scenario	Shaking time before acidification [d]	Shaking time after acidification [d]
Untreated	Before Treatment (T0)	30	-
S-nZVI	Uncontrolled pH (T1)	23, 56	-
OSF-nZVI		23, 56	-
S-mZVI		30, 31	-
mZVI		30, 62	-
S-nZVI	pH Adjusted to Field pH (T2)	56	4
OSF-nZVI		56	4
S-mZVI		31	3
mZVI		62	4

4.2.3.1. Phosphate Extraction

Phosphate extraction parameters were chosen based on modelling results and literature review (e.g. Wenzel *et al.*, 2001a; Larios, Fernández-Martínez and Rucandio, 2013). More details are shown in Appendix II.a. A 0.5 M PO₄ solution was prepared at pH 8.0. For this, Na₂HPO₄ and NaH₂PO₄ were mixed in a molar ratio of 0.48:0.02 in ultrapure water in a volumetric glass flask. The pH of the solution was checked in a 30 mL aliquot. In case the pH was < 8.0, 0.5 M Na₂HPO₄ solution was added stepwise until the pH reached 8.0. In case the pH was > 8.0, 0.5 M NaH₂PO₄ solution was added accordingly. The PO₄³⁻ extraction solution was stored for a maximum of 7 days at room temperature. 50 mL of 0.5 M PO₄³⁻ solution was added to 0.50 g solid sample (L/S ratio: 100). The suspensions were equilibrated for 16 h with an end-over-end shaker at a shaking speed of 4.5/9. After the shaking period, the suspensions were left to settle for ca. 15 min and a 5-mL aliquot was withdrawn for pH measurements. Measured pH values were 7.9 ± 0.03 in all extracts (Appendix Table 12), i.e., very close to the pH of the extraction solution before contact with the solid sample. The remaining supernatant was filtered through a single use 0.2 µm syringe filter (Sarstedt[®], polyethersulphone membrane, 26 mm, Methacrylate-butadiene-styrene housing, sterile). The filtered extracts were acidified to 4 % HNO₃ until analysis of As and Fe concentrations.

4.2.3.2. Oxalate Extraction

Oxalate extraction was performed according to the standardised procedure by van Reeuwijk (2002). A 0.2 M oxalate solution was prepared at pH 3.0. (NH₄)₂C₂O₄ and H₂C₂O₄ were mixed in a molar ratio of 0.11:0.09 in ultrapure water in a volumetric glass flask and transferred to a polypropylene bottle. The pH of the solution was checked in a 30 mL aliquot. In case the pH was < 3.0, 0.2 M (NH₄)₂C₂O₄ solution was added stepwise until the pH was 3.0. In case the pH was > 3.0, 0.2 M H₂C₂O₄ solution was added accordingly. The solution was stored

in the dark at room temperature for a maximum of 7 days. 50 mL of 0.2 M oxalate solution was added to 0.50 g dried sample (L/S ratio: 100). The suspensions were equilibrated for 4 h in the dark with an end-over-end shaker at a shaking speed of 4.5/9. After the shaking period, the suspensions were centrifuged at 4,000 rpm for 15 min (Allegra X15R Beckman Coulter Centrifuge, rotor length: 207.8 mm). The supernatant (ca. 45 mL) was filtered through a single use 0.2 μm syringe filter (Sarstedt[®] polyethersulphone membrane, 26 mm, Methacrylate-butadiene-styrene housing, sterile). Throughout the extraction procedure, exposure to daylight was avoided to prevent photochemically induced dissolution of crystalline Fe phases.

4.2.4. Digestion of Solid Samples

0.50 g \pm 1 % of the dried solid phase after centrifuging and filtering the mixtures described in section 4.2.2 was weighed in duplicates into 80 mL PTFE vessels (Milestone Ethos[®] Easy). The samples were digested with aqua regia using a microwave according to ISO 11466:1995 (Milestone Ethos[®] Easy Advanced Microwave Digestion System, MAXI-44 rotor). Samples were selected to match the samples used in phosphate and oxalate extractions (Table 6). Samples with the shortest shaking time of every ZVI treatment at T1 and samples of every ZVI treatment at T2 were used, respectively. Additionally, 0.50 g \pm 1 % of dried and sieved sediment that has not been in contact with AGW or sorbents (see section 4.3) was used. Digests were filtered using a funnel and filter paper (Munktell filter paper, OOM, 7-10 μm), diluted with ultrapure water, and stored at +4 °C until analysis of As and Fe concentrations.

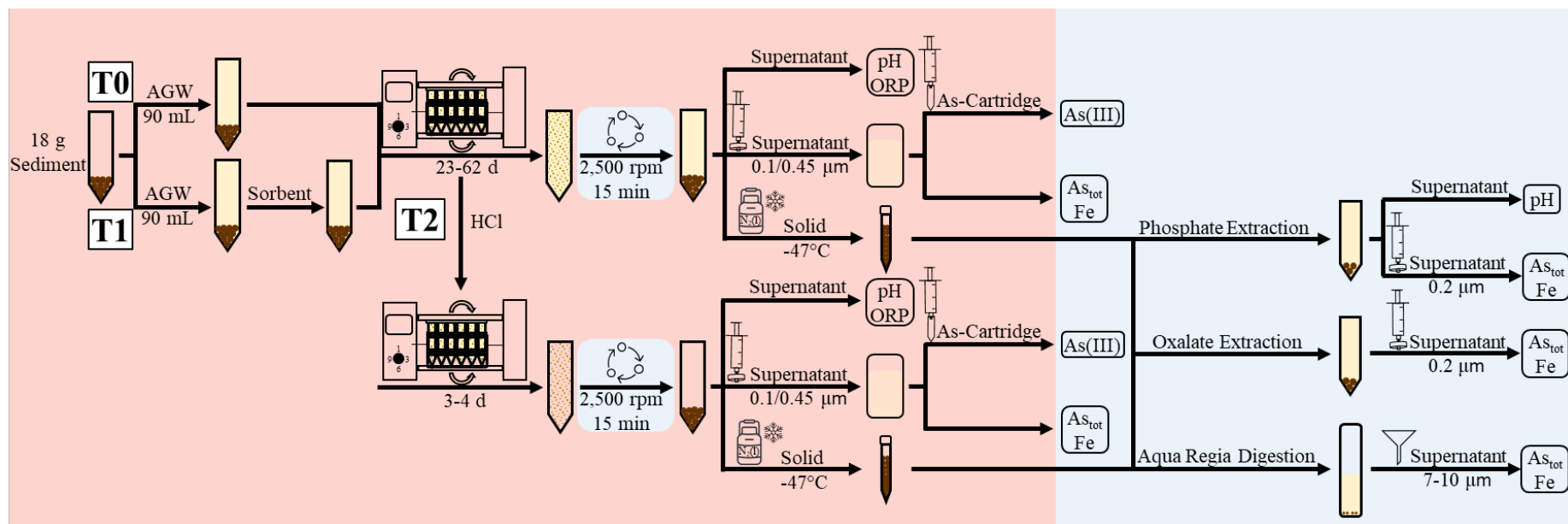


Figure 6: Experimental Workflow. Red: anoxic conditions; blue: oxic conditions. T0: before treatment; T1: uncontrolled pH. T2: pH adjusted to field pH. AGW: Artificial Groundwater; ORP: Oxidation Reduction Potential.

4.3. pH-dependent Arsenic Solubility under Oxidic Conditions

The procedure was adapted from SS-EN-14429 (SSI, 2015). A subsample of sediment sample 1904 (see section 4.1) was oven-dried for 5 days at 50 °C. The dried sample was sieved through a 2 mm sieve and $5.0 \pm 4\%$ was added to 50 mL centrifugal tubes (Sarstedt polypropylene, sterile). 50 ml of 10 mM NaNO₃ solution prepared in ultrapure water was added to each tube (L/S ratio: 10). To cover the pH range of the experiments in section 4.2, the pH of the individual tubes was adjusted within the pH range 5-11 in 0.5-unit steps, resulting in 13 different pH values. The amounts of acid (HNO₃) and base (NaOH) required to achieve the target pH values were assessed with pre-tests (see Appendix III.a). Solutions of 2 M NaOH and HNO₃ were prepared in ultrapure water by diluting 65 % concentrated HNO₃ and dissolving NaOH powder, respectively. Further dilutions to 0.5 and 0.1 M NaOH and HNO₃, respectively and 0.05 M NaOH were prepared in ultrapure water. 25 to 100 µL acid or base was added to the mixtures of sediment and NaNO₃ in order to avoid dilution effects (see Appendix Figure 20 for precise values). Samples were prepared in duplicates. Two samples were prepared without acid or base addition to assess the natural pH of the system. Suspensions were equilibrated for 5 ½ days with an end-over-end shaker at a shaking speed of 4.5/9. After the shaking period, the suspensions were centrifuged at 4,000 rpm for 15 min (Allegra X15R Beckman Coulter Centrifuge, rotor length: 207.8 mm). A 5 mL aliquot was withdrawn for pH measurements (Hach® Analytical GK2401C Combination pH Electrode) and the remaining supernatant (ca. 45 mL) was filtered through a 0.45 µm syringe filter (Pall® Acrodisc®, Supor® Membrane (polyethersulphone), 32 mm, acrylic housing, non-sterile). 15 mL of the filtered sample were transferred to 15 mL tubes, acidified to 1 % HNO₃ and kept at 4 °C until measurement of As, Fe, Ca, K, Mn and Na. 10 mL of the filtered sample was transferred to 15 mL tubes and stored at -20 °C in the dark until measurement of PO₄³⁻ and dissolved organic carbon (DOC). PO₄³⁻ was measured with an Auto Analyser (QuAAtro; method Q-064-05; SS EN ISO 15681-2). DOC was measured with a Shimadzu TOC – VCPH with TNM-1 module (SS-EN 1484).

4.4. Data Processing

4.4.1. Classification of Fractions

In order to investigate the binding affinity of As at different treatments, four different As fractions were defined according to their solubility and extractability. The Fe fractions were classified in a similar way. It is important to stress that the classification of fractions is operationally defined based on literature review. In order to validate these assumptions, additional analytical tools such as synchrotron-based X-ray absorption is required (Formentini *et al.*, 2017, 2021).

Fractionation of Iron

Fraction 1 (Fe_{F1}) represents the dissolved Fe in AGW after reaction according to section 4.2.2. (i.e. sediment and/or ZVI sorbent with AGW):

$$Fe_{F1} = Fe_{AGW}$$

(3) Dissolved Iron (Fe_{F1})

Fraction 2 (Fe_{F2}) represents the Fe concentration after reaction according to section 4.2.2 (i.e. sediment and/or ZVI sorbent with AGW) that is extracted by phosphate (PE) according to section 4.2.3.1. Of note, Fe dissolution by phosphate extraction was not expected; nevertheless, some Fe was detected in those extracts (see Appendix Figure 18). However, no significant impact on the validity of the phosphate-extracted As is expected. This fraction was calculated as follows:

$$Fe_{F2} = Fe_{PE}$$

(4) Phosphate extractable Iron (Fe_{F2})

Fraction 3 (Fe_{F3}) consists of amorphous Fe-(hydr)oxides such as ferrihydrite, hereafter called “amorphous Fe” (Schwertmann, 1973, 1991; Schwertmann, Schulze and Murad, 1982; Loeppert and Inskeep, 1996). It comprises the Fe concentration of the solid phase after reaction according to section 4.2.2 (i.e. sediment and/or ZVI sorbent with AGW) that got dissolved by oxalate extraction (OE) according to section 4.2.3.2:

$$Fe_{F3} = Fe_{OE}$$

(5) Amorphous Iron (Fe_{F3})

Fraction 4 (Fe_{F4}) is predominantly composed of crystalline Fe-(hydr)oxides (Keon *et al.*, 2001; Wenzel *et al.*, 2001b). It was calculated by deducting F1, F2, and F3 from total Fe (Fe_{tot}):

$$Fe_{F4} = Fe_{tot} - F1 - F2 - F3$$

(6) Crystalline Iron (Fe_{F4})

Total Iron (Fe_{tot}) of the untreated sample (T0) was obtained by microwave assisted aqua regia digestion (ARD) of a sediment sample that has not been in contact with AGW or sorbents (section 4.3). Fe_{tot} of the four ZVI treatments was obtained by summing the dissolved Fe concentration measured in the AGW (Fe_{F1}) with the Fe concentration measured by aqua regia digestion (section 4.2.4) of the solid sample after reaction according to section 4.2.2 (i.e. sediment and ZVI sorbent with AGW):

$$Fe_{tot} = Fe_{ARD} + Fe_{F1}$$

(7) Total Iron (Fe_{tot}) of the ZVI treatments

Fractionation of Arsenic

For As, fraction 1 (F1), fraction 2 (F2), and fraction 4 (F4) were obtained in the same manner as for Fe. Fraction 3 (F3) was obtained in an adapted manner. The meaning attributed to each of these fractions for As are the following.

Fraction 1 (F1) represents dissolved As in AGW after reaction described in section 4.2.2 (i.e. sediment and/or ZVI sorbent with AGW):

$$F1 = As_{AGW}$$

(8) Dissolved Arsenic (F1)

Fraction 2 (F2) reflects specifically sorbed As, i.e. physically accessible As (Keon *et al.*, 2001; Wenzel *et al.*, 2001a; Loeppert *et al.*, 2002; Dong, Guan and Lo, 2012). It comprises the As concentration of the solid phase after reaction according to section 4.2.2 (i.e. sediment and/or ZVI sorbent with AGW) that got dissolved by competitive phosphate extraction (PE) according to section 4.2.3.1:

$$F2 = As_{PE}$$

(9) Specifically sorbed As (F2)

Fraction 3 (F3) reflects As that is either strongly bound to or occluded in amorphous Fe (Keon *et al.*, 2001; Wenzel *et al.*, 2001; Kumpiene *et al.*, 2012). Some As bound to reactive aluminium (Al) phases, such as amorphous Al, may also be extracted by oxalate, but this amount is assumed to play a minor role in the ZVI treatments as Fe predominates. F3 was assessed by deducting the As extracted in F2 from the As extracted with oxalate (OE) (section 4.2.3.2):

$$F3 = As_{OE} - F2$$

(10) Strongly bound Arsenic to amorphous Iron (F3)

Fraction 4 (F4) reflects the As in the residual fraction. F4 comprises As that is predominantly either strongly bound to or occluded in crystalline Fe (Keon *et al.*, 2001). In the same manner as described in F3, some As bound to crystalline Al phases may also be included in this fraction, as well as As associated with silicates (Keon *et al.*, 2001). However, these amounts are assumed to play a minor role in the ZVI treatments. Other As bearing recalcitrant minerals such as pyrite and amorphous As_2S_3 may also be included in this fraction and their amount may

change with addition of ZVI treatments (Keon *et al.*, 2001). This fraction was calculated as follows:

$$F4 = AS_{\text{tot}} - F1 - F2 - F3$$

(11) *Residual Arsenic (F4)*

Total concentration of As (Tot) was obtained and calculated as described for Fe for the untreated sample (T0) and the four ZVI treatments, respectively:

$$\text{Tot} = AS_{\text{ARD}} + F1$$

(12) *Total Arsenic (Tot)*

4.4.2. Statistical Analysis

Data from all timepoints for T0, and T1 and T2 per ZVI treatment was averaged. Averaging was done considering that the conditions at ca. 30 d were near to equilibrium conditions and small deviations (i.e., a few days) between samplings were considered negligible. Mean concentrations of a given parameter were calculated in case of two or more values per sample ($n \geq 2$). Error bars were calculated for $n=2$ as absolute deviation (AD) from the mean and for $n > 2$ as standard deviation (SD). Significant differences ($p < 0.05$) were assessed with one way ANOVA with post hoc Tukey HSD in case of $n \geq 2$, normal distribution, and homogeneity of variances and with Kruskal-Wallis with post hoc Bonferroni in case of disregard of minimum one requirement.

4.4.3. Differences of Arsenic Fractionation (F1-F4)

The changes in As fractionation between the untreated sediment (T0) and the ZVI treatments at T1 and T2 were calculated by subtracting the mean concentration (mg/kg) of each fraction (F1-F4) of the untreated sediment (T0) from the corresponding fraction (mg/kg) in each ZVI treatment at T1 and T2 according to the following equation:

$$\Delta_{Fi} = Fi_{Si, Ti} - Fi_{T0}$$

(13) *Differences of Arsenic Fractionation (F1-F4)*

Where:

F_i : F1-F4

S_i : ZVI treatment (S-nZVI, OSF-nZVI, mZVI, S-mZVI)

T_i : T1, T2

Differences of As fractionation between T1 and T2 were calculated in the same manner to the equation above, by subtracting the mean As concentration (mg/kg) of each fraction (F1-F4) at T1 from the mean As concentration (mg/kg) of the corresponding fraction at T2.

4.5. Simulations with Visual MINTEQ

Dissolved As(III) and As(V) concentrations in the untreated sediment (sample 1904) were simulated at different pH-values and redox potentials using the geochemical equilibrium model Visual MINTEQ version 3.1 (Gustafsson, 2013). The model was calibrated using the data obtained by pH-dependent As solubility under oxic conditions (section 4.3).

Visual MINTEQ captures speciation of dissolved components, sorption and desorption to Fe-(hydr)oxides, binding to soil organic matter (SOM), and precipitation/dissolution of minerals. Sorption to Fe-(hydr)oxides was simulated with the CD-MUSIC surface charge model based on Hiemstra and Van Riemsdijk (1996) with adapted surface charge parameters according to Tiberg *et al.* (2013). Crystalline Fe-(hydr)oxides and clay minerals were disregarded due to their smaller sorption capacity and thus assumed minor influence on As sorption in the considered experiments (Tiberg *et al.*, 2013). Amorphous Al-(hydr)oxides were not included in the modelling due to missing data. However, there is no separate model for Al-(hydr)oxides and they are assumed to behave as ferrihydrite in the model. Since the output of the model initially overestimated the As sorption (see below), ferrihydrite concentrations were reduced in order to reflect measured dissolved As concentrations. Thus, missing input of Al-(hydr)oxides in the model does not seem to make a difference in this case. Consequently, oxalate extractable Fe of the untreated sediment, i.e., ferrihydrite (section 4.2.3.2), was used as an input parameter for inorganic sorbents. A fixed value of ferrihydrite was used for all pH values because dissolution of ferrihydrite was assumed to occur to a minor extent in the considered pH range (Fastlund, 2018). At negative Eh, i.e., reducing conditions, as it was simulated in some scenarios (see below), dissolution of ferrihydrite may have an increased impact. However, enhanced dissolution of ferrihydrite was assumed to occur only at $\text{pH} < 7$, i.e., outside the pH range of the batch experiments (see section 5.2.1).

Complexation to organic matter was simulated with the Stockholm Humic Model (SHM) with acid-base parameters according to Gustafsson and Van Schaik (2003). The ratio of “active” dissolved organic matter (DOM) to dissolved organic carbon (DOC) was set to 2, and DOM was assumed to consist of 100% fulvic acid (FA). Data from pH-dependent As solubility experiments (section 4.3) was used for DOC model input. Data from Fastlund (2018) was used for total organic carbon (TOC) input since TOC in the sediment sample used in the present study was not measured. It was assumed that 50 % of soil organic matter (SOM) is active, i.e. participates in proton and metal binding, and 50 wt% of SOM is carbon (C) (Tiberg *et al.*, 2016). Active SOM was assumed to consist of 50 % humic acid (HA) and 50 % fulvic acid (Tiberg *et al.*, 2016). However, no sorption of As to SOM and DOM was simulated by the model. Further details of used models and specified parameters can be found in Tiberg *et al.* (2016) and Fastlund (2018).

An overview of model input parameters is given in Table 7, the precise values used for the model input are shown in Appendix Table 13. Major cations (Na^+ , Ca^{2+} , K^+ , Mn^{2+} , $\text{P}(\text{PO}_4^{3-})$) were measured in the supernatants of pH-dependent As solubility experiments (section 4.3) and fixed as “total dissolved” concentrations in the model. NO_3^- concentrations were calculated according to added NaNO_3 and HNO_3 from pH-dependent As solubility experiments (section 4.3 and Appendix Figure 20). Geochemically active As, i.e. As that is assumed to participate in sorption/desorption processes, was obtained by oxalate extraction of dried and sieved sediment (see section 4.2.3.2). Redox potentials, if applicable, from untreated sediment (T0), and means of T1 and T2 (Figure 8) were added as “fixed Eh” in the model. The temperature was set to 22 °C and the pH was set as “fixed” to the pH value measured in the supernatant of pH-dependent As solubility experiments (section 4.3). For simulations at fixed Eh, $\text{H}_3\text{AsO}_3/\text{AsO}_4$ was added as a redox pair. “Ferrihydrite aged” was added as an “infinite” solid phase.

Fastlund (2018) conducted experiments similar to 4.3 and modelling with sediments from the same contaminated site and showed that dissolved As concentrations were underestimated by the model. It was assumed that this was caused by overestimation of active sorption sites of ferrihydrite. Consequently, ferrihydrite concentrations were reduced from 100 % to 10 % in 10 % steps in order to assess a ferrihydrite concentration which reflects best the measured dissolved As concentrations. These simulations were conducted in the same manner in this work, with As(V) at unspecified redox conditions as input parameters (see Appendix Figure 21). At 30 % ferrihydrite concentration, based on oxalate extractable Fe, the root mean square error (RMSE) between measured and simulated As concentrations was lowest and this concentration was used in all further simulations.

Table 7: Model Input Parameters

Component	Specification in the Model	Origin
pH	Fixed at	pH-dependent As solubility (see 4.3)
ORP	Fixed Eh [mV]	Untreated sediment (T0), means of T1 and T2 (see Figure 8)
Na ⁺	Fixed total dissolved***	pH-dependent As solubility (see 4.3)
NO ₃ ⁻	-	Calculated according to added NaNO ₃ and HNO ₃ (see Appendix Figure 20)
Ca ²⁺	Fixed total dissolved***	pH-dependent As solubility (see 4.3)
K ⁺	Fixed total dissolved***	pH-dependent As solubility (see 4.3)
Mn ²⁺	Fixed total dissolved***	pH-dependent As solubility (see 4.3)
P(PO ₄ ³⁻)	Fixed total dissolved***	pH-dependent As solubility (see 4.3)
Fe	Ferrihydrite (aged), infinite solid phase	Visual Minteq simulates dissolved concentration
Ferrihydrite	Ferrih-CD-MUSIC (Tiberg <i>et al.</i> , 2013)	30 % of oxalate extracted Fe converted to ferrihydrite (89 g/mol)
As(V)	-	Oxalate extraction (see 4.2.3.2)
DOC	SHM	pH-dependent As solubility (see 4.3)
FA and HA	SHM	Data from Fastlund (2018)

***: Input concentrations fixed at measured dissolved values

5. Results

5.1. Iron in the Solid Phase (Fe_{F3} , Fe_{F4})

In the untreated sediment (T0), the total Fe concentration (Fe_{tot}) was 7.3 g/kg (Table 8). This was constituted of 0.68 g/kg amorphous Fe (Fe_{F3}), i.e., 9.3 % total Fe, and 6.7 g/kg crystalline Fe (Fe_{F4}), i.e., 90.7 % total Fe.

In the four ZVI treatments, the highest total Fe concentration was observed in the mZVI treatment (18.9 g/kg), followed by the nanosorbent treatments S-nZVI and OSF-nZVI (10.6 and 10.4 g/kg, respectively), and the S-mZVI treatment (9.68 g/kg). This corresponds to an Fe concentration added via the ZVI sorbents of 11.5, 3.29, 3.11, and 2.34 g/kg, or 1.2, 0.33, 0.31, and 0.23 wt% for the mZVI, S-nZVI, OSF-nZVI, and S-mZVI treatment, respectively.

At uncontrolled pH (T1) and at pH adjusted to field pH (T2), the absolute concentration of amorphous Fe (Fe_{F3}) and crystalline Fe (Fe_{F4}) increased in all four ZVI treatments compared to the untreated sediment (T0). However, the percentage of Fe in all four ZVI treatments at T1 and T2 increased only for Fe_{F3} and decreased for Fe_{F4} compared to the untreated sediment.

At T1, compared to the untreated sediment (T0), the concentration of amorphous Fe (Fe_{F3}) increased to 9.3 g/kg (49.3 %) in the mZVI treatment, followed by the nanosorbent treatments OSF-nZVI and S-nZVI (3.0 g/kg, 28.6 %; 2.9 g/kg, 27.3 %) and the S-mZVI treatment (2.3 g/kg, 24.2 %). The concentration of crystalline Fe (Fe_{F4}) increased to 9.6 g/kg in the mZVI treatment, followed by the nanosorbent treatments S-nZVI and OSF-nZVI (7.7 g/kg, 7.5 g/kg) and the S-mZVI treatment (7.1 g/kg). The percentage of crystalline Fe (Fe_{F4}) decreased to 71.4, 72.7, and 73.5 % in the OSF-nZVI, S-nZVI, and S-mZVI treatment, followed by the mZVI treatment (50.6 %).

At T2 compared to the untreated sediment (T0), the concentration of amorphous Fe (Fe_{F3}) increased to 6.5 g/kg (34.2 %) in the mZVI treatment, followed by the nanosorbent treatments OSF-nZVI and S-nZVI (2.4 g/kg, 22.9 %; 2.2 g/kg, 20.4 %) and the S-mZVI treatment (1.4 g/kg, 14.0 %). The concentration of crystalline Fe (Fe_{F4}) increased to 8.6 g/kg in the mZVI treatment, followed by the S-nZVI treatment (7.7 g/kg), and the OSF-nZVI and S-mZVI treatments (7.2 g/kg

for both treatments). The percentage of crystalline Fe (Fe_{F4}) decreased to 69.1, 72.5, and 74.5 % in the OSF-nZVI, S-nZVI, and S-mZVI treatment, followed by the mZVI treatment (45.3 %).

At T2 compared to T1, amorphous Fe concentrations (Fe_{F3}) decreased in all four ZVI treatments. This is consistent with the increased dissolved Fe concentrations in all four ZVI treatments at T2 compared to T1 (see Figure 12).

Table 8: Iron concentration in the solid phase (Fe_{F3} , Fe_{F4} , Fe_{tot}) [mg/kg]. T0: untreated sediment. T1: uncontrolled pH. T2: pH adjusted to field pH. Fe_{F3} : amorphous Iron. Fe_{F4} : crystalline Iron. Fe_{tot} : total Iron.

Treatment	Scenario	Fe_{F3}		Fe_{F4}		Fe_{tot}	Fe_{tot} added via sorbent	
		g/kg	%	g/kg	%	g/kg	g/kg	wt%
Untreated	T0	0.68±0.01	9.3	6.65±0.00	90.7	7.33±0.52	-	-
S-nZVI	T1	2.90±0.1	27.3	7.72±0.14	72.7	10.6±1.1	3.29±0.97	0.33
OSF-nZVI		2.99±0.1	28.6	7.45±0.11	71.4	10.4±1.1	3.11±0.91	0.31
S-mZVI		2.34±0.2	24.2	7.11±0.19	73.5	9.68±0.7	2.34±0.44	0.23
mZVI		9.32±0.8	49.3	9.56±0.77	50.6	18.9±1.3	11.55±1.21	1.2
S-nZVI	T2	2.16±0.1	20.4	7.70±0.06	72.5	10.6±1.1	3.29±0.97	0.33
OSF-nZVI		2.39±0.0	22.9	7.22±0.06	69.1	10.4±1.1	3.11±0.91	0.31
S-mZVI		1.35±0.0	14.0	7.21±0.04	74.5	9.68±0.7	2.34±0.44	0.23
mZVI		6.46±0.3	34.2	8.55±0.44	45.3	18.9±1.3	11.55±1.21	1.2

5.2. Solution Chemistry

5.2.1. pH

The pH in the untreated system containing artificial groundwater (AGW) and As-contaminated sediment (T0) was slightly alkaline (7.4) (Figure 7).

At uncontrolled pH (T1) compared to the untreated system (T0), the pH in AGW increased statistically significant in the S-nZVI, OSF-nZVI, and mZVI treatments (Figure 7). The highest pH was measured in the mZVI treatment (10.0), followed by the OSF-nZVI (9.4), and S-nZVI treatment (9.2). The pH in AGW in the S-mZVI treatment was 7.5 at T1, i.e. not statistically significant different from T0.

At T2, the pH in AGW of all four ZVI treatments was adjusted to field pH, i.e. pH 7.0. Figure 7 shows that, indeed, the pH of all four ZVI treatments at T2 was similar to T0 (7.2, 7.1, 6.8, 6.8 for S-nZVI, OSF-nZVI, S-mZVI, and mZVI, respectively).

The most pronounced pH difference between T1 and T2 was observed in the mZVI treatment (decrease in 3.2 pH units; Figure 7). The pH of the OSF-nZVI, S-nZVI, and S-mZVI treatment decreased by 2.3, 2.0, and 0.7 pH units from T1 to T2, respectively.

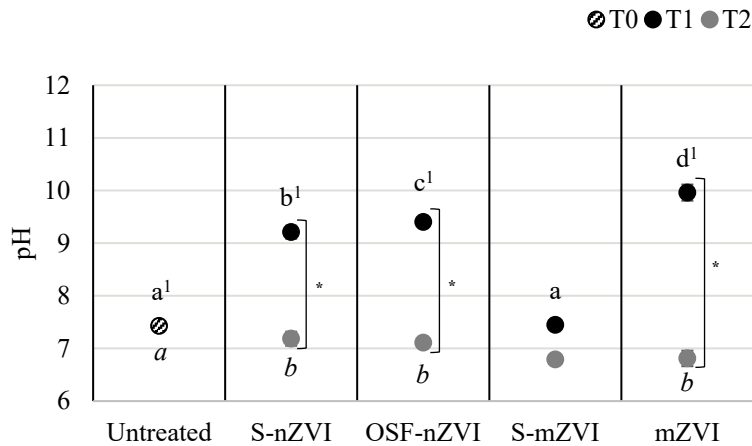


Figure 7: pH in AGW. T0: untreated Sediment. T1: uncontrolled pH. T2: pH adjusted to field pH. Values show means ($n \geq 2$). Error bars express standard deviation ($n > 2$). For S-mZVI, error bars express absolute deviation (T1, $n = 2$) and only one value is shown for T2. Statistically significant differences ($p < 0.05$) are shown for Kruskal-Wallis with post-hoc Bonferroni, and (1) one-way ANOVA with post-hoc Tukey HSD. Non-Italic letters refer to statistical differences within treatments at T1 and between T0 and T1. Italic letters refer to statistical differences within treatments at T2 and between T0 and T2. Square brackets with asterisks indicate differences between T1 and T2 proven with Kruskal-Wallis with post-hoc Bonferroni.

5.2.2. Oxidation Reduction Potential

The ORP in the untreated system containing artificial groundwater (AGW) and As-contaminated sediment (T0) was slightly negative (-5.4 mV) (Figure 8).

At uncontrolled pH (T1) compared to T0, the ORP in AGW of all four ZVI treatments decreased statistically significant (Figure 8). The lowest ORP was measured in the mZVI treatment (-295 mV), followed by the OSF-nZVI (-279 mV), the S-nZVI (-263 mV), and S-mZVI treatment (-248 mV).

At T2, the ORP in the S-nZVI, OSF-nZVI, and mZVI treatments was -136, -129, and -91 mV, respectively, which was less negative compared to T1 but still statistically significant below T0 (Figure 8). The ORP in the S-mZVI treatment changed unnotably from T1 to T2 to -219 mV and was thus below the other ZVI treatments at T2.

Comparing T2 with T1, the highest ORP increase was observed in the mZVI treatment (204 mV), followed by the OSF-nZVI (150 mV), and S-nZVI treatment (127 mV), however, no change was statistically significant (Figure 8).

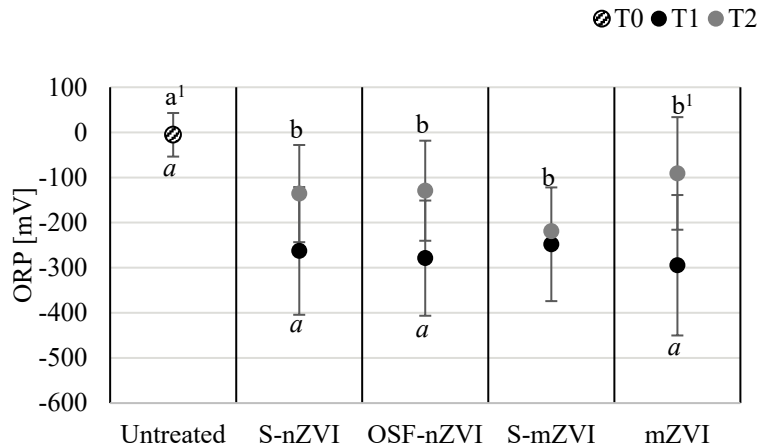


Figure 8: ORP [mV] in AGW. T0: untreated sediment. T1: uncontrolled pH. T2: pH adjusted to field pH. Values show means ($n \geq 2$). Error bars express standard deviation ($n > 2$). For S-mZVI, error bars express absolute deviation (T1, $n = 2$) and only one value is shown for T2. Significant differences ($p < 0.05$) are shown for Kruskal-Wallis with post-hoc Bonferroni, and (1) one-way ANOVA with post-hoc Tukey HSD. Non-Italic letters refer to differences within treatments at T1 and between T0 and T1. Italic letters refer to differences within treatments at T2 and between T0 and T2.

5.2.3. Dissolved Arsenic (F1)

In the untreated system containing AGW and As-contaminated sediment (T0), the dissolved As concentration (F1) was 1238 $\mu\text{g/L}$, accounting for 14.6 % of the total As in the sediment (Figure 9).

At uncontrolled pH (T1) and at pH adjusted to field pH (T2), the dissolved As concentration (F1) significantly decreased in all four ZVI treatment compared to the untreated sediment (T0).

At uncontrolled pH (T1) compared to T0, the microsorbent treatments S-mZVI and mZVI showed the highest decrease, reducing the dissolved As concentration by 99 % to 16.4 and 11.9 $\mu\text{g/L}$, respectively (Figure 9). They were followed by the OSF-nZVI, and S-nZVI treatments, which reduced the dissolved As concentration by 94 % to 73.6 $\mu\text{g/L}$ and 85 % to 183 $\mu\text{g/L}$, respectively.

At pH adjusted to field pH (T2) compared to T0, the S-mZVI treatment showed the highest decrease, reducing the dissolved As concentration by 99 % to 12.9 $\mu\text{g/L}$, followed by the OSF nZVI, mZVI, and S-nZVI treatment that reduced the dissolved As concentration by 97 % to 35.2 $\mu\text{g/L}$, 96 % to 50.2 $\mu\text{g/L}$ and 92 % to 104 $\mu\text{g/L}$, respectively (Figure 9).

At pH adjusted to field pH (T2) compared to uncontrolled pH (T1), the dissolved As concentration decreased in the nanosorbent treatments OSF-nZVI and S-nZVI, (by 38.3, and 79.3 $\mu\text{g/L}$, respectively), and increased in the mZVI treatment (by 38.3 $\mu\text{g/L}$; Figure 9). However, none of these changes were significant. The change in dissolved As concentration in the S-mZVI treatment was neglectable.

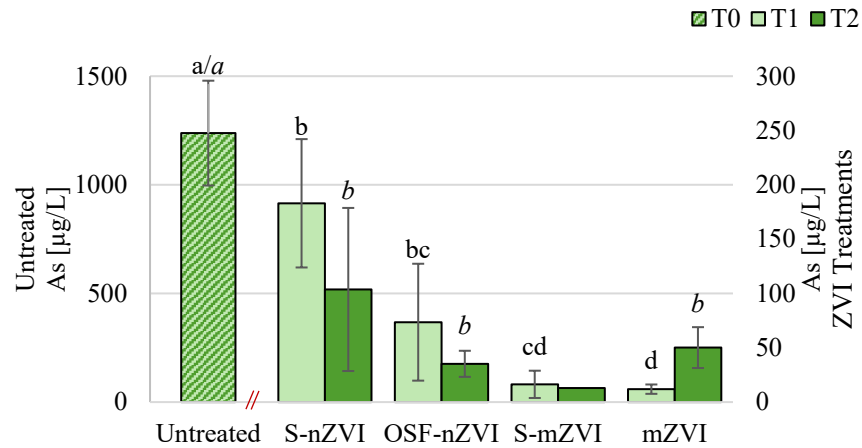


Figure 9: Dissolved As [$\mu\text{g/L}$] in AGW (F1). T0: untreated sediment. T1: uncontrolled pH. T2: pH adjusted to field pH. Values show means ($n \geq 2$). Error bars express standard deviation ($n > 2$). For S-mZVI, error bars express absolute deviation (T1, $n=2$) and only one value is shown for T2. Significant differences ($p < 0.05$) are shown for Kruskal-Wallis with post-hoc Bonferroni, and (1) one-way ANOVA with post-hoc Tukey HSD. Non-Italic letters refer to differences within treatments at T1 and between T0 and T1. Italic letters refer to differences within treatments at T2 and between T0 and T2.

5.2.4. Arsenic Speciation

Plotting the measured pH and ORP at T0, T1 and T2 in the Eh-pH speciation diagram of As shows the theoretical speciation of As at the corresponding conditions (Figure 10). It needs to be kept in mind that the As speciation may change depending on the total As concentration and the concentration and composition of the background electrolyte which is why this diagram only serves to give a rough idea of the situation (precise values for these parameters of the illustrated Eh-pH diagram could not be found in the literature). In the untreated sediment (ORP: -5 mV, pH: 7.4), the speciation of dissolved As (F1) is located on the equilibrium line between As(V) and As(III) ($\text{HAsO}_4^{2-}/\text{H}_3\text{AsO}_3$). Therefore, As(III) and As(V) are expected to occur at equal amounts. Despite the significant increase in pH (to on average 9.5) and decrease in ORP (to on average -279 mV) in the nanosorbent treatments (S-nZVI and OSF-nZVI) and in one of the microsorbent treatments (mZVI) at T1, As(III) and As(V) are expected to occur at equal amounts at these conditions. This is hence similar to the untreated sediment, with only a change in the hydrolysis species ($\text{HAsO}_4^{2-}/\text{H}_2\text{AsO}_3^-$). On the other hand, the near neutral pH (7.1) in the S-mZVI treatment at similar ORP conditions as the other ZVI treatments (-248 mV), H_3AsO_3 (As(III)) is expected to be the dominant species.

At T2, the As(III) species H_3AsO_3 is expected to be dominant in all four ZVI treatments due to lower pH (on average 7.0) while maintaining the ORP in the reducing region (on average -144 mV).

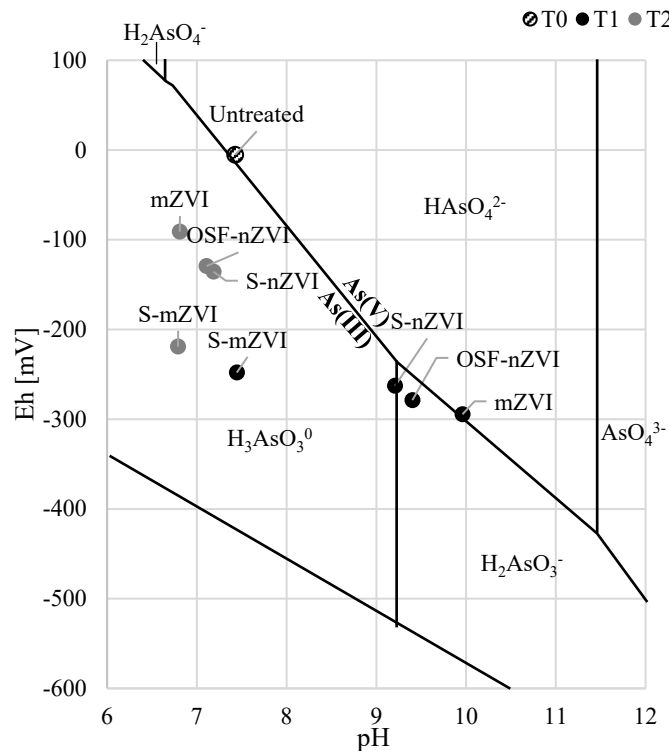


Figure 10: Measured Eh-pH data points plotted in the Eh-pH diagram for the aqueous arsenic species in the system As-O₂-H₂O at 25°C and 1 bar total pressure (adapted from Smedley and Kinniburgh (2002), p. 521).

The measured dissolved As(III) share shows that, in fact, more As(III) (984 µg/L; 80 % total dissolved As) was present in the untreated sediment than what was predicted by the Eh-pH diagram (Figure 11A, B). From T0 to T1, the measured dissolved As(III) share decreased in all four ZVI treatments to at least 26 % total dissolved As (S-mZVI), contradicting expected unchanged or increasing As(III) shares by the Eh-pH diagram. At T2 compared to T1, the As(III) share shows an increasing trend in all four ZVI treatments (except for mZVI) up to 55 % (S-mZVI), which is consistent with the decrease in pH and with the theoretical Eh-pH diagram. In the mZVI treatment, the As(III) share remains unchanged at T1 and T2 conflicting with the Eh-pH diagram. Deviations between measured and expected As speciation may be explained by limitations of ORP measurements, incomplete separation of As(III) and As(V) by the As-speciation cartridge and potential kinetically constrained redox reactions. In the four ZVI treatments, deviations may also be an indication for processes induced by sorbents that may not be directly reflected in changing ORP and pH. Due to total dissolved As concentrations below 183 µg/L in all four ZVI treatments at T1 and T2 (Figure 11B), imprecise performance of the As-speciation cartridge and analytical measurement inaccuracy may predominate.

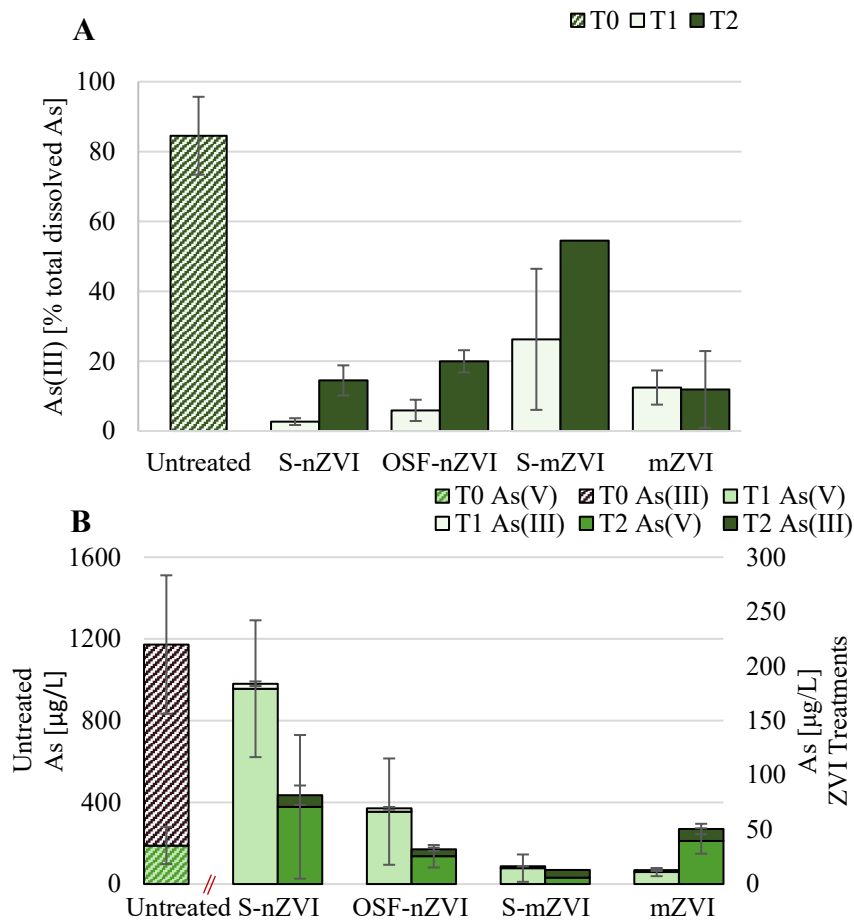


Figure 11: A: Dissolved As(III) [% total dissolved As]. B: Dissolved As(III) and As(V) [µg/L]. T0: untreated sediment. T1: uncontrolled pH. T2: pH adjusted to field pH. Values are means ($n \geq 2$). Error bars express standard deviation ($n > 2$). For S mZVI, error bars express absolute deviation (T1, $n = 2$) and only one value is available for T2.

5.2.5. Dissolved Iron (Fe_{F1})

In the untreated system containing only sediment and AGW (T0), 1.1 mg/L Fe was dissolved (Fe_{F1}), accounting for 0.1 % of the total Fe in the solid phase (Figure 12). At uncontrolled pH (T1) compared to the untreated sediment (T0), dissolved Fe concentrations of all ZVI treatments (except S-mZVI) were lower. At pH adjusted to field pH (T2) compared to T1 and T0, dissolved Fe concentrations sharply increased for all four ZVI treatments.

At T1, the dissolved Fe concentration in the S-nZVI, OSF-nZVI, and mZVI treatments was 0.05, 0.03, 0.01 mg/L (< 0 %), respectively (Figure 12). In the S-mZVI treatment, significantly more Fe was dissolved: 37.8 mg/L (2.3 %). This can be attributed to the significantly lower pH in the S-mZVI treatment (7.5) compared to the other three ZVI treatments at T1 (on average 9.5), resulting in enhanced Fe dissolution.

At T2, the dissolved Fe concentration was higher in all four treatments compared to T1 and T0, with statistical significance for the S-nZVI, OSF-nZVI, and mZVI

treatments. In the mZVI treatment, 653 mg/L Fe was dissolved. This represented 19.9 % of the total Fe and it was the highest increase from T1 to T2. In the nanosorbent treatments OSF-nZVI and S-nZVI, 141 and 128 mg/L Fe was dissolved, which accounted for 7.5 and 7.0 % total Fe, respectively. This is also a rather sharp increase from T1 to T2. In the S-mZVI treatment, 188 mg/L Fe (11.4 % total Fe) was dissolved, which was the lowest increase from T1 to T2.

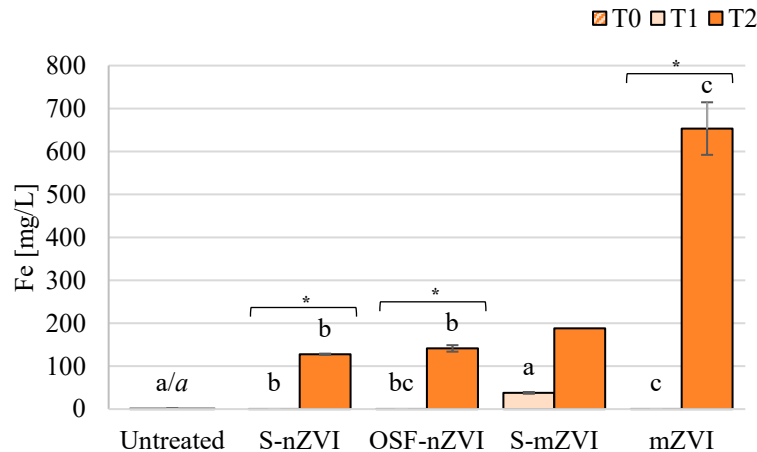


Figure 12: Dissolved Fe [mg/L] (Fe_{F1}). T0: untreated sediment. T1: uncontrolled pH. T2: pH adjusted to field pH. Values are means ($n \geq 2$). Error bars express standard deviation ($n > 2$). For S-mZVI, error bars express absolute deviation (T1, $n=2$) and only one value is shown for T2. Significant differences ($p < 0.05$) are shown for Kruskal-Wallis with post-hoc Bonferroni, and (1) one-way ANOVA with post-hoc Tukey HSD. Non-italic letters refer to differences within treatments at T1 and between T0 and T1. Italic letters refer to differences within treatments at T2 and between T0 and T2. Square brackets with asterisks indicate differences between T1 and T2 proven with Kruskal-Wallis with post-hoc Bonferroni.

5.3. Fractionation of Arsenic in the solid phase (F2-F4)

Table 9 summarises the concentration of total As and the As concentrations detected in F1 (dissolved), F2 (specifically sorbed), F3 (strongly bound to amorphous Fe) and F4 (residual) for the three different treatment scenarios: T0 (untreated sediment); T1 (ZVI treatments at uncontrolled pH); and T2 (ZVI treatments at pH adjusted to field pH). Data from dissolved As (F1) was converted to mg/kg by taking into account the L/S ratio in the batch experiments, and is displayed as a reference.

The total As concentration in the untreated sediment was 50.2 mg/kg.

The amount of specifically sorbed As (F2) in the untreated sediment was 7.4 mg/kg (14.6 %). At T1, the highest concentration of As in F2 was measured in the S-nZVI treatment (9.1 mg/kg), followed by the S-mZVI, OSF-nZVI and mZVI treatment (8.4, 6.8, 6.5 mg/kg, respectively). At T2, the highest concentration of As in F2 was observed in the S-mZVI treatment (16.3 mg/kg), followed by the mZVI, S-nZVI and the OSF-nZVI treatment (11.5, 10.7, 9.3 mg/kg, respectively).

The amount of As strongly bound to amorphous Fe (F3) in the untreated sediment was 20.4 mg/kg (40.5 %). At T1, the highest concentration of As in F3 was observed in the mZVI treatment (29.3 mg/kg), followed by the OSF-nZVI, S-nZVI, and S-mZVI treatment (28.5, 25.4, 23.6 m/kg, respectively). At T2, the highest concentration of As in F3 was observed in the OSF-nZVI treatment (31.9 mg/kg), followed by the S-nZVI, mZVI, and S-mZVI treatment (25.8, 19.6, 6.5 mg/kg, respectively).

The amount of As in the residual fraction (F4) in the untreated sediment was 15.2 mg/kg (30.3 %). At T1, the highest concentration of As in F4 was observed in the S-mZVI treatment (18.1 mg/kg), followed by the S-nZVI treatment (14.6 mg/kg), and the OSF-nZVI and mZVI treatment (14.4 mg/kg, respectively). At T2, the highest concentration of As in F4 was observed in the S-mZVI treatment (27.3 mg/kg), followed by the mZVI, S-nZVI, and OSF-nZVI treatment (18.9, 13.1, 8.8 mg/kg, respectively).

Table 9: Arsenic fractionation (F1-F4) [mg/kg]. T0: Untreated sediment. T1: uncontrolled pH. T2: pH adjusted to field pH.

Treatment	Scenario	F1		F2		F3		F4		As _{tot}	
		mg/kg	%	mg/kg	%	mg/kg	%	mg/kg	%	mg/kg	%
Untreated	T0	7.33±1.0	14.6	7.36±0.2	14.6	20.4±0.9	40.5	15.2±1.7	30.3	50.2±4.7	100
S-nZVI	T1	1.08±0.4	2.16	9.13±0.9	18.2	25.4±1.3	50.6	14.6±1.6	29.1	50.2±4.7	100
OSF-nZVI		0.44±0.3	0.87	6.83±1.2	13.6	28.5±2.2	56.8	14.4±2.5	28.7	50.2±4.7	100
S-mZVI		0.10±0.1	0.19	8.43±1.1	16.8	23.6±2.4	47.0	18.1±2.7	36.0	50.2±4.7	100
mZVI		0.07±0.0	0.14	6.48±0.8	12.9	29.3±1.7	58.3	14.4±1.9	28.6	50.2±4.7	100
S-nZVI	T2	0.61±0.4	1.22	10.7±0.0	21.2	25.8±3.0	51.4	13.1±3.0	26.1	50.2±4.7	100
OSF-nZVI		0.21±0.1	0.42	9.34±0.4	18.6	31.9±2.4	63.4	8.84±2.4	17.6	50.2±4.7	100
S-mZVI		0.08	0.15	16.3±0.7	32.5	6.50±0.9	12.9	27.3±1.1	54.4	50.2±4.7	100
mZVI		0.30±0.1	0.59	11.5±0.4	22.8	19.6±0.5	39.0	18.9±0.7	37.5	50.2±4.7	100

In order to better illustrate the changes of distribution of As in the solid phase (F2-F4) in the four ZVI treatments compared to the untreated sediment, the changes in As fractionation between the untreated sediment (T0) and the ZVI treatments at T1 and T2 are shown in Figure 13 and Figure 14. The effect of lowered pH (T2) on the ZVI sorbent performance is illustrated by the differences in As fractionation between T1 and T2 in Figure 15. Differences of dissolved As concentrations (F1) are shown as a reference.

5.3.1. Sorbent Performance at Uncontrolled pH (T1) vs. Untreated Sediment (T0)

As already shown in Figure 9, the dissolved As concentration in AGW (F1) decreased significantly in all four ZVI treatments at uncontrolled pH (T1) compared

to the untreated sediment (T0). In all four ZVI treatments, F1 decreased on average by 6.9 mg/kg (Figure 13).

The amount of specifically sorbed As (F2) increased in the S-nZVI and S-mZVI treatments by 1.8 and 1.1 mg/kg, respectively (Figure 13, F2). However, changes are not statistically significant. The change of F2 in the OSF-nZVI and mZVI treatments was neglectable.

The amount of As strongly bound to amorphous Fe (F3) increased in all four treatments. In the sulphidated treatments S-nZVI and S-mZVI, F3 increased by 5.1 and 3.3 mg/kg, respectively. In the non-sulphidated treatments OSF-nZVI and mZVI, F3 increased by 8.2 and 8.9 mg/kg, respectively. For the non-sulphidated treatments, F3 was the only fraction that increased. Overall, F3 was the solid fraction with the highest redistribution of As in all four treatments.

Redistribution of As to the residual fraction (F4) was only observed in the S-mZVI treatment (2.9 mg/kg). However, it was not statistically significant.

The total redistribution of As between all four fractions (F1-F4) from T1 to T0 was similar for all four ZVI treatments (6.9-8.9 mg/kg).

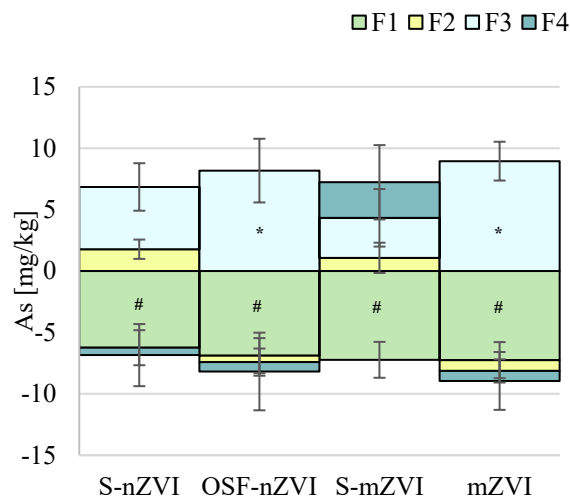


Figure 13: As fractionation change in ZVI treatments at uncontrolled pH (T1) compared to the untreated sediment (T0) illustrated as absolute difference [mg/kg] of means at T1 and T0 of each fraction. Symbols show significant differences ($p < 0.05$) of absolute values between T0 and T1 in each fraction (#: one-way ANOVA with post-hoc Tukey HSD; *: Kruskal-Wallis with post-hoc Bonferroni).

5.3.2. Sorbent Performance at pH Adjusted to Field pH (T2) vs. Untreated Sediment (T0)

As already shown in Figure 9, the dissolved As concentration in AGW (F1) decreased significantly in all four ZVI treatments at pH adjusted to field pH (T2) compared to the untreated sediment (T0). In all four ZVI treatments, F1 decreased by 6.7-7.3 mg/kg (Figure 14, F1).

The amount of specifically sorbed As (F2) at T2 compared to T0 increased in all four ZVI treatments (Figure 14, F2). The highest increase was observed in the S-

mZVI treatment (9.0 mg/kg) followed by the mZVI and S-nZVI treatment (4.1 and 3.3 mg/kg, respectively), and the OSF-nZVI treatment (2.0 mg/kg), with the first three being statistically significant.

The amount of As strongly bound to amorphous Fe (F3) increased in the nanosorbent treatments S-nZVI (5.5 mg/kg) and OSF-nZVI (11.5 mg/kg) and decreased in the S-mZVI (-13.9 mg/kg) treatment (Figure 14, F3). However, only the last two changes were statistically significant. In the S-mZVI treatment, F3 decreased by 13.9 mg/kg. The change of F3 in the mZVI treatment was neglectable.

The amount of As in the residual fraction (F4) decreased in the nanosorbent treatments and increased in the micro-sorbent treatments (Figure 14, F4). In the nanosorbent treatments S-nZVI and OSF-nZVI, F4 decreased by 2.1 and 6.4 mg/kg, respectively. However, no change was statistically significant. In the micro-sorbent treatments S-mZVI and mZVI, F4 increased by 12.1 and 3.7 mg/kg, respectively, with the former increase being statistically significant.

The total redistribution of As between all four fractions (F1-F4) was the highest in the S-mZVI treatment (21.2 mg/kg), followed by the OSF-nZVI treatment (13.5 mg/kg), and the S-nZVI and mZVI treatment (8.8 and 7.8 mg/kg, respectively).

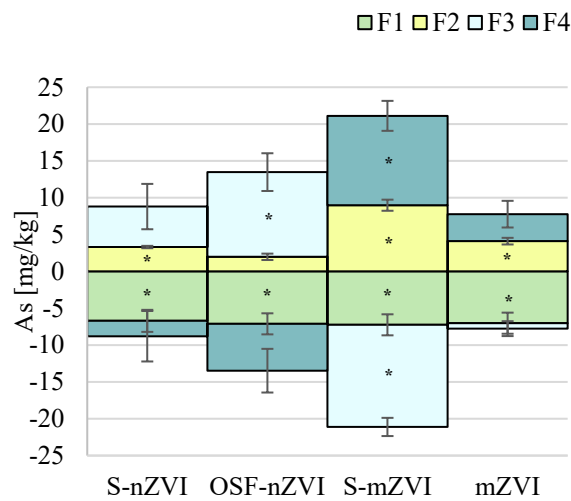


Figure 14: As fractionation change in ZVI treatments at pH adjusted to field pH (T2) compared to the untreated sediment (T0) illustrated as absolute difference [mg/kg] of means at T2 and T0 of each fraction. Asterisks show significant differences ($p < 0.05$) of absolute values between T0 and T2 in each fraction assessed with Kruskal-Wallis with post-hoc Bonferroni.

5.3.3. Sorbent Performance at pH Adjusted to Field pH (T2) vs. Uncontrolled pH (T0)

The amount of specifically sorbed As (F2) increased in all four treatments from T1 to T2 (Figure 15, F2). In the micro-sorbent treatments S-mZVI and mZVI, F2 increased significantly by 7.9 and 4.5 mg/kg, respectively. In the nanosorbent

treatments OSF-nZVI and S-nZVI, F2 increased by 0.42 and 2.5 mg/kg, respectively. However, neither of these changes were statistically significant.

The amount of As strongly bound to amorphous Fe (F3) decreased significantly in the sulphidated treatments S-nZVI and S-mZVI by 17.1 and 9.7 mg/kg, respectively (Figure 15, F3). F3 increased in the OSF-nZVI treatment by 3.3 mg/kg. However, this change was not significant. In the S-nZVI treatment, F3 changed unnotably.

The amount of As associated in the residual fraction (F4) decreased in the nanosorbent treatments and increased in the microsorbent treatments (Figure 15, F4). In the nanosorbent treatments S-nZVI and OSF-nZVI, F4 decreased by 1.5 and 5.6 mg/kg, respectively. In the microsorbent treatments S-mZVI and mZVI, F4 increased by 9.2 mg/kg and 4.5 mg/kg, respectively. However, none of these changes were statistically significant.

The total redistribution of As between all four fractions (F1-F4) was the highest in the S-mZVI treatment (17.1 mg/kg), followed by the mZVI and OSF-nZVI treatment (9.7 and 5.8 mg/kg, respectively). The total change of the As fractionation in the S-nZVI treatment was marginal (2.0 mg/kg).

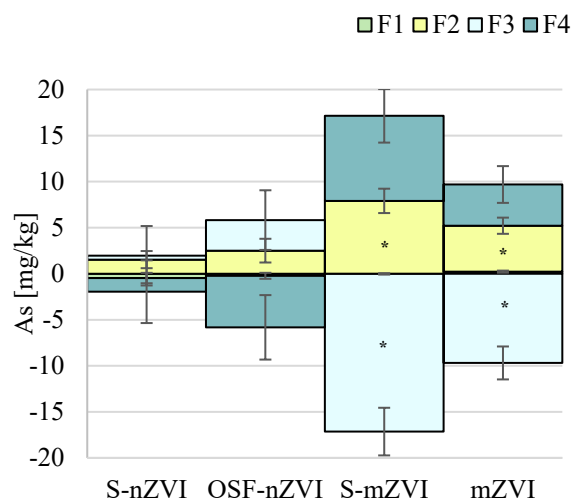


Figure 15: As fractionation change in ZVI treatments at pH adjusted to field pH (T2) compared to uncontrolled pH (T1) illustrated as absolute difference [mg/kg] of means at T2 and T1 of each fraction. Asterisks show significant differences ($p < 0.05$) of absolute values between T1 and T2 in each fraction assessed with Kruskal-Wallis with post-hoc Bonferroni.

5.4. Modelled pH-dependent Dissolved Arsenic Concentrations at Changing Redox Conditions

Dissolved As concentrations of the untreated sediment were simulated at three different ORP values, i.e., -5 mV (mean measured ORP at T0), -275 mV (mean measured ORP of all four ZVI treatments at T1), and -120 mV (mean measured ORP of all four ZVI treatments at T2) for the pH range 5-11.3 (Figure 8).

Simulations are based on pH-dependent As solubility experiments of the untreated sediment (section 4.3; for further modelling details see section 4.5).

Simulated dissolved As(V) concentrations at unspecified redox conditions are shown as a reference. Simulations of As(V) sorption using 30 % ferrihydrite from the oxalate extractable Fe of the untreated sediment, corresponded well to measured concentrations of As(V) at low pH (4-6) and high pH (9-11.3). Sorption of As(V) was somewhat overestimated by the model between pH 6-9 (see Appendix Figure 21).

Simulations at specified ORP show that with decreasing ORP, the sorption maximum of As shifts towards higher pH. At -5 mV, the As sorption maximum was simulated between 7 and 7.5. At -120 mV, it shifted towards pH 8.3 and at -275 mV towards pH 8.9.

The concentration of dissolved As measured in the untreated sediment (T0) was markedly higher than the simulated concentrations when using ORP -5 mV and corresponded more to simulations at -120 and -275 mV. This indicates that either other processes than sorption control As solubility in the untreated sediment or that the ORP of T0 was overestimated. This is in agreement with the As(III) share in the untreated sediment being higher than predicted by the Eh-pH diagram (see 5.2.4).

All treatments at T1 and T2 showed markedly lower As concentrations compared to the simulated ones at -275 and -120 mV. This indicates that the decrease in dissolved As concentrations after ZVI sorbent addition was only caused to a minor extent by the pH and ORP changes induced by ZVI sorbent addition, and to a major extent by addition of new binding sites by the ZVI sorbents and thus increased As immobilisation.

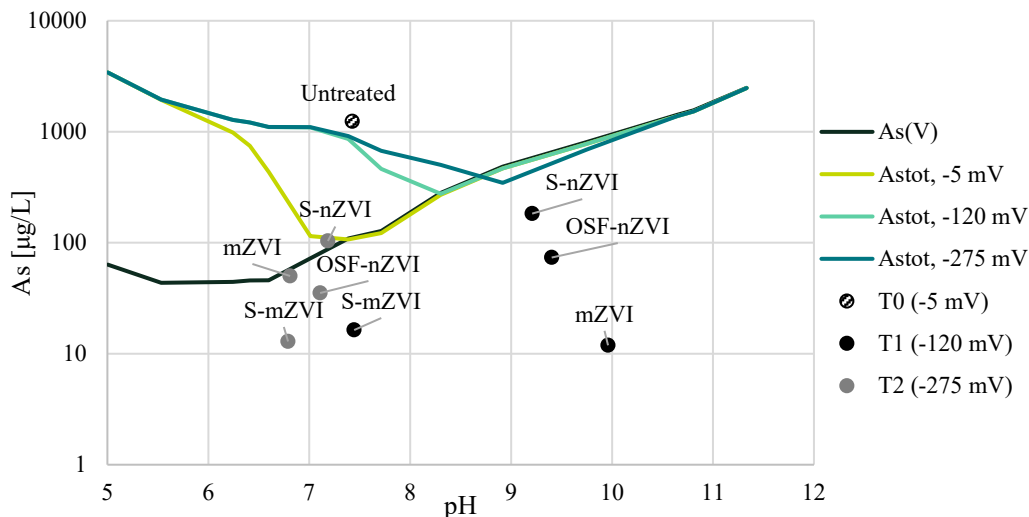


Figure 16: Simulated pH-dependent dissolved As concentrations of the untreated sediment at -5, -120, and -275 mV. Simulations were conducted with Visual Minteq ver. 3.1. Simulated dissolved As(V) and dissolved total As (As_{tot}) concentrations at T0, T1, and T2 are displayed as a reference.

6. Discussion

6.1. Field Conditions

Total concentrations of all measured elements in the untreated sediment (i.e., Ba, Cd, Co, Cr, Cu, Hg, Ni, Pb, V, Zn), except for As, were below soil guideline values for sensitive land use set by the Swedish Environmental Protection Agency (SEPA, 2016; precise values see Appendix Table 14). The total As concentration of the sediment (50.2 mg/kg) was 5 times higher than the threshold value for Sensitive Land Use of 10 mg/kg (SEPA, 2016). This indicates that the As contamination may pose a risk to humans and the environment. Even though the guidelines apply predominantly for soils above the groundwater surface, they serve as a qualitative reference to assess the contamination status due to lacking guideline values for soils below the groundwater surface (i.e., sediments).

Fractionation of As in the untreated sediment indicated that it is predominantly strongly bound to amorphous Fe (F3, 40.5 %) and to the residual fraction (F4, 30.3 %). The residual fraction may comprise association of As with e.g. organic matter or sulphide compounds, however it is assumed that due to the high affinity of As towards Fe compounds, F4 is dominated by As associated with crystalline Fe-oxides (Loeppert *et al.*, 2002). Danila *et al.* (2020) conducted a sequential extraction of a CCA-contaminated soil targeting amongst others amorphous and crystalline Fe-oxides as well as organic matter and sulphide compounds. They showed that indeed As predominates in the former two fractions. Therefore, it can be assumed that ca. 70 % of As (F3+F4) is strongly bound to crystalline and amorphous Fe compounds in the sediment. The remaining 30 % are equally comprised by dissolved As (F1) and specifically sorbed As (F2).

The concentration of dissolved As (1238 µg/L) of the untreated sediment sample in AGW largely exceeds the As drinking water threshold limit of 10 µg/L indicating the need for remediation action (WHO, 2017). Moreover, the equally high concentration of specifically sorbed As (F2) may become dissolved by changing conditions such as pH, ORP, dissolved anions or natural organic matter (Caporale *et al.*, 2013).

6.2. Changing Conditions Induced by Sorbents

Significantly increasing pH upon ZVI addition was reported in various field trials (Zhang, 2003; Henn and Waddill, 2006; Wei *et al.*, 2010; Otaegi and Cagigal, 2017). A pH increase of 2-3 units from neutral to alkaline pH, as shown here, is typical for ZVI remediation (Zhang, 2003). The opposite trend is observed for ORP after ZVI addition, i.e., with ORP decreasing to values below zero, typically by 300 to 600 mV. The measured ORP decrease in the experiments from T0 to T1 for all four ZVI treatments of on average 270 mV is at the lower end of this range (Wei *et al.*, 2010; Otaegi and Cagigal, 2017).

An increasing pH and a decreasing ORP can be explained by the corrosion of ZVI that takes place after suspension in water according to equation (2) (Ponder *et al.*, 2000). In the present study, the concentration of dissolved oxygen was <1 mg/L which is typical for anoxic aquifers (Appendix Table 11). In those cases, H₂O and As serve as the main electron acceptors (Wei *et al.*, 2010).

There were no statistically significant differences in ORP between the four ZVI treatments at uncontrolled pH (T1) and pH adjusted to field pH (T2) (Figure 8). This indicates that expected differences in the Fe corrosion of the four ZVI sorbents were not reflected in the ORP.

On the contrary, there were statistically significant differences in pH between the four ZVI sorbents at uncontrolled pH (T1). The S-mZVI treatment did not induce a significant pH change at uncontrolled pH (T1) compared to the untreated sediment (T0) whereas all other treatments significantly increased the pH (on average to pH 9.5) (Figure 7). This may indicate different processes induced by different sorbents, e.g., varying extent of Fe corrosion or matrix effects. The missing pH increase in the S-mZVI treatment at T1 may be explained by reduced corrosion of the Fe(0) core as a result of the sulphidation (Singh *et al.*, 2021). Further, the S-mZVI sorbent was dissolved in 40-50 % glycerine whereas the other ZVI sorbents were dissolved in water (S-nZVI, OSF-nZVI) or obtained as a powder (mZVI) (Table 11) which may have resulted in different matrix effects. Interestingly, a significant pH increase was observed in the S-nZVI treatment, which contained sulphidated ZVI sorbents, too. This may be explained by the different coating procedure, i.e., Na₂S was used for S-nZVI, and FeS was used for S-mZVI (Regenesis, no date; Brumovský *et al.*, 2020). Consequently, coating with Na₂S does not seem to sufficiently prevent corrosion of the Fe core.

All four ZVI sorbents increased the amount of amorphous Fe (F3) by on average 2.1 g/kg in the S-nZVI, OSF-nZVI, and S-mZVI treatment and by 8.6 g/kg in the mZVI treatment at uncontrolled pH (T1) compared to the untreated sediment (T0) (Table 8). This accounts for on average 72 % amorphous Fe (F3) of each ZVI sorbent, indicating the formation of amorphous Fe-(hydr)oxides such as ferrihydrite caused by the corrosion of the Fe(0) core (Shi *et al.*, 2015). This was also observed in other ZVI-amended soils, where 77 % of the added ZVI sorbent was observed as

amorphous Fe six years after application (Tiberg *et al.*, 2016). Since less than 2.3 % of the total Fe was dissolved in all four ZVI treatments at T1 (Figure 12), the remaining Fe can be almost exclusively assigned to crystalline Fe (F4). This means that on average 28 % of the added Fe by ZVI sorbents was still present as Fe(0) at T1. At pH adjusted to field pH (T2), on average 12 % of the total Fe was dissolved (Figure 12), and the concentration of amorphous Fe (F3) decreased to on average 45 % for all four ZVI sorbents whereas the concentration of crystalline Fe (F4) unnotably changed (average 22.7 % for all four ZVI sorbents) (Table 8). This indicates dissolution induced by acidification of previously formed amorphous Fe corrosion products for all four ZVI sorbents. Interestingly, the previously concluded difference in corrosion of the S-mZVI treatment compared to the other three ZVI treatments was not reflected in the measured Fe concentrations. Consequently, other processes such as matrix effects may explain the differences in pH of the ZVI treatments or differences in corrosion of the Fe(0) core were not sufficiently reflected in the extractions.

In order to clarify this issue, further experiments that analyse the electronic structure and surface morphology of the ZVI sorbents, e.g., transmission electron microscopy or synchrotron-based X-ray absorption measurements are required.

6.3. Arsenic Removal Efficiency

All four ZVI sorbents successfully decreased dissolved As concentrations (F1) by at least 85 % at T1 (i.e. uncontrolled pH) with slightly changing As removal efficiencies at T2 (i.e. pH adjusted to field pH) (Figure 9). S-mZVI showed the highest removal efficiency (99 %) at T1 and T2. In general, experiments conducted at T1 were assumed to reflect the short-term sorbent performance, i.e., during the first 30 days after theoretical field injection (Wei *et al.*, 2010; Otaegi and Cagigal, 2017). Experiments conducted at T2 aimed at reflecting long-term sorbent performance, assuming that the pH of the aquifer following sorbent injection tends to drift back to field pH over time (Otaegi and Cagigal, 2017). Therefore, it can be concluded that all four ZVI sorbents significantly decreased dissolved As concentrations (F1) in the short-term (T1) and in the long-term (T2).

S-nZVI showed a lower As removal efficiency (on average 89 %) than OSF-nZVI (on average 96 %) at T1 and T2 which contradicts findings reported in the literature. For instance, Singh *et al.* (2021) and Wu *et al.* (2018) showed markedly increased As(III) removal efficiencies of S-nZVI compared to nZVI under anoxic conditions. However, in both experiments, “regular” nZVI particles were used. On the contrary, in our experiments, oxidic-shell-free particles were used that lack an oxidic shell prior to As removal experiments (see section 4.2.1). These particles show significantly improved As removal efficiencies at anoxic conditions compared to “regular” nZVI particles (Tuček *et al.*, 2017; Kašlík *et al.*,

2018). Brumovský *et al.* (2020, 2021) compared the remediation of trichlorethylene (TCE) and Cr(VI) at anoxic, idealised, and simulated field conditions of oxidic-shell-free nZVI (NANOFER 25P from NanoIron) and S-nZVI (NANOFER 25DS; same as in the experiments of the thesis) and showed increased TCE removal for S-nZVI particles. This indicates that As(III) removal may show opposing trends with increased removal for OSF-nZVI compared to S-nZVI. However, measured dissolved As concentrations (F1) in the S-nZVI and OSF-nZVI treatment at T1 and T2 showed a high standard deviation and were not statistically different (Figure 9) which indicates the need for further measurements with more replicates in order to enable a profound data analysis.

The microsorbents S-mZVI and mZVI showed the same As removal efficiency (99 %) at T1. At T2, S-mZVI showed an increased As removal efficiency (99 %) compared to mZVI (96 %) at T2. This indicates that for microsorbents, sulphidation does not influence the As removal efficiency in the short-term (T1). In the long-term (T2), the decrease in As removal efficiency of non-sulphidated microsorbents (mZVI) may be explained by enhanced Fe dissolution (19.9 %) in the mZVI treatment compared to the S-mZVI treatment (11.4 %). Consequently, already immobilised As may be remobilised by dissolution of binding sites. Gu *et al.* (2017) compared the TCE remediation of mZVI particles and S-mZVI particles (with homogeneously distribution of Fe and S within the S-mZVI particles as compared to the core-shell structure of the S-mZVI particles in this study) at anoxic conditions at pH 7 and showed significantly increased remediation with S-mZVI. They attributed this to decreased hydrolysis of water and thus increased electron efficiency of the S-mZVI particle towards contaminant removal. Wu *et al.* (2018) explained increased As(III) removal efficiency of S-nZVI compared to nZVI particles with increasing surface roughness and shell thickness and thus increased binding sites for As removal. This may represent additional explanations for the increased performance of S-mZVI compared to S-nZVI at T2. Interestingly, both studies contradict the experimental data of this study. Even though, both studies used altered particles and conditions compared to the ones in the thesis they serve as a general reference as no studies have been conducted comparing microsized sulphidated and non-sulphidated ZVI sorbents used in this study. Missing increased As removal efficiency in the S-mZVI treatment compared to the mZVI treatment may be explained by the application of a 5 times increased Fe dose in the mZVI treatment. Consequently, the increased supply of binding sites for the immobilisation of As in the mZVI treatment may have overshadowed the benefits of the sulphidation in the S-mZVI treatment.

The increased As removal efficiency of microsorbents (99 % for both) compared to nanosorbents (on average 90 %) at T1 contradicts findings reported in the literature. Indeed, Danila *et al.* (2020) showed increased As removal efficiencies of nZVI compared to mZVI in a CCA contaminated soil. The measured differences

may be explained by formation of aggregates of the two nanosorbents at given conditions which lead to a reduced reactive surface area and thus a reduced As removal efficiency in the nanosorbent treatments compared to the micro-sorbent treatments. Indeed, it was observed in previous studies that the used S-nZVI particles (NANOFER 25DS) form 1 μm aggregates in natural groundwater and 4 μm aggregates in the supplied slurry (Brumovský *et al.*, 2021). Similarly, Schmid *et al.* (2015) stated formation of 4 μm aggregates in the supplied slurry of used OSF nZVI particles (NANOFER 25). However, for a more profound statement, particle size measurements of the used ZVI sorbents at solution conditions applied in the present study need to be conducted.

Additionally, differences in As removal efficiency of un-sulphidated nano- and micro-sorbents OSF nZVI and mZVI may be explained by the ca. 4 times increased Fe dosage of mZVI compared to OSF-nZVI (Table 8). However, it needs to be kept in mind that OSF-nZVI have a higher reactive surface area compared to mZVI (>25, 5.15 m^2/g , respectively).

Differences in As removal efficiency of sulphidated nano- and micro-sorbents S-nZVI and S-mZVI may be further explained by the different coating processes. As it was stated by the supplier, S-nZVI were coated with Na_2S and S-mZVI were coated with FeS (Regenesis, no date; Brumovský *et al.*, 2020). This may lead to physical restriction of the Fe core of S-nZVI which may impair the As removal efficiency. Nevertheless, Brumovský *et al.* (2020) have shown the formation of amorphous FeS sheets on the surface of the Fe(0) core immediately after preparation. Consequently, the impact of differences in S coating on the As removal experiments needs to be evaluated with further experiments such as analysis of the electronic structure and surface morphology of the S-ZVI particles.

The increase in As removal efficiency of nanosorbents S-nZVI and OSF-nZVI at controlled pH (T2) compared to uncontrolled pH (T1) support findings reported in the literature. For instance, Tuček *et al.* (2017) and Wu *et al.* (2018) showed that more dissolved As is removed by OSF-nZVI and S-nZVI at pH 7 compared to pH 9, respectively. This can be possibly explained by reduced corrosion of the Fe(0) core and thus reduced formation of sorption sites, reduced sorption due to increased electrostatic repulsion of As(III) and ZVI sorbents, and decreased reduction of As and thus formation of immobile As(0) phases (Bang *et al.*, 2005; Tuček *et al.*, 2017; Wu *et al.*, 2018)

Despite the significant decrease in dissolved As concentrations (F1) in the nanosorbent treatments S-nZVI and OSF-nZVI at T1 and T2 to on average 144 and 55 $\mu\text{g}/\text{L}$, respectively, they still strongly exceeded the drinking water threshold for As (10 $\mu\text{g}/\text{L}$; WHO, 2017). Dissolved As concentrations of micro-sorbent treatments S-mZVI and mZVI marginally exceeded 10 $\mu\text{g}/\text{L}$ at T1 (13 and 12 $\mu\text{g}/\text{L}$, respectively). Nonetheless, the mZVI treatment markedly exceeded dissolved As concentrations at T2 (50 $\mu\text{g}/\text{L}$).

However, the Dutch intervention values for As in groundwater (60 µg/L) which apply for the assessment of contaminated groundwater in Sweden, were not exceeded in the two micro-sorbent treatments (S-mZVI and mZVI) (VROM, 2000). Concentrations above this threshold indicate a serious contamination of the groundwater and thus a risk of harmful effects to the environment and humans (INSURE, 2017). Thus, a serious contamination of the groundwater can be excluded by treating the aquifer with both micro-sorbents S-mZVI and mZVI.

6.4. Arsenic Immobilisation Mechanisms

6.4.1. Uncontrolled pH (T1)

Even though it is expected that changing pH and ORP conditions induced by ZVI addition at the simulated short-term scenario (uncontrolled pH, T1) may change the As speciation and thus mobilise As, it is assumed that predominantly the amount of dissolved As at T0 reacted with the sorbents. This can be supported by looking at the modelling results (Figure 16) and the As redistribution between all four fractions (F1-F4) from T0 to T1 (Figure 13). Figure 16 indicates that the dissolved As concentration (F1) in the untreated system (T0) is expected to slightly decrease or remain similar due to changing pH and ORP conditions induced by the ZVI sorbents at T1 (7.5 for S-mZVI and on average 9.5 for the other three ZVI sorbents, ca. -275 mV for all four ZVI sorbents) regardless of the addition of new binding sites by the ZVI sorbents. Therefore, no new solubilisation of As from the sediment is expected from T0 to T1. Further, the redistribution of As towards the solid fractions (F2-F4) at T1 (on average 7.8 mg/kg) corresponds in all four ZVI treatments to the dissolved As concentration (F1) in the untreated system at T0 (7.3 mg/kg). This may either be caused by immobilisation of As by pre-existing sediment sites or new binding sites added via sorbents. Immobilisation processes with pre-existing sediment sites are assumed to be dominated by sorption, i.e. specifically sorbed As (F2), since time-spans longer than the ones applied in the experiments (max. 66 days) are required for As to form stronger bonds with sediment components. Therefore, the increase in the As share in F2 can be attributed to both sorption onto the sediment or the sorbents. However, the observed increase in the share of As in F3 and F4, i.e. As bound to amorphous Fe and in the residual fraction, is assumed to be attributed solely to interactions with ZVI sorbents.

Surprisingly, only a minor change in specifically sorbed As (F2) was observed for the sulphidated treatments S-nZVI and S-mZVI, whereas no change was observed for the non-sulphidated treatments OSF-nZVI and mZVI at T1. This contradicts literature findings which showed that sorption of As to ZVI sorbents is one of the dominant immobilisation pathways (Wu *et al.*, 2018; Wang *et al.*, 2021).

In all four ZVI treatments, As was predominantly immobilised by binding strongly onto amorphous Fe (F3). This may indicate either occlusion in or coprecipitation with amorphous Fe (Keon *et al.*, 2001). In fact, it was stated in numerous studies that coprecipitation of As(III) with ZVI particles by formation of Fe-As-hydroxides was a dominant pathway (Lackovic *et al.*, 2000; Yan, *et al.*, 2012; Li *et al.*, 2014). This is also supported by the increasing share of amorphous Fe (F3) by addition of ZVI sorbents (Table 8).

In the S-mZVI treatment, besides an increasing F3 share, As in the residual fraction (F4) increased. This may indicate formation of either strong bonds with crystalline Fe (F4), or, more likely, formation of As sulphides. Indeed, formation of As₂S₃ was observed in experiments with As(III) and S-nZVI as well as mackinawite (FeS) (Wolthers *et al.*, 2005; Singh *et al.*, 2021). The dissolved sulphide concentration was below the detection limit (<10 µg/L) in the S-mZVI treatment at T1 (Appendix Table 15). This may support the hypothesis of the formation of solid S compounds such as As-sulphides with the FeS core. On the other hand, this could also indicate missing dissolution of the FeS core and thus missing reaction of dissolved S²⁻ with As. In order to finally clarify the formation of As sulphides, further experiments involving synchrotron-based X-ray absorption measurements are required.

Wu *et al.* (2018) conducted a sequential extraction of an anoxic system containing As(III) and nZVI as well as S-nZVI, respectively, and observed a decrease in As associated in the residual fraction (F4) and an increase in specifically sorbed As (F2) and As strongly bound to amorphous Fe (F3) in the S-nZVI compared to the nZVI treatments, respectively. A similar trend for F2 was observed in this study when comparing the sulphidated and non-sulphidated ZVI treatments. However, F3 shows an opposing trend as described by Wu *et al.* (2018) with an increasing F3 share in the non-sulphidated ZVI treatments compared to the sulphidated ZVI treatments. But, as it was mentioned earlier, Wu *et al.* (2018) used “regular” nZVI compared to oxidic-shell-free and micro-sized ZVI in this study, which may lead to altering immobilisation processes.

6.4.2. pH Adjusted to Field pH (T2)

Figure 16 indicates that the dissolved As concentration (F1) in the untreated system is expected to increase slightly or remain similar from pH and ORP at T1 (7.5 for S-mZVI and ca. 9.5 for the other three ZVI sorbents, ca. -275 mV for all four ZVI sorbents) to pH and ORP at T2 (ca. 7.0, and -120 mV for all four ZVI treatments) regardless of the addition of new binding sites by the ZVI sorbents. Therefore, minor new solubilisation of As from the sediment is expected from T1 to T2. Consequently, redistribution of As in the solid phase (F2-F4) from T1 to T2 can be attributed to a smaller extent to redistribution of As in the sediment and to a greater extent to redistribution of As on the binding sites of the ZVI sorbents.

From T1 to T2, no major As redistribution in the solid phase (F2-F4) in the S-nZVI treatment was assessed (Figure 15). This supports the assumption that only minor remobilisation of As from the sediment induced by changing ORP and pH conditions from T1 to T2 occurs. In the OSF-nZVI treatment, only minor changes were assessed in the As fractionation in the solid phase (F2-F4) from T1 to T2. Therefore, it can be concluded that nanosorbents OSF-nZVI and nZVI were not significantly affected by the lowering of the pH to field pH. This may indicate that equilibrium conditions were achieved in the nanosorbent treatments at T1 and that the As immobilisation of the nanosorbents was not affected by acidification simulating long-term sorbent performance.

In the micro-sorbent treatments S-mZVI and mZVI significantly changing As fractionation was observed from T1 to T2 (17.1, 9.7 mg/kg, respectively; Figure 15). This may indicate that equilibrium conditions were not achieved in the micro-sorbent treatments during the experimental timeframe (max. 66 d) and that the As immobilisation of the micro-sorbents was affected by acidification simulating long-term sorbent performance.

Danila *et al.* (2020) simulated nZVI and mZVI sorbent ageing by heating ZVI treated mining-contaminated soil samples at 500 °C for 1 h in order to accelerate the formation of crystalline Fe compounds. It was observed that more As was dissolved and exchangeable in both sorbent treatments due to the release of As bound to amorphous Fe. The effect was more pronounced for nZVI compared to mZVI amended soil due to enhanced crystallisation of amorphous Fe in the nZVI treatment. This contradicts the results of this study which showed that nanosorbents were more stable in the simulated long-term scenario (T2) compared to micro-sorbents. However, Danila *et al.* (2020) focused simulation of long-term sorbent performance on the composition of the solid Fe compounds and not on the pH as in the present study. Consequently, further experiments altering additional parameters of the treatment systems are required to draw final conclusions on the long-term behaviour of the four ZVI sorbents.

In the S-mZVI treatment at T2, the total redistribution of As between all four fractions (F1-F4; 17.1 mg/kg) significantly exceeded the total redistribution of As at T1 (7.2 mg/kg) (Figure 15). This indicates possible As redistribution in the sediment in the S-mZVI treatment at T2 additionally to redistribution of As on the S-mZVI sorbent surfaces. This is surprising since the pH decrease in the S-mZVI treatment from T1 to T2 was marginal (0.7 pH-units, Figure 7) and no redistribution of As in the sediment was observed for the nanosorbent treatments at similar pH and ORP conditions than S-mZVI at T2. In the S-mZVI treatment at T2, As was redistributed from being strongly bound to amorphous Fe (F3) to specifically sorbed As (F2) and As associated in the residual fraction (F4) to a similar extent (7.9 and 9.2 mg/kg, respectively). An increased As share in the residual fraction may be explained by increasing formation of As sulphides with the FeS shell of the

S-mZV sorbent as indicated at T1 (see section 6.4.1) (Wolthers *et al.*, 2005; Singh *et al.*, 2021). The increased F2 As share may be explained by redistribution of As in the sediment from being strongly bound to amorphous Fe (F3) towards specifically sorbed As (F2). This indicates that conditions induced by S-mZVI at T2 shift As fractionation in the sediment towards a more available fraction (F3 to F2). However, further experiments quantifying the binding of As to sediment and sorbent compounds are required (e.g. involving synchrotron-based X-ray absorption measurements) in order to finally clarify the processes induced by acidification in the S-mZVI treatment.

In the mZVI treatment at T2, the amount of As redistribution between all four fractions (F1-F4) corresponded well to the As redistribution at T1 (9.7 and 8.9 mg/kg, respectively). This indicates redistribution of As on the mZVI sorbent surfaces. Interestingly, As co-precipitated with amorphous Fe (F3) at T1 is redistributed to a similar extent to specifically sorbed As (F2) and As associated in the residual fraction (F4) (4.5 and 5.0 mg/kg, respectively). This indicates that the pH decrease (T2) caused remobilisation of As bound on the mZVI sorbent (F3 to F2). On the other hand, the pH decrease (T2) caused a stronger immobilisation of As (F3 to F4). This may indicate the formation of recalcitrant phases such as an intermetallic structure with the Fe(0) core or As(0) between the oxidic shell and the Fe(0) core as observed in experiments with As(III) and nZVI and OSF-nZVI under anoxic conditions (Yan, Vasic, *et al.*, 2012; Tuček *et al.*, 2017; Singh *et al.*, 2021). Formation of this phase only at T2 can be explained by the need of protons for the reduction of As(III) under anoxic conditions (Tuček *et al.*, 2017). Thus, Tuček *et al.* (2017) observed significantly decreasing As(III) removal efficiencies with OSF-nZVI at pH>7 under anoxic conditions and explained them with a limited supply of protons. Interestingly, this trend was not indicated in the OSF-nZVI treatment at T2 which corresponded well to the experiments conducted by (Tuček *et al.*, 2017). Further, Yan *et al.* (2012) only observed As(III) reduction with nanosized but not microsized ZVI sorbents. In order to finally clarify the formation of recalcitrant As phases in the mZVI treatments at T2, further experiments involving synchrotron-based X-ray absorption measurements are required.

6.5. Assessment of the Overall Sorbent Performance

In order to assess the suitability of the four ZVI sorbents used in this study for the remediation of the As-contaminated anoxic aquifer in Hjärtevad, factors governing the performance of the ZVI sorbents were defined (Table 10), namely As removal efficiency, As immobilisation strength, stability against changing conditions (i.e. pH adjustment to field pH; T1 to T2), and pH perturbation induced by ZVI addition. The impact of each factor was assessed for each of the four ZVI sorbents for the two different remediation scenarios: uncontrolled pH (T1) and pH adjusted to field

pH (T2), except for stability. The importance of the individual factors on the overall sorbent performance increases from left to right (Table 10) and performance of each ZVI sorbent for each factor was assessed in relation to the other ZVI sorbents in three categories: red, indicating lowest performance; yellow, indicating moderate performance; green, indicating highest performance. Table 10 indicates that S-mZVI showed the best overall performance of all four ZVI sorbents, in particular in terms of As removal efficiency, As immobilisation strength and pH perturbation. However, the S-mZVI treatment was the treatment with the lowest stability against changing conditions induced by pH adjustment to field pH (T2). Therefore, further experiments assessing the long-term performance of S-mZVI may be required in order to finally validate the overall suitability of the sorbent. mZVI showed an overall moderate performance with a high As removal efficiency at T1, a high As immobilisation strength at T2, a moderate As removal efficiency at T2, and a moderate stability against changing conditions. OSF-nZVI and S-nZVI were assessed as the least suitable sorbents with only one factor showing highest performance, namely high stability against pH decrease. However, all ZVI sorbents significantly decreased dissolved As concentration in the short-term (T1) and the long-term (T2) and evaluation of the overall best performance was solely based on comparison between the four ZVI sorbents used in the present study. In order to finally assess the most suitable ZVI sorbent for in-situ field application in the anoxic aquifer in Hjärtevad, additional factors such as mobility and costs need to be considered, too.

Table 10: Assessment of the overall sorbent performance of all four ZVI sorbents in relation to each other based on selected factors. T1: uncontrolled pH. T2: pH adjusted to field pH. Red: lowest performance; Yellow: moderate performance; Green: highest performance.

Treatment	As Removal Efficiency ¹		As Immobilisation Strength ²		Stability ³	pH Perturbation ⁴
	T1	T2	T1	T2	T1→T2	T1
S-nZVI	●	●	●	●	●	●
OSF-nZVI	●	●	●	●	●	●
S-mZVI	●	●	●	●	●	●
mZVI	●	●	●	●	●	●

¹: Higher As removal efficiency indicates better sorbent performance. ²: Immobilisation strength was assessed by immobilisation in F4, higher As immobilisation strength indicates better sorbent performance. ³: Stability against changing conditions (i.e. acidification), higher stability indicates better sorbent performance. ⁴: Lower pH perturbation relative to the untreated sediment (T0) indicates better sorbent performance.

7. Conclusions

- Micro- and nanosized, sulphidated and non-sulphidated zerovalent iron sorbents are suitable for the remediation of arsenic under anoxic conditions
- Arsenic is mainly immobilised by formation of coprecipitates (Fe-As-hydroxides) by reaction with zerovalent iron sorbents
- Acidification does not significantly impact the arsenic removal efficiency of zerovalent iron sorbents
- Arsenic immobilisation strength of nanosized zerovalent iron sorbents is not affected by acidification
- Arsenic immobilisation strength of microsized zerovalent iron sorbents is affected by acidification
- S-mZVI is the most suitable zerovalent iron sorbent for the remediation of the As-contaminated anoxic aquifer in Hjärtevad

Nevertheless, some limitations of the present study need to be kept in mind and further experiments for a more profound data interpretation may be required. These involve mainly synchrotron-based X-ray absorption measurements in order to validate the assumptions drawn from the extraction data, adjustment of additional parameters in order to better simulate long-term sorbent performance (e.g., increase in shaking time after acidification), and application of further experiments at conditions closer to the field conditions (e.g., lowering of the L/S ratio).

References

- Ahmad, A. and Bhattacharya, P. (2019) 'Arsenic in Drinking Water: Is 10 $\mu\text{g/L}$ a Safe Limit?', *Current Pollution Reports*, 5(1), pp. 1–3. doi: <https://doi.org/10.1007/s40726-019-0102-7>.
- Amstaetter, K. *et al.* (2010) 'Redox Transformation of Arsenic by Fe(II)-Activated Goethite ($\alpha\text{-FeOOH}$)', *Environmental Science & Technology*, 44(1), pp. 102–108. doi: <https://doi.org/10.1021/es901274s>.
- Bae, S. and Hanna, K. (2015) 'Reactivity of Nanoscale Zero-Valent Iron in Unbuffered Systems: Effect of pH and Fe(II) Dissolution', *Environmental Science & Technology*, 49(17), pp. 10536–10543. doi: <https://doi.org/10.1021/acs.est.5b01298>.
- Bang, S. *et al.* (2005) 'Chemical reactions between arsenic and zero-valent iron in water', *Water Research*, 39(5), pp. 763–770. doi: <https://doi.org/10.1016/j.watres.2004.12.022>.
- BANG, S., KORFIATIS, G. and MENG, X. (2005) 'Removal of arsenic from water by zero-valent iron', *Journal of Hazardous Materials*, 121(1–3), pp. 61–67. doi: <https://doi.org/10.1016/j.jhazmat.2005.01.030>.
- Bowell, R. J. *et al.* (2014) 'The Environmental Geochemistry of Arsenic -- An Overview --', *Reviews in Mineralogy and Geochemistry*, 79(1), pp. 1–16. doi: <https://doi.org/10.2138/rmg.2014.79.1>.
- Brumovský, M. *et al.* (2020) 'Core–Shell Fe/FeS Nanoparticles with Controlled Shell Thickness for Enhanced Trichloroethylene Removal', *ACS Applied Materials & Interfaces*, 12(31), pp. 35424–35434. doi: <https://doi.org/10.1021/acsami.0c08626>.
- Brumovský, M. *et al.* (2021) 'Sulfidated nano-scale zerovalent iron is able to effectively reduce in situ hexavalent chromium in a contaminated aquifer', *Journal of Hazardous Materials*, 405, p. 124665. doi: <https://doi.org/10.1016/j.jhazmat.2020.124665>.
- Caporale, A. G. *et al.* (2013) 'Effect of competing ligands on the sorption/desorption of arsenite on/from Mg-Fe layered double hydroxides (Mg-Fe-LDH)', *Chemical Engineering Journal*, 225, pp. 704–709. doi: <https://doi.org/10.1016/j.cej.2013.03.111>.
- Cundy, A. B., Hopkinson, L. and Whitby, R. L. D. (2008) 'Use of iron-based technologies in contaminated land and groundwater remediation: A review', *Science of the Total Environment*, 400, pp. 42–51. doi: <https://doi.org/10.1016/j.scitotenv.2008.07.002>.
- Danila, V. *et al.* (2020) 'Immobilisation of metal(loid)s in two contaminated soils using micro and nano zerovalent iron particles: Evaluating the long-term stability', *Chemosphere*, 248, p. 126054. doi: <https://doi.org/10.1016/j.chemosphere.2020.126054>.
- Dixit, S. and Hering, J. G. (2003) 'Comparison of Arsenic(V) and Arsenic(III) Sorption onto Iron Oxide Minerals: Implications for Arsenic Mobility',

Environmental Science & Technology, 37(18), pp. 4182–4189. doi: <https://doi.org/10.1021/es030309t>.

Dong, H., Guan, X. and Lo, I. M. C. (2012) ‘Fate of As(V)-treated nano zero-valent iron: Determination of arsenic desorption potential under varying environmental conditions by phosphate extraction’, *Water Research*, 46(13), pp. 4071–4080. doi: <https://doi.org/10.1016/j.watres.2012.05.015>.

Fan, D. *et al.* (2017) ‘Sulfidation of Iron-Based Materials: A Review of Processes and Implications for Water Treatment and Remediation’, *Environmental Science & Technology*, 51(22), pp. 13070–13085. doi: <https://doi.org/10.1021/acs.est.7b04177>.

Farquhar, M. L. *et al.* (2002) ‘Mechanisms of Arsenic Uptake from Aqueous Solution by Interaction with Goethite, Lepidocrocite, Mackinawite, and Pyrite: An X-ray Absorption Spectroscopy Study’, *Environmental Science & Technology*, 36(8), pp. 1757–1762. doi: 10.1021/es010216g.

Fastlund, M. (2018) *Arseniks löslighet i grundvattenakviferen i Hjärtevad, Examensarbete 30 hp SLU, Uppsala Universitet*. Available at: <http://www.diva-portal.org/smash/record.jsf?pid=diva2%3A1185715&dswid=2114>.

Fendorf, S. *et al.* (1997) ‘Arsenate and chromate retention mechanisms on goethite. 1. Surface structure’, *Environmental Science and Technology*, 31(2), pp. 315–320. doi: <https://doi.org/10.1021/es950653t>.

Filip, J. *et al.* (2014) ‘Anaerobic Reaction of Nanoscale Zerovalent Iron with Water: Mechanism and Kinetics’, *The Journal of Physical Chemistry C*, 118(25), pp. 13817–13825. doi: <https://doi.org/10.1021/jp501846f>.

Flora, S. J. S. (2015) ‘Arsenic’, in *Handbook of Arsenic Toxicology*, pp. 1–49. doi: <https://doi.org/10.1016/B978-0-12-418688-0.00001-0>.

Formentini, T. A. *et al.* (2017) ‘Radical change of Zn speciation in pig slurry amended soil: Key role of nano-sized sulfide particles’, *Environmental Pollution*, 222, pp. 495–503. doi: <https://doi.org/10.1016/j.envpol.2016.11.056>.

Formentini, T. A. *et al.* (2021) ‘Redistribution of Zn towards light-density fractions and potentially mobile phases in a long-term manure-amended clayey soil’, *Geoderma*, 394, p. 115044. doi: <https://doi.org/10.1016/j.geoderma.2021.115044>.

Gao, X. *et al.* (2013) ‘Mobility of arsenic in aquifer sediments at Datong Basin, northern China: Effect of bicarbonate and phosphate’, *Journal of Geochemical Exploration*, 135, pp. 93–103. doi: <https://doi.org/10.1016/j.gexplo.2012.09.001>.

Geosyntec (2020) ‘Memorandum - Recommendations for Amendment Dosages, Monitoring Parameters, and Sampling Frequency for TUFFO and Telia Project ISCR Bench Tests Former Telia Company Wood Treatment Site - Hjärtevad, Småland, Sweden’, pp. 1–4.

Gil-Díaz, M. *et al.* (2016) ‘A nanoremediation strategy for the recovery of an As-polluted soil’, *Chemosphere*, 149, pp. 137–145. doi: <https://doi.org/10.1016/j.chemosphere.2016.01.106>.

Goh, K.-H. and Lim, T.-T. (2005) ‘Arsenic fractionation in a fine soil fraction and influence of various anions on its mobility in the subsurface environment’, *Applied Geochemistry*, 20(2), pp. 229–239. doi: <https://doi.org/10.1016/j.apgeochem.2004.08.004>.

Gu, Y. *et al.* (2017) ‘Mechanochemically Sulfidated Microscale Zero Valent Iron: Pathways, Kinetics, Mechanism, and Efficiency of Trichloroethylene

Dechlorination', *Environmental Science & Technology*, 51(21), pp. 12653–12662. doi: <https://doi.org/10.1021/acs.est.7b03604>.

Gustafsson, J. P. (2013) 'Visual MINTEQ ver. 3.1.' Available at: <https://vminteq.lwr.kth.se>.

Gustafsson, J. P. and Van Schaik, J. W. J. (2003) 'Cation binding in a mor layer: batch experiments and modelling', *European Journal of Soil Science*, 54(2), pp. 295–310. doi: <https://doi.org/10.1046/j.1365-2389.2003.00526.x>.

Han, Y. and Yan, W. (2016) 'Reductive Dechlorination of Trichloroethene by Zero-valent Iron Nanoparticles: Reactivity Enhancement through Sulfidation Treatment', *Environmental Science & Technology*, 50(23), pp. 12992–13001. doi: <https://doi.org/10.1021/acs.est.6b03997>.

Hao, L. *et al.* (2018) 'A critical review on arsenic removal from water using iron-based adsorbents', *RSC Advances*. Royal Society of Chemistry, 8(69), pp. 39545–39560. doi: <https://doi.org/10.1039/C8RA08512A>.

Henn, K. W. and Waddill, D. W. (2006) 'Utilization of nanoscale zero-valent iron for source remediation—A case study', *Remediation Journal*, 16(2), pp. 57–77. doi: <https://doi.org/10.1002/rem.20081>.

Hepure (2016) 'Ferox Target zero valent iron powder'. Available at: <http://hepure.com/wp-content/uploads/2017/04/Ferox-Target-SDS.pdf>.

Herath, I. *et al.* (2018) 'Thiolated arsenic in natural systems: What is current, what is new and what needs to be known', *Environment International*, 115(January), pp. 370–386. doi: <https://doi.org/10.1016/j.envint.2018.03.027>.

Hiemstra, T. and Van Riemsdijk, W. H. (1996) 'A Surface Structural Approach to Ion Adsorption: The Charge Distribution (CD) Model', *Journal of Colloid and Interface Science*, 179(2), pp. 488–508. doi: <https://doi.org/10.1006/jcis.1996.0242>.

Hongshao, Z. and Stanforth, R. (2001) 'Competitive Adsorption of Phosphate and Arsenate on Goethite', *Environmental Science & Technology*, 35(24), pp. 4753–4757. doi: <https://doi.org/10.1021/es010890y>.

Huang, H.-H. (2016) 'The Eh-pH Diagram and Its Advances', *Metals*, 6(1), p. 23. doi: <https://doi.org/10.3390/met6010023>.

INSURE (2017) 'EQS Limit and Guideline Values for Contaminated Sites'. Available at: https://www.meteo.lv/fs/CKFinderJava/userfiles/files/EQS_limit_and_guideline_values.pdf.

Kanel, S. R. *et al.* (2005) 'Removal of Arsenic(III) from Groundwater by Nanoscale Zero-Valent Iron', *Environmental Science & Technology*, 39(5), pp. 1291–1298. doi: <https://doi.org/10.1021/es048991u>.

Kašlík, J. *et al.* (2018) 'Nanoarchitecture of advanced core-shell zero-valent iron particles with controlled reactivity for contaminant removal', *Chemical Engineering Journal*, 354, pp. 335–345. doi: <https://doi.org/10.1016/j.cej.2018.08.015>.

Keon, N. E. *et al.* (2001) 'Validation of an Arsenic Sequential Extraction Method for Evaluating Mobility in Sediments', *Environmental Science & Technology*, 35(13), pp. 2778–2784. doi: <https://doi.org/10.1021/es001511o>.

Kim, E.-J. *et al.* (2011) 'Facile Synthesis and Characterization of Fe/FeS Nanoparticles for Environmental Applications', *ACS Applied Materials & Interfaces*, 3(5), pp. 1457–1462. doi: <https://doi.org/10.1021/am200016v>.

Kumpiene, J. *et al.* (2021) ‘LONG-TERM stability of arsenic in iron amended contaminated soil’, *Environmental Pollution*, 269, p. 116017. doi: <https://doi.org/10.1016/j.envpol.2020.116017>.

Kumpiene, J., Fitts, J. P. and Mench, M. (2012) ‘Arsenic fractionation in mine spoils 10 years after aided phytostabilization’, *Environmental Pollution*, 166, pp. 82–88. doi: <https://doi.org/10.1016/j.envpol.2012.02.016>.

Lackovic, J. A., Nikolaidis, N. P. and Dobbs, G. M. (2000) ‘Inorganic Arsenic Removal by Zero-Valent Iron’, *Environmental Engineering Science*, 17, pp. 29–39. doi: <https://doi.org/10.1089/ees.2000.17.29>.

Larios, R., Fernández-Martínez, R. and Rucandio, I. (2013) ‘Assessment of a sequential extraction procedure for arsenic partitioning and application to samples from different pollution sources’, *Analytical Methods*, 5(16), p. 4096. doi: <https://doi.org/10.1039/c3ay40102b>.

Li, S. *et al.* (2014) ‘Zero-valent iron nanoparticles (nZVI) for the treatment of smelting wastewater: A pilot-scale demonstration’, *Chemical Engineering Journal*, 254, pp. 115–123. doi: <https://doi.org/10.1016/j.cej.2014.05.111>.

Liu, Y. and Lowry, G. V. (2006) ‘Effect of Particle Age (Fe 0 Content) and Solution pH On NZVI Reactivity: H₂ Evolution and TCE Dechlorination’, *Environmental Science & Technology*, 40(19), pp. 6085–6090. doi: <https://doi.org/10.1021/es060685o>.

Loeppert, R. H. *et al.* (2002) ‘Quantity and Speciation of Arsenic in Soils by Chemical Extraction’, in Cai, Y. and Braids, O. C. (eds) *Biogeochemistry of Environmentally Important Trace Elements*. Washington, DC: American Chemical Society, pp. 42–56. doi: <https://doi.org/10.1021/bk-2003-0835.ch004>.

Loeppert, Richard H. and Inskeep, W. P. (1996) ‘Iron’, in Sparks, D. L. *et al.* (eds) *Methods of Soil Analysis: Part 3 Chemical Methods*, 5.3. Madison, WI, USA: Soil Science Society of America, American Society of Agronomy (SSSA Book Series), pp. 639–664. doi: <https://doi.org/10.2136/sssabookser5.3.c23>.

Manning, B. A. *et al.* (2002) ‘Arsenic(III) and Arsenic(V) Reactions with Zerovalent Iron Corrosion Products’, *Environmental Science & Technology*, 36(24), pp. 5455–5461. doi: <https://doi.org/10.1021/es0206846>.

Martin, M. *et al.* (2014) ‘Surface Interactions of Arsenite and Arsenate on Soil Colloids’, *Soil Science Society of America Journal*, 78, pp. 157–170. doi: <https://doi.org/10.2136/sssaj2013.04.0133>.

Matschullat, J. (2000) ‘Arsenic in the geosphere — a review’, *Science of The Total Environment*, 249, pp. 297–312. doi: [https://doi.org/10.1016/S0048-9697\(99\)00524-0](https://doi.org/10.1016/S0048-9697(99)00524-0).

Mohan, D. and Pittman, C. U. (2007) ‘Arsenic removal from water/wastewater using adsorbents—A critical review’, *Journal of Hazardous Materials*, 142, pp. 1–53. doi: <https://doi.org/10.1016/j.jhazmat.2007.01.006>.

Otaegi, N. and Cagigal, E. (2017) ‘NanoRem Pilot Site – Nitrastur, Spain: Remediation of Arsenic in Groundwater Using Nanoscale Zero-valent Iron’, *CL:AIRE NanoRem Bulletin*, 12, pp. 1–6. Available at: <http://www.nanorem.eu/Displaynews.aspx?ID=938>.

Peng, X. *et al.* (2017) ‘Effect of Arsenic on the Formation and Adsorption Property of Ferric Hydroxide Precipitates in ZVI Treatment’, *Environmental Science & Technology*, 51(17), pp. 10100–10108. doi: <https://doi.org/10.1021/acs.est.7b02635>.

Phenrat, T. *et al.* (2009) ‘Adsorbed Polyelectrolyte Coatings Decrease Fe₀ Nanoparticle Reactivity with TCE in Water: Conceptual Model and Mechanisms’, *Environmental Science & Technology*, 43(5), pp. 1507–1514. doi: <https://doi.org/10.1021/es802187d>.

Polya, D. A. *et al.* (2019) ‘Groundwater arsenic biogeochemistry – Key questions and use of tracers to understand arsenic-prone groundwater systems’, *Geoscience Frontiers*, 10(5), pp. 1635–1641. doi: <https://doi.org/10.1016/j.gsf.2019.05.004>.

Ponder, S. M., Darab, J. G. and Mallouk, T. E. (2000) ‘Remediation of Cr(VI) and Pb(II) Aqueous Solutions Using Supported, Nanoscale Zero-valent Iron’, *Environmental Science & Technology*, 34(12), pp. 2564–2569. doi: <https://doi.org/10.1021/es9911420>.

Ramos, M. A. V. *et al.* (2009) ‘Simultaneous Oxidation and Reduction of Arsenic by Zero-Valent Iron Nanoparticles: Understanding the Significance of the Core–Shell Structure’, *The Journal of Physical Chemistry C*, 113(33), pp. 14591–14594. doi: <https://doi.org/10.1021/jp9051837>.

van Reeuwijk, L. . (2002) *Procedure for Soil Analysis - ISRIC - TechPaper 09. Sixth Edition*. Technical. Wageningen, The Netherlands: International Soil Reference and Information Centre. Available at: https://www.isric.org/sites/default/files/ISRIC_TechPap09.pdf.

Regenesis (no date) ‘Zero-Valent Iron Technical Bulletin - Benefits of Sulfidation’. Available at: https://regenesis.com/wp-content/uploads/2019/02/S-MicroZVI_SpecSheet-7-1.pdf.

Sasaki, K. *et al.* (2009) ‘Sorption and speciation of arsenic by zero-valent iron’, *Colloids and Surfaces A: Physicochemical and Engineering Aspects*, 347, pp. 8–17. doi: <https://doi.org/10.1016/j.colsurfa.2008.10.033>.

Schmid, D. *et al.* (2015) ‘Measuring the reactivity of commercially available zero-valent iron nanoparticles used for environmental remediation with iopromide’, *Journal of Contaminant Hydrology*, 181, pp. 36–45. doi: <https://doi.org/10.1016/j.jconhyd.2015.01.006>.

Schwertmann, U. (1973) ‘Use of Oxalate for Fe Extraction from Soils’, *Canadian Journal of Soil Science*, 53(2), pp. 244–246. doi: <https://doi.org/10.4141/cjss73-037>.

Schwertmann, U. (1991) ‘Solubility and dissolution of iron oxides’, in Chen, Y. and Hadar, Y. (eds) *Iron Nutrition and Interactions in Plants*. Dordrecht, The Netherlands: Springer Netherlands, pp. 3–27. doi: <https://doi.org/10.1007/BF00011851>.

Schwertmann, U., Schulze, D. G. and Murad, E. (1982) ‘Identification of Ferrihydrite in Soils by Dissolution Kinetics, Differential X-ray Diffraction, and Mössbauer Spectroscopy’, *Soil Science Society of America Journal*, 46(4), pp. 869–875. doi: 10.2136/sssaj1982.03615995004600040040x.

SEPA (2009) ‘Naturvårdsverket: Riktvärden för förorenad mark - Modellbeskrivning och vägledning’, 5976, pp. 1–272. Available at: <https://www.naturvardsverket.se/Om-Naturvardsverket/Publikationer/ISBN/5900/978-91-620-5976-7/>.

SEPA (2016) ‘Datablad för arsenik’. Available at: <https://www.naturvardsverket.se/upload/stod-i-miljoarbetet/vagledning/fororenade-omraden/arsenik.pdf>.

SGU (2013) 'Sveriges geologiska undersökning: Bedömningsgrunder för grundvatten', *Rapport 2013:01*, 1, p. 238. Available at: <http://resource.sgu.se/produkter/sgurapp/s1301-rapport.pdf>.

Shi, Z. *et al.* (2015) 'Methods for characterizing the fate and effects of nano zerovalent iron during groundwater remediation', *Journal of Contaminant Hydrology*, 181, pp. 17–35. doi: <https://doi.org/10.1016/j.jconhyd.2015.03.004>.

Singh, P. *et al.* (2021) 'Kinetics and mechanism of arsenic removal using sulfide-modified nanoscale zerovalent iron', *Chemical Engineering Journal*, 412, p. 128667. doi: [10.1016/j.cej.2021.128667](https://doi.org/10.1016/j.cej.2021.128667).

SIS (2015) 'Swedish Standard Institute: Karaktärisering av avfall - Bestämning av lakegenskaper - pH-inverkan på lakning vid initial tillsättning av syra/bas. SS-EN 14429:2015'. Available at: <https://www.sis.se/produkter/miljo-och-halsoskydd-sakerhet/avfall/allmant/ssen144292015/>.

Smedley, P. . and Kinniburgh, D. . (2002) 'A review of the source, behaviour and distribution of arsenic in natural waters', *Applied Geochemistry*, 17(5), pp. 517–568. doi: [https://doi.org/10.1016/S0883-2927\(02\)00018-5](https://doi.org/10.1016/S0883-2927(02)00018-5).

Su, C. and Puls, R. W. (2001a) 'Arsenate and Arsenite Removal by Zerovalent Iron: Effects of Phosphate, Silicate, Carbonate, Borate, Sulfate, Chromate, Molybdate, and Nitrate, Relative to Chloride', *Environmental Science & Technology*, 35(22), pp. 4562–4568. doi: <https://doi.org/10.1021/es010768z>.

Su, C. and Puls, R. W. (2001b) 'Arsenate and Arsenite Removal by Zerovalent Iron: Kinetics, Redox Transformation, and Implications for in Situ Groundwater Remediation', *Environmental Science & Technology*, 35(7), pp. 1487–1492. doi: <https://doi.org/10.1021/es001607i>.

Sun, Y. *et al.* (2016) 'The influences of iron characteristics, operating conditions and solution chemistry on contaminants removal by zero-valent iron: A review', *Water Research*, 100, pp. 277–295. doi: <https://doi.org/10.1016/j.watres.2016.05.031>.

SWECO (2019) 'Miljöutredning Etapp 2 - Utredning rörande Föroreningsförhållandena vid den f.d. Impregnerings-anläggningen i Hjaltevad, Eksjö kommun.', *Sweco Environment AB*, pp. 1–185.

Tanboonchuy, V. *et al.* (2011) 'Impact of selected solution factors on arsenate and arsenite removal by nanoiron particles', *Environmental Science and Pollution Research*, 18(6), pp. 857–864. doi: <https://doi.org/10.1007/s11356-011-0442-3>.

Tanboonchuy, V., Grisdanurak, N. and Liao, C.-H. (2012) 'Background species effect on aqueous arsenic removal by nano zero-valent iron using fractional factorial design', *Journal of Hazardous Materials*, 205–206, pp. 40–46. doi: <https://doi.org/10.1016/j.jhazmat.2011.11.090>.

Tiberg, C. *et al.* (2013) 'Phosphate effects on copper(II) and lead(II) sorption to ferrihydrite', *Geochimica et Cosmochimica Acta*, 120, pp. 140–157. doi: <https://doi.org/10.1016/j.gca.2013.06.012>.

Tiberg, C. *et al.* (2016) 'Immobilization of Cu and As in two contaminated soils with zero-valent iron – Long-term performance and mechanisms', *Applied Geochemistry*, 67, pp. 144–152. doi: <https://doi.org/10.1016/j.apgeochem.2016.02.009>.

Tuček, J. *et al.* (2017) 'Zero-Valent Iron Nanoparticles Reduce Arsenites and Arsenates to As(0) Firmly Embedded in Core–Shell Superstructure: Challenging Strategy of Arsenic Treatment under Anoxic Conditions', *ACS Sustainable*

Chemistry & Engineering, 5(4), pp. 3027–3038. doi: <https://doi.org/10.1021/acssuschemeng.6b02698>.

VROM (2000) 'Ministerie van Volkshuisvesting, Ruimtelijke Ordening en Milieubeheer: Dutch Target and Intervention Values, 2000 (the New Dutch List) - APPENDIX A'. Available at: https://www.esdat.net/environmental_standards/dutch/appendixs_i2000dutch_environmental_standards.pdf.

Wang, S. and Mulligan, C. N. (2006) 'Effect of natural organic matter on arsenic release from soils and sediments into groundwater', *Environmental Geochemistry and Health*, 28(3), pp. 197–214. doi: <https://doi.org/10.1007/s10653-005-9032-y>.

Wang, X. *et al.* (2021) 'Advances in metal(loid) oxyanion removal by zerovalent iron: Kinetics, pathways, and mechanisms', *Chemosphere*, 280, p. 130766. doi: <https://doi.org/10.1016/j.chemosphere.2021.130766>.

Wang, Y. *et al.* (2010) 'Evidence for Different Surface Speciation of Arsenite and Arsenate on Green Rust: An EXAFS and XANES Study', *Environmental Science & Technology*, 44, pp. 109–115. doi: <https://doi.org/10.1021/es901627e>.

Wei, Y.-T. *et al.* (2010) 'Influence of nanoscale zero-valent iron on geochemical properties of groundwater and vinyl chloride degradation: A field case study', *Water Research*, 44, pp. 131–140. doi: <https://doi.org/10.1016/j.watres.2009.09.012>.

Wenzel, W. W. *et al.* (2001a) 'Arsenic fractionation in soils using an improved sequential extraction procedure', *Analytica Chimica Acta*, 436(2), pp. 309–323. doi: [10.1016/S0003-2670\(01\)00924-2](https://doi.org/10.1016/S0003-2670(01)00924-2).

Wenzel, W. W. *et al.* (2001b) 'Arsenic fractionation in soils using an improved sequential extraction procedure', *Analytica Chimica Acta*, 436(2), pp. 309–323. doi: [https://doi.org/10.1016/S0003-2670\(01\)00924-2](https://doi.org/10.1016/S0003-2670(01)00924-2).

Wenzel, W. W. (2013) 'Arsenic', in Alloway, B. J. (ed.) *Heavy Metals in Soils - Trace Metals and Metalloids in Soils and their Bioavailability*. 3rd edn. Dordrecht: Springer Netherlands (Environmental Pollution), pp. 241–282. doi: https://doi.org/10.1007/978-94-007-4470-7_9.

WHO (2004) *World Health Organisation: Guidelines for drinking water quality, Third Edition, Vol. 1. Recommendations*. 3rd edn, *Environmental Pollution Series A, Ecological and Biological*. 3rd edn. Geneva, Switzerland. Available at: https://www.who.int/water_sanitation_health/dwq/GDWQ2004web.pdf.

WHO (2017) *World Health Organisation: Guidelines for Drinking-water Quality: fourth edition incorporating the first addendum*. 4th edn. Geneva, Switzerland. Available at: <https://www.who.int/publications/i/item/9789241549950>.

Wolthers, M. *et al.* (2005) 'Arsenic mobility in the ambient sulfidic environment: Sorption of arsenic(V) and arsenic(III) onto disordered mackinawite', *Geochimica et Cosmochimica Acta*, 69(14), pp. 3483–3492. doi: <https://doi.org/10.1016/j.gca.2005.03.003>.

Wu, D. *et al.* (2018) 'Enhanced As(III) Sequestration Using Sulfide-Modified Nano-Scale Zero-Valent Iron with a Characteristic Core-Shell Structure: Sulfidation and As Distribution', *ACS Sustainable Chemistry & Engineering*, 6(3), pp. 3039–3048. doi: <https://doi.org/10.1021/acssuschemeng.7b02787>.

Yan, W. *et al.* (2010) 'Multi-tiered distributions of arsenic in iron nanoparticles: Observation of dual redox functionality enabled by a core-shell structure', *Chemical Communications*, 46(37), pp. 6995–6997. doi: <https://doi.org/10.1039/c0cc00000a>.

<https://doi.org/10.1039/c0cc02311f>.

Yan, W., Ramos, M. A. V., *et al.* (2012) 'As(III) Sequestration by Iron Nanoparticles: Study of Solid-Phase Redox Transformations with X-ray Photoelectron Spectroscopy', *The Journal of Physical Chemistry C*, 116(9), pp. 5303–5311. doi: <https://doi.org/10.1021/jp208600n>.

Yan, W., Vasic, R., *et al.* (2012) 'Intraparticle Reduction of Arsenite (As(III)) by Nanoscale Zerovalent Iron (nZVI) Investigated with In Situ X-ray Absorption Spectroscopy', *Environmental Science & Technology*, 46(13), pp. 7018–7026. doi: <https://doi.org/10.1021/es2039695>.

Yan, W. *et al.* (2013) 'Iron nanoparticles for environmental clean-up: recent developments and future outlook', *Environ. Sci.: Processes Impacts*, 15, pp. 63–77. doi: <https://doi.org/10.1039/C2EM30691C>.

Yuan, C. and Lien, H.-L. (2006) 'Removal of Arsenate from Aqueous Solution Using Nanoscale Iron Particles', *Water Quality Research Journal*, 41(2), pp. 210–215. doi: <https://doi.org/10.2166/wqrj.2006.024>.

Zhang, W. (2003) 'Nanoscale iron particles for environmental remediation: An overview', *Journal of Nanoparticle Research*, 5, pp. 323–332. doi: <https://doi.org/10.1023/A:1025520116015>.

Zhu, H. *et al.* (2009) 'Removal of arsenic from water by supported nano zero-valent iron on activated carbon', *Journal of Hazardous Materials*, 172(2–3), pp. 1591–1596. doi: <https://doi.org/10.1016/j.jhazmat.2009.08.031>.

Zou, Y. *et al.* (2016) 'Environmental Remediation and Application of Nanoscale Zero-Valent Iron and Its Composites for the Removal of Heavy Metal Ions: A Review', *Environmental Science & Technology*, 50(14), pp. 7290–7304. doi: <https://doi.org/10.1021/acs.est.6b01897>.

Acknowledgements

I would like to give a special thanks to my main supervisor Thiago Formentini for his constant support and feedback throughout the thesis. Further, I want to thank my co-supervisors Markus Puschenreiter and Geert Cornelis for their support during few but very helpful meetings. Additionally, I would like to thank Dan Berggren Kleja for the opportunity to write my thesis in this project and his insightful peer-review. I would also like to thank Charlotta Tiberg for her support in the modelling part of the thesis. Lastly, I would also like to thank Mina Spångberg for her support in the laboratory.

Appendix

I. Groundwater Composition

Table 11: Groundwater composition in 2017 at groundwater sampling points (1708 and 1709) closest to sediment sampling point 1904 (16-17 m distance) and median values of 34 sampling points throughout the whole area (2016-2018) including the classification of the median values according to SGU's classification (1: very low – 5: too high). ¹: SGU (2013).

Variable	Unit	1708_2	1709_2	Median of the Area	SGU classification 1708/1709/Median
As _{tot}	µg/L	1450	321		5/5
As(III)	µg/L	1340	251		5/5
pH	-	6.8	6.5	6.9	3/3/3
HCO ₃	mg/L	59	38	87	3/3/4
EC	mS/m	11	12	20	1/1/1
ORP	mV	-10	-94	-156	-
Ca	mg/L	20	17	25	3/2/3
Mg	mg/L	3	3	3	2/2/2
Na	mg/L	5	5	6	2/2/2
K	mg/L	3	2	2	2/1/1
O ₂	mg/L	0	0.1	<1	1/1/1
NO ₃	mg/L	<2	<2	<2	1/1/1
NH ₄	mg/L	0.3	0.3	0.3	3/3/3
Fe	mg/L	6	18	7	5/5/5
Mn	mg/L	0.6	0.6	0.6	5/5/5
PO ₄ -P	mg/L	0.004	0.01	0.04	1/2/2
SO ₄	mg/L	15	21.5	17	2/2/2
Al	mg/L	0.05	0.04	0.04	2/2/2
Cl	mg/L	5	6	8	1/1/1
DOC	mg/L	3	2	4	>1.9 mg/L ¹

II. Phosphate Extraction

a. Justification of main phosphate extraction parameters

1. **100 L/S ratio:** ensuring representative sample amount, sufficient extraction volume and As concentration for analysis
2. **pH 8:** reduction of formation of Fe(III)PO_4 , close to pH conditions of the batch experiments
3. **0.5 M PO_4 :** sufficient competition efficiency of PO_4^{3-} for desorption of As(V) and As(III), minimising the selective bias of PO_4^{3-} towards As(V) as stated by Loeppert, Jain and El-haleem (2003). Modelling with Visual Minteq v. 3.1 was conducted with input data mimicking the field conditions and accounting for the added Fe concentrations by the sorbents as ferrihydrite. Two concentrations of added Fe (0.1, 0.5 %) were simulated reflecting the range of added Fe in the batch experiments (0.2-1%). Figure 17: Effect of different phosphate concentrations on As sorption onto ferrihydrite. Modelling was conducted with Visual Minteq ver. 3.1. shows that with increasing PO_4^{3-} concentrations more As gets desorbed and the effect of PO_4^{3-} selectivity towards As(V) is minimised. A final PO_4^{3-} concentration of 0.5 M was chosen in order to find the balance between sufficient As desorption and avoidance of matrix effects during ICP-MS analysis.

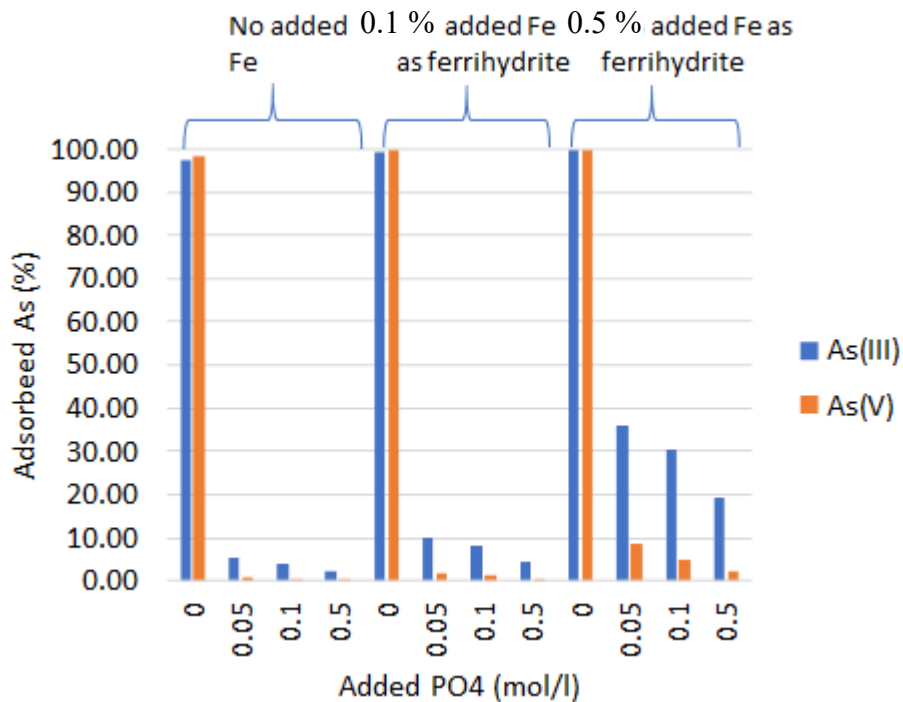


Figure 17: Effect of different phosphate concentrations on As sorption onto ferrihydrite. Modelling was conducted with Visual Minteq ver. 3.1.

b. Fe concentrations in phosphate extracts (Fe_{F2})

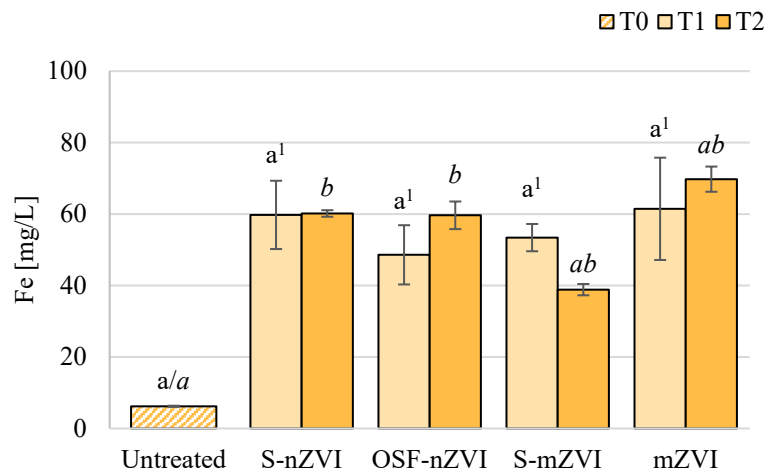


Figure 18: Phosphate extractable Fe [mg/L] (F_2). T0: Untreated Sediment. T1: Uncontrolled pH. T2: pH adjusted to field pH. Values show means ($n \geq 2$). Error bars express standard deviation ($n > 2$) or absolute deviation ($n = 2$). Significant differences ($p < 0.05$) are shown for Kruskal-Wallis with post-hoc Bonferroni, and (1) one-way ANOVA with post-hoc Tukey HSD. Non-italic letters refer to differences within treatments at T1 and between T0 and T1. Italic letters refer to differences within treatments at T2 and between T0 and T2.

c. pH and ORP values of the phosphate extracts

Table 12: pH in extracts after phosphate extractions.

Treatment	Scenario	Shaking time before acidification [d]	Shaking time after acidification [d]	pH
Untreated	Before Treatment (T0)	30	-	8.0
		30	-	8.0
S-nZVI	Uncontrolled pH (T1)	23	-	8.0
		23	-	7.9
		56	-	8.0
		56	-	8.0
OSF-nZVI		23	-	8.0
		23	-	8.0
		56	-	7.9
S-mZVI		56	-	8.0
	30	-	8.0	
	30	-	8.0	
	31	-	8.0	
mZVI	31	-	8.0	
	30	-	8.0	
	30	-	8.0	
	62	-	8.0	
S-nZVI		62	-	8.0
		56	4	8.0

	pH Adjusted to Field pH (T2)	56	4	8.0
OSF-nZVI		56	4	8.0
		56	4	8.0
		56	3	7.9
S-mZVI		31	3	8.0
		62	4	8.0
mZVI		62	4	8.0

III. pH-dependent Arsenic Solubility

a. Pre-tests

Pre-tests were conducted according to the procedure described in 4.3. 7 samples were prepared with different amounts of acid (HNO_3) and base (NaOH) (Figure 19). Samples were shaken for 5 days and the pH was directly measured in the supernatant after centrifugation.

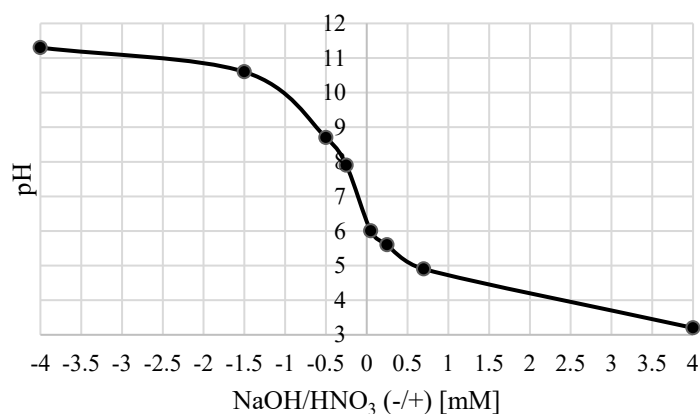


Figure 19: Added NaOH/HNO_3 concentrations [mM] and resulting pH of pre-tests of the unfiltered supernatant after 5 days shaking.

b. Main Experiments

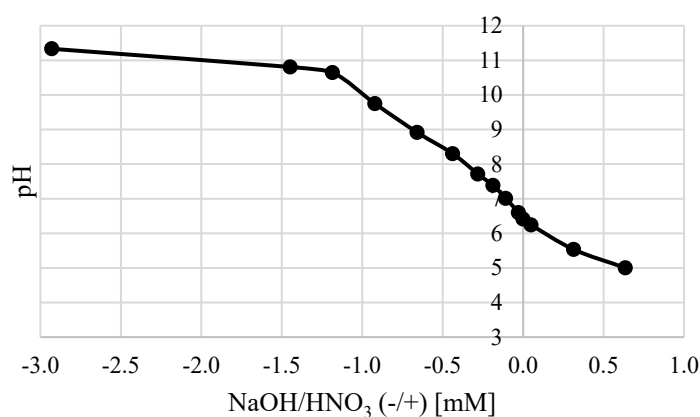


Figure 20: Added NaOH/HNO_3 concentrations [mM] and resulting average pH of the unfiltered supernatant after 5 1/2 days shaking.

IV. Modelling

a. Input data

Table 13: Input data for Visual Minteq.

pH-dependent solubility (section 4.3)	Calculated from HNO ₃ & NaNO ₃ addition	pH-dependent solubility (section 4.3)						Data from Fastlund (2018)		Oxalate Extraction			
		pH	NO ₃ ⁻ mg/L	Na ⁺ mg/L	Ca ²⁺ mg/L	K ⁺ mg/L	Mn ²⁺ mg/L	P(PO ₄ ³⁻) mg/L	DOC mg/L	FA g/l	HA g/l	As mg/L	Ferrihydrite g/l
		11.33	620.05	302.11	0.47	1.45	0.03	0.59	4.49	0.05	0.05	3.77	0.183
		10.81	620.05	269.57	0.57	1.48	0.03	0.48	3.85	0.05	0.05	3.77	0.183
		10.65	620.05	267.93	0.57	1.48	0.02	0.46	3.80	0.05	0.05	3.77	0.183
		9.75	620.05	254.66	0.67	1.44	0.02	0.32	2.80	0.05	0.05	3.77	0.183
		8.92	620.05	252.32	0.89	1.48	0.02	0.24	2.20	0.05	0.05	3.77	0.183
		8.30	620.05	248.52	1.33	1.57	0.02	0.15	1.70	0.05	0.05	3.77	0.183
		7.71	620.05	240.35	1.87	1.62	0.03	0.05	0.55	0.05	0.05	3.77	0.183
		7.39	620.05	243.15	2.05	1.60	0.04	0.05	1.75	0.05	0.05	3.77	0.183
		7.01	620.05	250.70	2.79	1.74	0.10	0.03	1.25	0.05	0.05	3.77	0.183
		6.60	620.05	242.51	3.57	1.80	0.15	0.01	0.80	0.05	0.05	3.77	0.183
		6.41	620.05	240.02	3.75	1.92	0.16	0.01	0.65	0.05	0.05	3.77	0.183
		6.24	623.15	248.26	4.04	1.84	0.18	0.01	0.75	0.05	0.05	3.77	0.183

5.53	639.54	236.13	6.03	2.04	0.29	0.01	0.55	0.05	0.05	3.77	0.183
5.00	659.47	242.50	8.30	2.37	0.37	0.03	0.45	0.05	0.05	3.77	0.183

b. Optimisation of Ferrihydrite

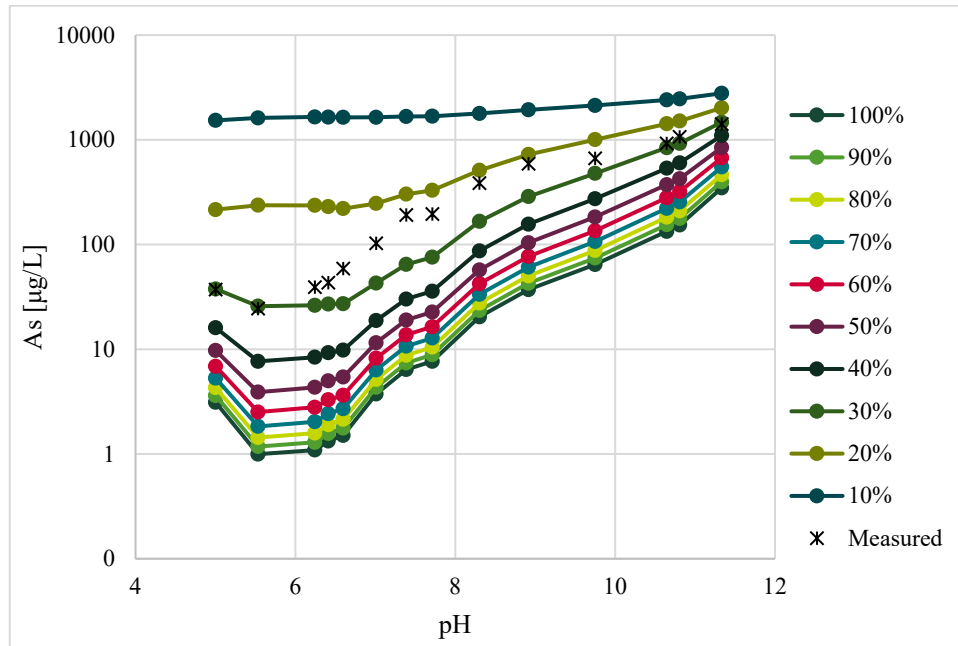


Figure 21: Simulation of As solubility with changing Ferrihydrite concentrations. 100 % represent 0.18 g/L ferrihydrite. Measured means measured As concentrations in the supernatant of experiments in section 4.3.

V. Total Concentrations of metals in the sediment

Table 14: Total Concentrations [mg/kg] of metals in the sediment of sampling point 1904 analysed by hot-plate digestion (SE-SOP-0021). 1: Chrome VI (predominant in groundwater).

Element	Concentration [mg/kg]	Guideline values (Sensitive Land Use) (SEPA, 2009) [mg/kg]
Ba	8.01	200
Cd	<0.1	0.5
Co	1.56	15
Cr	56.4	80(2) ¹
Cu	25.6	80
Hg	<0.2	0.25
Mn	83.1	-
Ni	3.09	40
Pb	3.74	50
V	8.24	100
Zn	16.7	250

VI. Dissolved Sulphide

Dissolved sulphide (Table 15) was measured in the filtered supernatants of the centrifuged samples of the three different remediation scenarios (see section 4.2.2). It was measured colorimetrically according to the USEPA Methylene Blue Method Nr. 8131 with a HACH colorimeter (DOC316.53.01136).

Table 15: Dissolved Sulphide [$\mu\text{g/L}$] in the untreated sediment (T0), in ZVI treatments at uncontrolled pH (T1), and at pH adjusted to field pH (T2).

Treatment	Scenario	Sulphide [$\mu\text{g/L}$]
Untreated	T0	<10
S-nZVI	T1	15±10
OSF-nZVI		<10
S-mZVI		<10
mZVI		<10
S-nZVI		T2
OSF-nZVI	<10	
S-mZVI	<10	
mZVI	<10	